ABSTRACT

Title of Document: ROLE OF BK CHANNELS IN CARDIAC FUNCTION

Michael Lai, Ph.D., 2015

Directed By: Associate Professor Andrea Meredith, Department of Physiology

Large-conductance voltage- and Ca^{2+}-activated potassium (BK) channels are critical modulators of cellular excitability throughout the cardiovascular and nervous systems. The first aim of this work focuses on a novel role for BK channels in regulating cardiac pacing. Recently, BK channels were implicated in heart rate regulation, but the underlying mechanism was unclear. We hypothesized that BK channels regulate heart rate by modulating the intrinsic excitability of sinoatrial node cells (SANCs), the predominant cardiac pacemaking cells. We found that BK channel protein was expressed in SANCs, and that elimination of BK currents via pharmacological inhibition and genetic ablation reduces SANC excitability. Additionally, we characterized the properties of BK currents from SANCs. Our results indicate that BK channels are novel regulators of SANC function, and suggest that BK channels can serve as a novel therapeutic target for treating heart rate disorders.

The second aim of this work focuses on the effect of single-nucleotide polymorphisms (SNPs) on BK current properties. There are approximately 100 known non-synonymous SNPs in human *KCNMA1*, the gene that encodes BK channels, but few have been characterized or linked with disease. We hypothesized that SNPs in *KCNMA1* associated with disease, or located in domains of the BK channel gating ring that mediate Ca^{2+}-dependent activation would alter BK current properties. We determined that the effects of SNPs on BK current properties were Ca^{2+} concentration-dependent. Also, we found that SNP-induced alterations in current kinetics influenced the amplitude of BK currents evoked by action potential waveforms. These results indicate that SNPs in *KCNMA1* can modulate BK current properties and could contribute to the diversity of BK currents evoked by physiological stimuli.

ROLE OF BK CHANNELS IN CARDIAC FUNCTION

By

Michael Henry Lai

Dissertation submitted to the Faculty of the Graduate School of the
University of Maryland, College Park, in partial fulfillment
of the requirements for the degree of
Doctor of Philosophy
2015

Advisory Committee:
Associate Professor Andrea Meredith, Advisor/Co-Chair
Professor John Fisher, Co-Chair
Associate Professor Adam Hsieh
Associate Professor Matthew Trudeau
Professor Sergei Sukharev

Dedication

To discovery

Acknowledgements

I would like to thank several people that have helped and supported me throughout my graduate school tenure, as without them this would not have been possible:

- First and foremost, I would like to thank my advisor Andy for her unwavering support. There have been several times where aspects of this project have seemed impossible and without her encouragement I would not have carried this project to the end. Thanks Andy for making me a better scientist.
- My family …sorry I haven't been available as much as you would have liked me to be…I was working, not goofing around, I promise!
- The members of my committee for helpful comments throughout my project.
- Numerous colleagues that I've had throughout my time in Baltimore; first and foremost my labmates, past (Jenna, Chris, Jessica, Betsy) and present (Josh, Sono, Amber).
- Joe Mauban for helping me numerous times with equipment issues, training on microscopes, and listening to me whine during lunch.
- The Trudeau, Chung, Lederer, and Welling labs for helpful advice and reagents.
- The Interdisciplinary Training Program in Muscle Biology and Cardiovascular Cell Biology training grants for financial support.
- Last but not least, I would like to thank my fiancée Julie. Thanks for putting up with a lot of my complaining, and for reminding me that science can still be fun, even if things don't work.

Table of Contents

List of Tables

List of Figures

List of Abbreviations

AC: adenylate cyclase
ACh: acetylcholine
AmpB: amphotericin B
ANS: autonomic nervous system
AP: action potential
APD_{50}: action potential duration at 50% repolarization
AV: atrioventricular
BK: big potassium
Ca_V: voltage-gated calcium channel
CTX: charybdotoxin
DD: diastolic depolarization
DMSO: dimethyl sulfoxide
dV/dt: derivative of voltage over time
ECGs: electrocardiograms
HCN: hyperpolarization cyclic nucleotide gated
HEK: human embryonic kidney
HRP: horseradish peroxidase
ISO: isoproterenol
IbTX: iberiotoxin
I-V: current-voltage
$I_{Ca,L}$: L-type calcium current
$I_{Ca,T}$: T-type calcium current
I_f: funny current
$I_{K,ACh}$: acetylcholine activated potassium current
$I_{K,r}$: rapid delayed rectifier potassium current
$I_{K,s}$: slow delayed rectifier potassium current
I_{Na}: sodium current
I_{NCX}: sodium/calcium exchange current
$I_{T,o}$: transient outward current
IK: intermediate conductance
G-V: conductance-voltage
KB: kraft-bruhe
***Kcnma1*$^{-/-}$:** mice lacking expression of BK channels
K_i: inhibition constant
mbr5: mouse brain clone 5
MDP: maximum diastolic potential
NE: norepinephrine
PAX: paxilline
PKA: protein kinase A
P_O: open probability
P-R: conduction through AV node
Q-T: ventricular depolarization and repolarization
RCK: regulator of K^+ conductance
RT-PCR: reverse transcriptase polymerase chain reaction

RyRs: ryanodine receptors
SAN: sinoatrial node
SANCs: sinoatrial node cells
SCN: suprachiasmatic nucleus
SNP: single nucleotide polymorphism
SR: sarcoplasmic reticulum
SERCA: sarcoplasmic reticulum Ca^{2+} ATP-ase pump
SK: small-conductance
τ: time constant
TM: transmembrane
T-P: interval between ventricular repolarization and next atrial depolarization
TSA: tyramide signal amplification
TTX: tetrodotoxin
VSD: voltage-sensing domain
VSM: vascular smooth muscle
V_{Th}: threshold potential
WT: wild-type

Chapter 1: Introduction

BK ($K_{Ca}1.1$, Maxi-K) channels are large-conductance Ca^{2+}- and voltage activated potassium channels that are that are gated by membrane depolarization and elevation of intracellular Ca^{2+} (Marty, 1983). BK channels are encoded by a single *Kcnma1* (*slo1*) gene (Butler et al., 1993; Meredith et al., 2004), and the pore-forming subunit of the channel consists of a tetramer of α-subunits (Shen et al., 1994). Each α-subunit is defined by seven transmembrane domains that regulate voltage sensing and form the channel pore, an extracellular NH_2 (N) terminus, and an intracellular -COOH (C) terminus that forms the channel gating ring and regulates Ca^{2+} sensitivity (Meera et al., 1997) (Figure 1). BK currents are classified by their large single-channel conductance, outward currents in response to membrane depolarization and/or intracellular Ca^{2+}, and sensitivity to specific toxins and inhibitors (Butler et al., 1993; Cui et al., 2009; Knaus et al., 1994; Latorre and Miller, 1983; Meera et al., 2000). BK current properties can be modulated through a variety of mechanisms, including posttranslational modifications, auxiliary subunits, and alternative splicing (Brenner et al., 2000; Davies et al., 2003; Xie and McCobb, 1998; Yan et al., 2008).

Physiologically, BK channels are essential regulators of excitability throughout the cardiovascular and nervous systems. In the cardiovascular system, BK channels are expressed throughout vascular smooth muscle, and opening of BK channels facilitates vasodilation (Nelson et al., 1995). Also, multiple reports indicate that activation of mitochondrial BK channels protects the heart against ischemic injury (Bentzen et al., 2009; Singh et al., 2013; Xu et al., 2002). In neurons, BK channels can regulate the repolarization and after-hyperpolarization phases of action potentials (Faber and Sah,

2002; Storm, 1987), as well as mediate neurotransmitter release (Raffaelli et al., 2004). Additionally, neuronal excitability can be mediated by changes in BK channel expression and current properties (Meredith et al., 2006; Shelley et al., 2013).

BK channels have profound clinical relevance due to their ubiquitous expression throughout the cardiovascular and nervous systems. BK channel dysfunction can contribute to several conditions, including hypertension, diabetes, and epilepsy (Du et al., 2005; England et al., 1993; McGahon et al., 2007; Wan et al., 2013). Because of the vast number of physiological roles for BK channels, it would be extremely beneficial to have therapies designed to selectively target and modulate BK currents in order to potentially treat pathophysiological conditions. Therefore, it is of utmost importance to continue to elucidate novel physiological roles for BK channels so that more effect treatments can be developed.

1.1 *BK channel structure*

The BK channel pore-forming subunit consists of a tetramer of α-subunits, and each α-subunit contains seven transmembrane domains (S0–S6) and an intracellular COOH-terminus (Meera et al., 1997) (Figure 1). The S1-S4 domains form the voltage-sensing domain (VSD), which regulates voltage-dependent gating of the channels, while the S5-S6 domains form the channel pore (Meera et al., 1997). Although the BK channel VSD and pore are similar in structure to other voltage-gated K^+ channels (Atkinson et al., 1991; Butler et al., 1993), BK channels contain a seventh transmembrane domain (S0) at the NH_2-terminal end (Meera et al., 1997; Wallner et al., 1996). The S0 domain modulates voltage-dependent gating (Koval et al., 2007), and is essential for α-subunit association with auxiliary β-subunits (Wallner et al., 1996), which are two

transmembrane domain proteins that regulate multiple current properties, including Ca^{2+} sensitivity and activation kinetics (Brenner et al., 2000a; McCobb et al., 1995).

The VSD consists of the S1-S4 transmembrane domains (Figure 1). The S4 domain is the primary voltage sensor, and it contains three positively charged arginine residues (R207, R210, R213) that are conserved across other K^+ channels and regulate the voltage-dependent activation (Cui and Aldrich, 2000; Díaz et al., 1998; Ma et al., 2006). In addition to the charged residues in S4, several other charged residues in S2 and S3 have been implicated in voltage-sensing, including D153, R167, and D186. TM domains S5 and S6 form the central pore and pore helix of the channel. The pore structure is similar to that of other K^+ channels, as it contains a K^+ selectivity filter (Brelidze et al., 2003; Heginbotham et al., 1994), as well as an external turret between S5-S6 that mediates toxin selectivity (Giangiacomo et al., 2008). Additionally, the pore contains a ring of eight glutamic acid residues (E321 and E324), which reside below the selectivity filter and enable the channel's large single-channel conductance (Brelidze et al., 2003).

The C-terminus of each BK channel α-subunit contains four additional hydrophobic segments (S7-S10)(Meera et al., 1997) that form the channel gating ring (Wu et al., 2010; Yuan et al., 2010; 2011) (Figure 1). Each C-terminus contains two "regulators of K^+ conductance" (RCK) domains (Wu et al., 2010; Yuan et al., 2011), and within these RCK domains are two high-affinity Ca^{2+} sensing sites (Schreiber and Salkoff, 1997; Xia et al., 2002; Zhang et al., 2010). The first residues identified to regulate Ca^{2+} sensing were within the "Ca^{2+}-bowl," a group of five consecutive aspartic acid residues in RCK2 (Schreiber and Salkoff, 1997). Through site-directed mutagenesis,

the negatively charged aspartic acids were neutralized through mutation to asparagine (5D5N), causing a 60-70 mV rightward shift in the conductance-voltage (G-V) curve compared to wild-type (WT) channels at low (4 μM Ca^{2+}) and saturating (1 mM) Ca^{2+} concentrations (Schreiber and Salkoff, 1997; Xia et al., 2002). Additionally, crystal structures of the BK channel gating ring suggest that Ca^{2+} binds directly within Ca^{2+} bowl and causes a conformational change that promotes opening of the pore (Yuan et al., 2011).

The mouse D362, D367 and E535 residues are the critical residues in the BK RCK1 domain that form the second high-affinity Ca^{2+} sensing site. Through alignment of the BK channel (*slo1*) sequence with *slo3*, a BK channel homologue that is regulated by pH rather than Ca^{2+}, it was determined that D362 and D367 were not conserved, suggesting that D362 and D367 may regulate Ca^{2+} sensing (Xia et al., 2002). It was then discovered that mutating D362/D367 to alanine caused a +100 mV positive shift in the G-V relationship compared to WT channels in saturating Ca^{2+} conditions. This indicated that D362/D367 were essential for Ca^{2+} sensitivity (Xia et al., 2002). Later, it was demonstrated that E535 was also an essential residue to the RCK1 Ca^{2+} sensitivity site, as E535A shifted the G-V relationship towards positive potentials in a similar manner compared to the D362A/D367A mutations (Zhang et al., 2010).

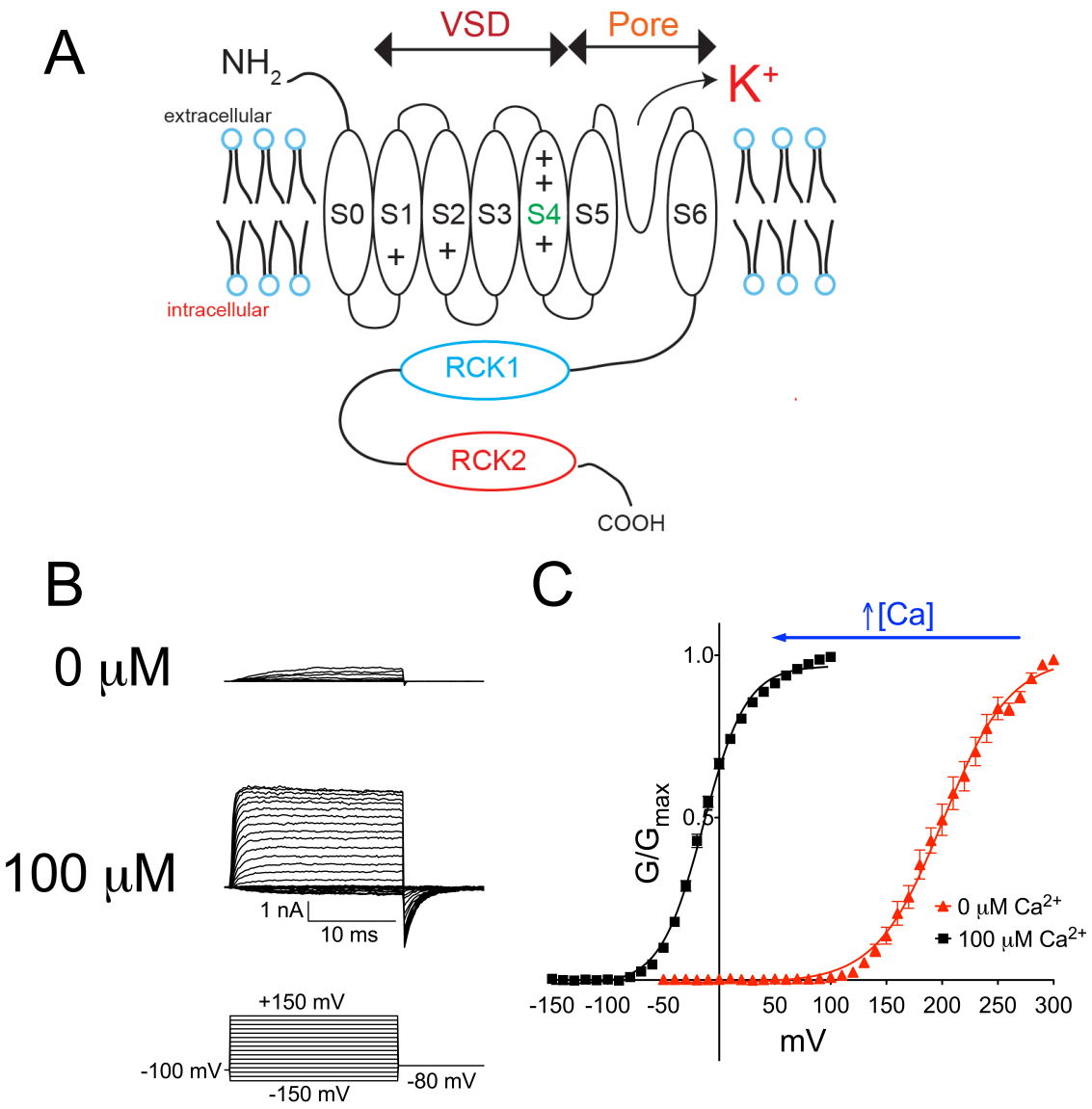

Figure 1: BK channel structure and currents

(A) Topology of a BK channel α-subunit. Each α-subunit has an extracellular N-terminus, voltage-sensing domain (VSD, S1-S4), pore (S5-S6), and an intracellular C-terminus. The C-terminus, which contains two RCK domains, forms the channel gating ring. Each RCK domain contains a high-affinity Ca^{2+} coordination site. (B) BK currents are activated by membrane depolarization and Ca^{2+}. BK currents were evoked using depolarizing voltage steps from BK channels in an inside-out patch configuration in symmetrical K^+ at the indicated concentration of Ca^{2+}. (C) Normalized conductance-voltage (G-V) relationship for BK currents at indicated Ca^{2+}. Current activation becomes more robust and the G-V relationship is shifted toward more negative potentials as intracellular Ca^{2+} is elevated.

1.2 *Allosteric regulation of BK currents by Ca^{2+} and voltage*

BK channels can open through solely Ca^{2+}- or voltage-dependent mechanisms; in zero-Ca^{2+} conditions, the single-channel open probability (P_O) increases with membrane depolarization due to voltage-sensor activation (Figure 2A, Figure 2C) (Meera et al., 1996; Rothberg and Magleby, 2000; Talukder and Aldrich, 2000). Alternatively, the P_O can be increased, even at hyperpolarized potentials where the voltage-sensor is not intrinsically activated, by elevation of intracellular Ca^{2+} (Figure 2B)(Rothberg and Magleby, 2000). Although these pathways can open the channel pore independently, the pathways are also uniquely allosterically coupled, as demonstrated by the Horrigan-Aldrich model (Horrigan and Aldrich, 2002) (Figure 3). In this model, P_O is described as a function of voltage-sensor activation and Ca^{2+} binding. A key aspect of the model is that changes in membrane potential or intracellular Ca^{2+} that affect the state of the voltage sensors or Ca^{2+} binding, respectively, will directly affect each other and will consequently affect P_O. Therefore, it is essential to identify residues that affect voltage- or Ca^{2+}-sensitivity in order to understand allosteric mechanisms of channel gating.

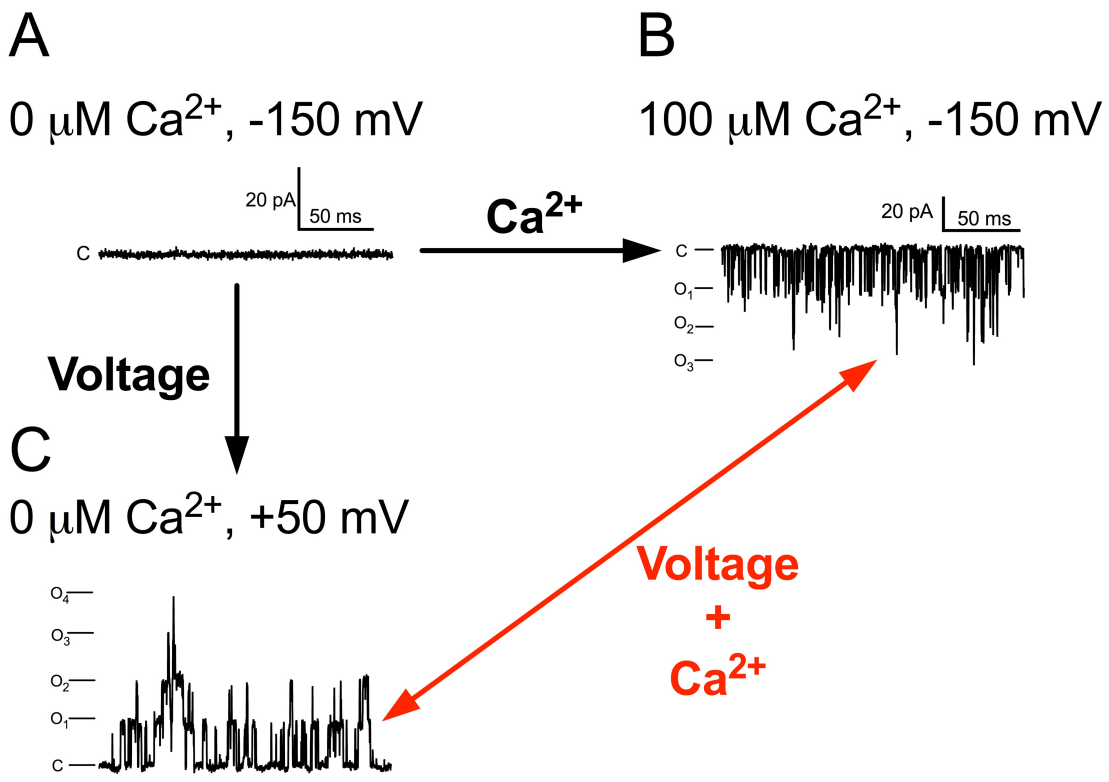

Figure 2: BK currents can be activated independently through either Ca^{2+} or voltage-dependent pathways

Single channel openings were recorded from BK channels in an inside-out patch configuration at the indicated Ca^{2+} concentrations and voltages. (A) BK channels have a low open probability (P_O) and are closed, as denoted by "C," in conditions where there is no Ca^{2+} and the membrane is hyperpolarized. Channels can open solely through Ca^{2+}-dependent (B) or voltage-dependent mechanisms (C). Because BK channels are allosterically activated, voltage- and Ca^{2+}-dependent activation are coupled. The number of channels opening at one time in (B) and (C) are denoted by "O". Single channel recordings in (A) and (C) were acquired from the same patch.

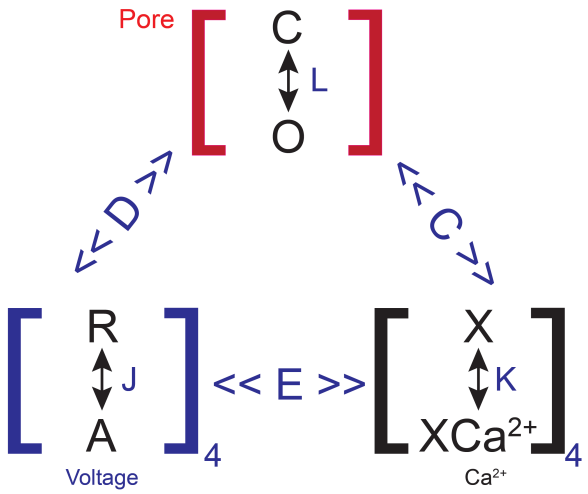

Figure 3: Horrigan-Aldrich model of allosteric activation of BK channels

Each BK channel subunit can be activated by voltage and Ca^{2+} (Horrigan and Aldrich, 2002). Because BK channels consist of a tetramer of α-subunits, the model incorporates four voltage sensors (blue brackets, left) and at least four high-affinity Ca^{2+} binding sites (black brackets, right). Each of the voltage sensors can transition between resting (*R*) and active (*A*) states, which is governed by an equilibrium factor *J*. Each Ca^{2+} binding site can transition between a Ca^{2+}-unbound (*X*) and Ca^{2+}-bound (*XCa*) state, which is governed by an equilibrium constant *K*. The channel pore can be either in the closed (*C*) or the open (*O*) state, which is governed by the equilibrium constant *L*. In Ca^{2+}-free conditions, the interaction between the voltage sensors and the channel pore is regulated by an allosteric factor *D*. In conditions where the voltage sensors are not activated, the interaction between Ca^{2+}-binding and the channel pore is regulated by an allosteric factor *C*. Furthermore, both voltage- and Ca^{2+} are coupled to channel gating through allosteric factor *E*. Figure adapted from Horrigan and Aldrich, 2002.

1.3 *Mechanisms that convey diversity to BK current properties*

BK currents can exhibit diverse properties, such different current kinetics, voltage sensitivities, and Ca^{2+} sensitivities. Differences in current properties allow BK channels to regulate excitability in multiple tissues, as the electrical stimuli that activate BK currents in different tissues often occur over different time scales, voltage ranges, and frequencies. BK current diversity can be attributed to multiple mechanisms, including alternative splicing of *Kcnma1* (Butler et al., 1993; Xie and McCobb, 1998), auxiliary subunits (Brenner et al., 2000a; Yan and Aldrich, 2010), and phosphorylation (Reinhart et al., 1991; Yan et al., 2008).

Alternative splicing is one mechanism that accounts for BK current diversity (Butler et al., 1993; Ha et al., 2000; Shelley et al., 2013; Xie and McCobb, 1998). Alternative splicing increases protein diversity from a single gene, as editing of pre-messenger RNA changes the encoded amino acid sequence, which can affect BK current properties (Shipston, 2001). Within the C-terminus, there are four splice sites (S1-S4) (Figure 4). Alternative splicing can directly affect BK current properties, which subsequently can modulate the excitability and function of cells such as those in the inner ear and adrenal gland (Ramanathan et al., 1999; Xie and McCobb, 1998). However, the effect of specific exons on current properties can be dependent on inclusion or exclusion of other exons (Johnson et al., 2011; Rosenblatt et al., 1997; Shelley et al., 2013). Therefore, it is essential to carefully consider the splice variant background of the BK channel prior to experiments. The alternative splice sites, the residues inserted at each splice site, and the effects of these residue sequences on current properties, can be found in Table 1.

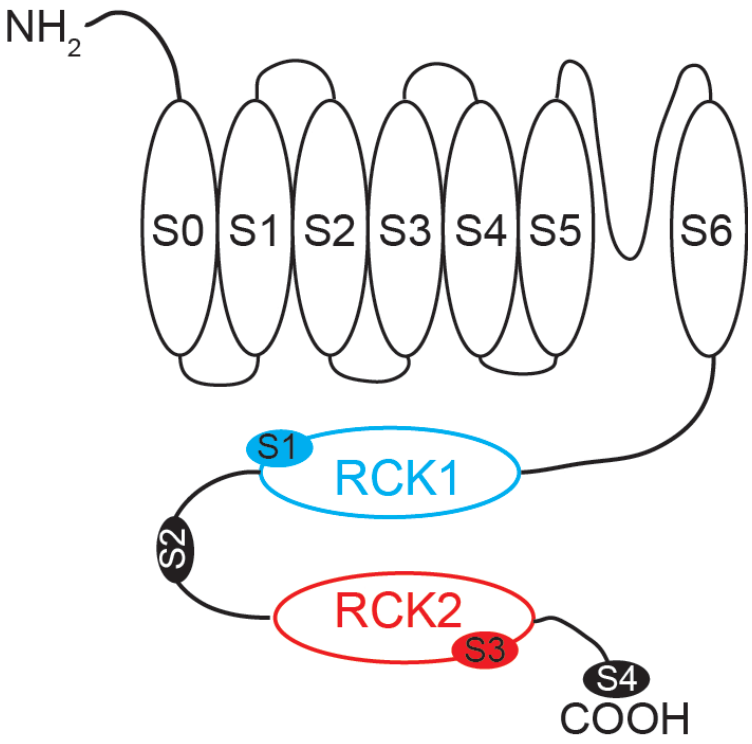

Figure 4: Alternative splice sites with BK channel α-subunit

Schematic of one BK channel α-subunit. Alternative splice sites (S1-S4) are denoted by shaded ovals in the C-terminus of the channel.

Splice Site	Amino Acid Sequences	Effect of amino acid sequences on BK current properties
1	SRKR	- induces right-shift in G-V and slows activation kinetics (Shelley et al., 2013)
2	1. L 2. LIYF 3. LIYSKMSIYKRMRRACCFDC GRSERDCSCMSGRVRGNVDT LERTFPLSSVSVNDCSTSFRAF 4. PKMSIYKRMRRACCFDCGRS ERDCSCMSGRVRGNVDTLER TFPLSSVSVNDCSTSFRAF 5. LKVAARSRYSKDPFEFKKETP NSRLVTEPV	- 2, 3: induce left-shifts in G-V, quickens activation kinetics (Xie and McCobb, 1998) - 4: left-shifts G-V, desensitizes channels to cAMP (Chen et al., 2005)
3	(A)KPGKLPLVSVNQEKNSGTHILMIT EL	-Eliminates reduction in Hill Coefficient (Ha et al., 2000)
4	1. NRKEMVYR 2. KKEMVYR 3. KYVQEERL 4. NATRMTRMGQAEKKWFTDE PDNAYPRNIQIKPMSTHMAN QINQYKSTSSLIPPIREVEDEC 5. NATRMTRMGQEKKWFTDEP DNAYPRNIQIKPMSTHMANQI NQYKSTSSLIPPIREVEDEC	- -VYR, -VEDEC regulate BK trafficking to cell membranes (Singh et al., 2013)

Table 1: BK channel alternative splice sites, possible amino acid sequences at each splice site, and effect of amino acid sequences on BK current properties

Auxiliary β- and γ-subunit proteins are another mechanism underlying BK current diversity. There are four β-subunit proteins (β1 - β4) whose expression levels are tissue-dependent (Behrens et al., 2000; Brenner et al., 2000a; Meera et al., 2000). Functionally, β-subunits generally enhance Ca^{2+}-dependent activation of BK currents, and modulate current activation and deactivation kinetics. Most work pertaining to physiological roles of BK β-subunits focuses on the β1 and β4 subunits. β1 subunits, which are primarily associated with smooth muscle, but also found in brain, colon, uterus, and bladder via northern blot (Behrens et al., 2000; Brenner et al., 2000a; Dworetzky et al., 1994; Tseng-Crank et al., 1996), generally cause an increase Ca^{2+} sensitivity. Co-expression of the α and β1 subunits induces large (+40 to +78 mV) hyperpolarizing shifts in the G-V relationship of BK currents at multiple Ca^{2+} concentrations compared to the α-subunit alone (McCobb et al., 1995). Also, genetic deletion of β1 subunits reduces the number of channel openings and amplitude of BK currents in response to Ca^{2+} spark events in arterial muscle (Brenner et al., 2000b). In addition to increasing Ca^{2+} sensitivity, β1 subunits also increase the time constants of activation (τ_{Act}) (Brenner et al., 2000a).

BK β4 subunits are primarily expressed in the brain but can also be detected in relatively low levels in tissues such as the heart, kidney, and lungs (Behrens et al., 2000; Brenner et al., 2000a; Meera et al., 2000). The effects β4 subunits on BK current properties are complex, as β4 can confer differential effects on the G-V relationship of BK currents depending on the intracellular Ca^{2+} concentration. When co-expressing BK α- and β4 subunits in symmetrical K^+ solutions at low intracellular Ca^{2+} concentrations (< 10 μM Ca^{2+}), β4 subunits slow current activation kinetics and shift the G-V curve to

more positive potentials (Brenner et al., 2000a). However, at Ca^{2+} concentrations greater than 10 μM, the β4 subunit shifts the G-V relationship in a negative direction, suggesting that at high Ca^{2+} concentrations, β4 subunits enhance Ca^{2+} sensitivity (Brenner et al., 2000a). In addition to complex effects on channel gating, β4 subunits also confer resistance to both iberiotoxin (IbTX) and charybdotoxin (CTX), two potent peptide toxin inhibitors of BK channels (Meera et al., 2000).

The β2 and β3 subunits, although less-studied physiologically than either β1 or β4, are distinct from the β1 and β4 subunits because they induce current inactivation. Inactivating BK currents exhibit a time-dependent reduction in current amplitude after initial activation (Solaro et al., 1995). The inactivation conferred by β2 and β3 subunits is Ca^{2+}-dependent, as the time constants of inactivation decrease as intracellular Ca^{2+} is increased (Wallner et al., 1999; Xia et al., 1999). Furthermore, β2 subunits cause a hyperpolarizing shift in the G-V relationship at multiple Ca^{2+} concentrations, suggesting that β2 subunits still enhance Ca^{2+} sensitivity even though they promote current inactivation (Brenner et al., 2000a; Wallner et al., 1999; Xia et al., 1999). The β3 subunit does not affect the G-V relationship in symmetrical K^+ solutions (Brenner et al., 2000a), and confers less inactivation than the β2 subunit (Uebele et al., 2000).

In addition to β-subunits, evidence for auxiliary γ subunits has emerged within the last few years. γ-subunits were first discovered in non-excitable prostate cancer cells, and co-expression of the BK α-subunit with the LRRC26 (γ1) subunit caused a 140 mV hyperpolarizing shift in G-V relationship (Yan and Aldrich, 2010). Therefore, it was proposed that BK channels α-subunits co-expressed with γ1 could open at extremely negative potentials even in non-excitable cells. Additional γ proteins, which also confer

negative shifts in the G-V relationship, are expressed in a tissue-dependent manner in several other tissues, including brain, testes, skeletal muscle, secretory glands, and colon (Yan and Aldrich, 2012).

1.4 ***BK channel inhibitors***

Physiological roles for BK channels are often established through pharmacological inhibition of BK currents. Paxilline (PAX) and iberiotoxin (IbTX) are two commonly used BK channel inhibitors. PAX is a lipophilic indole diterpene derived from the fungus *Penicillium paxilli* (Bilmen et al., 2002; Sanchez et al., 1996). The inhibition constant (K_i), or concentration required to block 50% of the current, of PAX with BK channels was found to be 1.9 nM in conditions where there is 10 μM intracellular Ca^{2+} (Sanchez et al., 1996). PAX is hypothesized to occlude the inner cavity of BK channels when the channels are in a closed state, and stabilize the channel in a closed configuration, therefore causing PAX to be termed a "closed-channel" blocker (Zhou and Lingle, 2014). Glycine 311 in the S6 transmembrane domain has an essential role in conferring sensitivity of BK channels to PAX inhibition, as mutations of G311 reduce the efficacy of PAX (Zhou et al., 2010). Because G311 mutations shift the G-V relationship of BK currents to more negative potentials, it is hypothesized that G311 causes the S6 domain to stay in a closed-channel conformation, which allows PAX to inhibit BK currents. However, the effect of PAX is reduced or eliminated in conditions where the BK channel open probability is increased, such as when the membrane is depolarized or when intracellular Ca^{2+} is elevated (Sanchez et al., 1996; Zhou and Lingle, 2014).

PAX has been utilized to identify several roles for BK currents in the cardiovascular and nervous systems because of its membrane permeability. In smooth muscle, PAX has been used to isolate BK currents from arteriolar smooth muscle (Wu et al., 2008), and causes a contractile response in mouse mesenteric arteries (Xu et al., 2011), indicating that BK currents regulate vasoconstriction. Furthermore, hearts subjected to ischemia/reperfusion injury and then treated with PAX and NS1619, a BK channel agonist, were more infarcted than hearts only treated with NS1619 (Xu et al., 2002). This indicated that BK channel activation confers cardioprotection against ischemic injury. In the brain, PAX has been used to identify the role of BK currents in the repolarization and afterhyperpolarization phases of neuronal action potentials (Faber and Sah, 2002). Additionally, PAX was used to identify that BK current inhibition could serve as an anticonvulsant therapy, as PAX reduces firing activity in post-seizure neocortical neurons (Shruti et al., 2008).

PAX is beneficial compared to other BK antagonists, such as IbTX, because PAX is lower in cost, is membrane-permeable (Hu et al., 2001), and its effects are not dependent on accessory β-subunits (Brenner et al., 2005; Imlach et al., 2008). However, PAX has several drawbacks, including its mechanism of action and its potential off-target effects. The efficacy of PAX is largely dependent on the channels' initial P_O, as PAX inhibits BK currents more effectively when BK channels are initially closed (Zhou and Lingle, 2014). Therefore, PAX may not be the most effective BK channel inhibitor in cell types that undergo constant depolarization, or exhibit consistent Ca^{2+} influx or intracellular Ca^{2+} release, all of which would increase the initial BK channel P_O. Also, PAX has been linked with inhibiting the sarcoplasmic reticulum ATPase pump (SERCA),

an essential Ca^{2+} cycling protein that replenishes Ca^{2+} back into the sarcoplasmic reticulum (SR), at concentrations between 5 and 50 μM (Bilmen et al., 2002).

IbTX is a highly potent, membrane impermeable peptide toxin inhibitor of BK channels, with an IC_{50} of approximately 3.6 nM (Meera et al., 2000). IbTX targets the extracellular face of BK channels and blocks the pore of the channel (Candia et al., 1992; Giangiacomo et al., 1992). Like PAX, IbTX has also been used to identify the physiological role of BK channels in systems such as the brain (Sausbier et al., 2004; Shao et al., 1999), heart (Imlach et al., 2010), and bladder (Heppner et al., 1997; Herrera et al., 2000; Meredith et al., 2004). The primary benefit of using IbTX is its high specificity and lack of known off-target effects. However, there are also several drawbacks to using IbTX as a BK channel inhibitor. In addition to being expensive compared to other BK inhibitors such as PAX or tetraethylammonium, and being membrane impermeable, the efficacy of IbTX is reduced by almost 1000-fold when the α-subunit is co-expressed with β4 subunits (Meera et al., 2000). Therefore, IbTX may not be the most suitable BK channel inhibitor in tissues where β-subunit expression is unknown.

1.5 ***BK currents regulate cardiovascular and neuronal function***

The physiological roles for BK currents are generally established through the use of pharmacology or genetically-modified animals. The physiological relevance of BK currents was originally discovered in *Drosophilia*, as deletion of the *slowpoke* (*slo*) gene eliminated a Ca^{2+}-dependent K^+ current and elongated the flight muscle action potentials (Elkins et al., 1986). In mammalian systems, BK currents are best characterized in smooth muscle and neurons. In smooth muscle, BK currents are often activated by Ca^{2+}

sparks, which are intracellular Ca^{2+} release events from ryanodine receptors (RyRs) on the sarcoplasmic reticulum (Nelson et al., 1995; Sausbier et al., 2005). Upon activation, BK channel-mediated efflux of K^+ causes membrane hyperpolarization and relaxation (Nelson et al., 1995), which allows BK currents to regulate blood pressure (Brenner et al., 2000b; Nelson et al., 1995; Sausbier et al., 2005), urinary bladder function (Heppner et al., 1997; Meredith et al., 2004), cerebrovascular circulation (Filosa et al., 2006) and erectile function (Werner et al., 2005).

In neurons, BK channels form complexes with voltage-gated Ca^{2+} channels (Berkefeld et al., 2006; Grimes et al., 2009), and upon activation BK currents contribute to the repolarization and afterhyperpolarization phases of neuronal action potentials (Storm, 1987), as well as neurotransmitter release (Wang et al., 2001). This allows BK currents to regulate functions such as locomotor control (Imlach et al., 2008; Sausbier et al., 2004) and circadian rhythmicity (Meredith et al., 2006; Montgomery et al., 2013). Furthermore, mutations that disrupt BK channel function can alter neuronal excitability and manifest itself in conditions such as epilepsy (Du et al., 2005).

1.6 ***Use of animal models to study BK currents***

Although performing experiments on BK channels expressed in heterologous cells or on tissue extracted from animals can provide insight into roles for BK channels, *in vivo* experiments are still the best method for understanding physiological roles for BK channels. Pharmacological BK inhibitors have been used to establish *in vivo* roles for BK channels, including in heart rate regulation (Imlach et al., 2010), locomotor function (Imlach et al., 2008), autonomic nerve activity (Kawada et al. 2010) and occurrence of seizures (Shruti et al., 2008). However, BK channel modulators can be expensive and

difficult to administer over long periods of time, and could have off-target effects on other channels or proteins (Bilmen et al., 2002; Park et al., 2007). Furthermore, inhibitors such as IbTX are not membrane permeable (Candia et al., 1992; Giangiacomo et al., 1992), which makes it difficult to target systems of interest *in vivo*.

To address these issues, genetically modified mice are often used to identify systemic roles for BK currents *in vivo*. The generation of *Kcnma1*$^{-/-}$ mice, which lack expression of functional BK channels (Meredith et al., 2004; Sausbier et al., 2004), addressed several shortcomings associated with administering BK channel blockers into living organisms. Genetic ablation of BK channels allows for the effects of chronic BK current inhibition to be studied while avoiding the off-target effects of BK channel inhibitors. Additionally, *Kcnma1*$^{-/-}$ mouse tissue can serve as a valuable negative control for BK channel expression when trying to demonstrate novel BK channel expression in tissues. *Kcnma1*$^{-/-}$ mice have been used to identify roles for BK currents in heart rate regulation (Imlach et al., 2010), circadian timekeeping (Meredith et al., 2006), urinary function (Meredith et al., 2004), and locomotor function (Meredith et al., 2004; Sausbier et al., 2004). However, there are drawbacks to using genetically modified animals; deletion of BK channels may cause unwanted compensatory effects, such as overexpression of other channels or proteins, which may undermine the true physiological effect of eliminating BK channel function. Also, because deletion of BK channels is global rather than tissue specific in these mice, expected observations such as elevated blood pressure may be due to unexpected mechanisms, such as changes in aldosterone levels, rather than strictly changes in vascular tone and relaxation (Sausbier et al., 2005).

Chapter 2: Specific Aims

The first aim of this dissertation focuses on the mechanism by which BK channels regulate heart rate. BK channels are essential regulators of excitability in cells throughout the cardiovascular and nervous system, and within the last five years a novel role for BK channels in heart rate regulation was discovered (Imlach et al., 2010). However, the mechanism by which BK channels regulate heart rate is poorly understood. The goal of Specific Aim 1 is to elucidate the pathway by which BK channel inhibitors cause a reduction in heart rate. *We hypothesized that BK channels expressed in sinoatrial node cells, the heart's predominant pacemaking cells, regulate heart rate.*

The second aim of this dissertation focuses on the effect of non-synonomous single-nucleotide polymorphisms (SNPs) on human BK current properties. SNPs are variations in nucleotide sequence that can lead to changes in the encoded BK channel amino acid sequence. Approximately 100 non-synonymous SNPs in the gene that encodes BK channels (*KCNMA1*) have been identified, but few have been linked with disease or electrophysiologically characterized. *We hypothesized that SNPs linked with pathophysiological conditions or located in domains known to regulate Ca^{2+}-dependent activation would alter BK current properties.*

Chapter 3: General Methodology

3.1 *Equipment used for electrophysiology*

Patch clamp recordings were performed using a Multiclamp 700B amplifier and Digidata 1440 (Axon Instruments, Sunnyvale, CA). Data were acquired and analyzed using pClamp 10 (Axon Instruments). Glass pipettes (TW150F-4, World Precision Instruments, Sarasota, FL) for recordings were pulled using a P-97 micropipette puller (Sutter Instruments, Novato, CA) and fire-polished using a MF-830 microforge (Narishige International, East Meadow, NY).

3.2 *Perforated patch action potential recordings from mouse sinoatrial node cells (SANCs)*

Action potential experiments from mouse sinoatrial node cells was performed via the amphotericin B-based perforated patch configuration (Figure 5C) as previously described (Rae et al., 1991; Wu et al., 2009). Amphotericin B (A9528, Sigma-Aldrich, St. Louis, MO) was resuspended in DMSO, and diluted in pipette solution at a concentration of 240 μg/mL. For recordings, the Multiclamp 700B was set in zero-current, current-clamp configuration, and data was acquired at 20 kHz. Access resistances for recordings were below 40 MΩ. Solutions used for recordings are listed in Chapter 4.

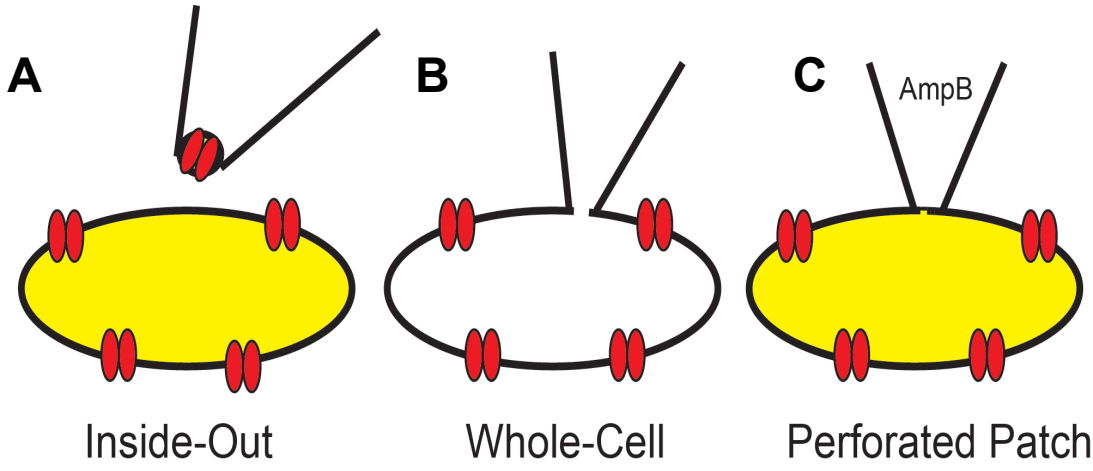

Figure 5: Electrophysiology recording configurations

BK currents and action potentials were recorded in one of three patch configurations; inside-out (A), whole-cell (B), or perforated-patch (C) configurations. In inside-out patch configuration (A), a patch of membrane containing BK channels is excised from the cell, exposing the intracellular side of the channel to the bath solution. This allows the BK currents to be recorded at different intracellular Ca^{2+} concentrations. In whole-cell configuration (B), the cell membrane is ruptured, dialyzing the cytosol with pipette solution, but allowing for electrical access to the entire cell. In perforated-patch configuration (C), amphotericin B (AmpB) in the pipette solution perforates the cell membrane, creating pores that only allow monovalent ions to permeate. This allows for electrical access to the cell without dialyzing the cell cytosol with the pipette solution.

3.3 *Whole-cell patch recordings*

Experiments recording native BK currents from mouse SANCs, as well as recording BK currents at nominal Ca^{2+} from HEK293T cells transfected with BK channel cDNA were performed in the whole-cell patch configuration (Figure 5B). Solutions and recording parameters are listed in Chapter 4.

3.4 *Inside-out patch clamp recordings from HEK293T cells*

BK currents were recorded at different intracellular Ca^{2+} concentrations using the inside-out patch configuration (Figure 5A). Internal and external solutions used for experiments are listed in Chapters 4 and 5. To determine the total Ca^{2+} required to reach desired free Ca^{2+} concentration, we utilized WebMaxC (http://web.stanford.edu/~cpatton/webmaxcS.htm). For calculations, we used a temperature of 20 °C, a pH of 7.2, and an ionic concentration of 0.16.

3.5 *HEK293T cell culture and transfections*

HEK293T cells (CRL-11268, ATCC, Manassas, VA) were cultured on 35 mm or 60 mm tissue culture dishes in media containing DMEM (Cat. #11995, Life Technologies), 10% fetal bovine serum (Cat #4315, Sigma-Aldrich), 1% penicillin/streptomycin (Cat. #30-002-Cl, Corning), and 1% L-glutamine (Cat. #25-005-Cl, Corning). Cells were maintained under sterile conditions in a 37 °C incubator supplied with 5% CO_2. BK channel constructs were transiently transfected into HEK cells using either Lipofectamine 2000 (Life Technologies, Grand Island, NY) or Trans-IT LT-1 (Mirus Bio, Madison, WI) transfection reagents. Using Lipofectamine, a 1/5 ratio of DNA/Lipofectamine (μg/μL) was used for transfections according to the

manufacturers' recommended protocol. Using LT-1, a 1.5/2 LT-1 ratio (μg/μL) was used, and transfections were performed according to the manufacturers' recommended protocol. Recordings were performed one to three days post transfection.

3.6 *DNA preparation*

Plasmid DNA was prepared by Bing Jiang (Bioinnovatise, Rockville, MD). Plasmid DNA was transformed into DH5α competent cells (Cat. #18265-017, Life Technologies) according to the manufacturer's protocol. Plasmid DNA was isolated and purified using a plasmid purification kit (Cat. #12163, Qiagen, Venlo, Netherlands). DNA was stored in sterile water and frozen at -20 °C for transfections.

3.7 *Data analysis*

The conductance of macroscopic currents obtained from inside-out patch recordings was determined by dividing the amplitude of the tail current 200 μs after the start of the repolarizing tail step by the voltage of the tail-step (Sweet and Cox, 2009). Conductance versus voltage (G-V) relationships were fit using either Origin 8.5 (Origin Lab, Northampton, MA) or Prism 5 (GraphPad, La Jolla, CA) to a Boltzmann fit equation:

$$G = Gmax/(1 + e^{ZF(V_{0.5}-V)/RT}$$

Activation and deactivation kinetics for inside-out patch recordings were fit to single exponential functions in pClamp 10 using the equation:

$$f(t) = \sum_{i=1}^{n} A_i e^{-t/\tau_i} + C$$

Chapter 4: The role of BK channels in regulating cardiac pacemaking

4.1 *Introduction*

Heart rate is regulated by the excitability of cells within the sinoatrial node (SAN), the heart's primary pacemaker. SAN cells (SANCs) are specialized cells within the right atrium that spontaneously evoke action potentials. Within the last five years, the BK channel inhibitors paxilline (PAX) and iberiotoxin (IbTX) were shown to cause a reduction in heart rate in mice *in vivo* and in isolated rat hearts (Imlach et al., 2010). Although a previous study suggested that disruption of *slo* lowers heart rate in *Drosophila melanogaster* (Johnson et al., 1998), the results by Imlach *et al.* were the first to suggest that BK channels regulate mammalian heart rates. However, the pathway by which BK channel inhibitors slow heart rate was not examined.

In this aim, we tested the hypothesis that BK channels expressed in SANCs regulate heart rate. This hypothesis was based on results demonstrating that PAX and IbTX caused an acute reduction in isolated rat heart rates (Imlach et al., 2010), which suggests that the BK channels regulating heart rate are expressed within the heart. To test this hypothesis, we investigated: 1) the effect of PAX on the electrocardiograms of mice *in vivo*, 2) the effect of BK channel inhibitors on mouse SANC firing rates and outward currents evoked from SANCs, 3) the expression of BK channels in mouse SANCs, and 4) the properties of BK currents evoked by BK channels cloned from mouse SANCs.

4.2 ***Background***

4.2.1 BK channels in the heart

Although BK channels and currents are well-characterized in several cell types throughout the cardiovascular and nervous systems, the role of BK channels in the heart is less-studied. Studies prior to 2010 did not indicate that BK channels regulate cardiomyocyte excitability, as IbTX, a membrane-impermeable BK channel inhibitor (Candia et al., 1992; Giangiacomo et al., 1992), did not alter ventricular myocyte action potentials (Takamatsu et al., 2003). BK channel subunits were previously been detected in human and rodent hearts via northern blot (Behrens et al., 2000; Brenner et al., 2000a; Tseng-Crank et al., 1994) and western blot (Singh et al., 2013; Xu et al., 2002)(Figure 30), and the majority of current work focuses on BK channels expressed in cardiac mitochondria. BK channel expression has been detected in cardiac mitochondria (BK_{Mito}) (Singh et al., 2013), and functionally, BK_{Mito} are thought to mediate cardioprotection against ischemia/reperfusion injury; the BK channel activators NS1619 and NS11021 reduce cardiac ischemic injury in rabbit (Xu et al., 2002), rat (Bentzen et al., 2009), and mouse (Singh et al., 2013) hearts. Supporting this hypothesis, *Kcnma1*$^{-/-}$ mice are not afforded cardioprotection when subjected to treatment with NS1619 (Singh et al., 2013).

However, in 2010, a novel role for BK channels in heart rate regulation was reported (Imlach et al., 2010). An acute reduction in heart rate was observed in wild-type (WT) mice but not *Kcnma1*$^{-/-}$ mice after PAX injection. Also, both PAX and IbTX caused reductions in isolated rat heart rates (Imlach et al., 2010). In combination, this data indicated for the first time that BK channels expressed in the heart modulate heart

rate, and regulate cardiac cell excitability. Furthermore, because of IbTX's lack of membrane permeability (Candia et al., 1992; Giangiacomo et al., 1992), this data suggested that membrane-bound BK channels mediate these effects.

Specific Aim 1 is designed to test the hypothesis that BK channels expressed in SANCs regulate heart rate. We formulated this hypothesis because SANCs are the predominant regulators of heart rate, and previous data suggests that BK channels expressed in the heart mediate the effects of BK channel inhibitors.

4.2.2 SANC physiology

Heart rate *in vivo* is initiated and maintained by spontaneous action potentials evoked by SANCs, a specialized subset of myocytes residing within the right atrium (Mangoni and Nargeot, 2008). Intrinsic excitability of SANCs is the result of finely controlled synergy between plasma membrane currents, and rhythmic Ca^{2+} release from the sarcoplasmic reticulum (SR)(Lakatta et al., 2010). The SANC action potential consists of three main phases; diastolic depolarization (DD), the upstroke, and repolarization (Figure 6).

DD is the action potential phase that initiates SANC excitability. During DD, the membrane spontaneously depolarizes from the maximum diastolic potential (MDP) to the threshold potential (V_{th})(Mangoni and Nargeot, 2008)(Figure 6). Although the mechanism that initiates the DD is highly controversial, it is thought that DD is the result of a synergy between a "voltage-clock" mechanism and a "Ca^{2+}-clock" mechanism (Lakatta et al., 2010). The voltage-clock mechanism of SANC automaticity is dependent on interaction of currents evoked by several different plasma membrane-bound ion channels. I_f current, which is an inward Na^+/K^+ current that is evoked by

hyperpolarization-activated cyclic nucleotide (HCN)-gated channels, activates robustly upon membrane hyperpolarization (DiFrancesco, 2006). Upon activation, I_f causes membrane depolarization that activates T- and L-type Ca^{2+} current during the later stages of DD (Mangoni et al., 2003; 2006), which promotes further membrane depolarization until V_{th} is reached. DD initiation via the Ca^{2+} clock occurs through rhythmic spontaneous local Ca^{2+} releases (LCRs) from the SR (Vinogradova et al., 2004), which activate the Na^+/Ca^{2+} exchange current *(I_{NCX})* on the plasma membrane and generates inward current that further promotes membrane depolarization that activates I_{Ca} (Bogdanov et al., 2001).

The upstroke phase of the SANC action potential follows DD. The upstroke is primarily mediated by $I_{Ca,L}$ current evoked by $Ca_V1.2$ channels (Mangoni et al., 2003). Inhibition of $I_{Ca,L}$ with agents such as nifedipine has differential effects on pacemaker cell excitability, as nifedipine completely eliminates action potentials evoked by central SANCs obtained from rabbits, while just slowing the firing rate of peripheral SANCs (Kodama et al., 1997). This is potentially due to variation in channel expression in different areas of the SAN. I_{Na} is also thought to regulate the action potential upstroke in peripheral rabbit SANCs, since tetrodotoxin (TTX) does not affect the excitability of central SANCs, but reduces the upstroke velocity and firing rate of peripheral SANCs (Kodama et al., 1997). I_{Na} is also essential in the upstroke of the mouse SANC action potential (Lei et al., 2004).

The repolarization phase of the SANC action potential is primarily attributed to activation of voltage-gated K^+ currents, such as $I_{K,r}$, $I_{K,s}$, and to a lesser extent $I_{T,o}$ which are the rapid ($I_{K,r}$) and slow ($I_{K,s}$) delayed rectifying K^+ currents, and transient outward

($I_{T,o}$) current (Cho et al., 2003; Clark et al., 2004; Kodama et al., 1999). $I_{K,r}$, which is activated upon membrane depolarization, repolarizes the membrane and contributes towards setting the maximum diastolic potential (MDP) of the action potential. Inhibition of $I_{K,r}$ with agents such as E-4031 elongates the repolarization phase of the action potential and causes depolarization of the MDP (Clark et al., 2004; Kodama et al., 1999). Depolarization of the MDP by $I_{K,r}$ block is hypothesized to slow SANC firing by reducing hyperpolarization that activates I_f, as well as by causing voltage-dependent inactivation of I_{Ca}. $I_{K,s}$, which also contributes to the repolarization phase of the action potential, activates slower and deactivates faster than $I_{K,r.}$ Although $I_{K,s}$ is not detectable in mouse SANCs (Cho et al., 2003; Mangoni et al., 2008), block of $I_{K,s}$ with 293B in porcine SANCs, which lack $I_{K,r}$, also causes MDP depolarization and a suppression of excitability (Ono et al., 2000). $I_{T,o}$ also contributes to the repolarization phase of the action potential, and block of $I_{T,o}$ with 4-AP causes elongation of the action potential duration and depolarization of the MDP (Boyett et al., 1998).

In vivo, SANCs automaticity is regulated by the autonomic nervous system (ANS), and vascular control of heart rate via the baroreceptor reflex. The sympathetic and parasympathetic branches of the ANS innervate the SAN and modulate SANC firing through release of catecholamines (sympathetic) or acetylcholine (parasympathetic) (Figure 7). The sympathetic nervous system regulates increases in heart rate through norepinephrine (NE) and epinephrine, which increase SANC action potential frequencies by activating β1-adrenergic receptors (Figure 7)(Mangoni and Nargeot, 2008). Alternatively, the parasympathetic branch facilitates reductions in SANC firing through

vagal nerve release of acetylcholine (ACh) which activates $I_{K,ACh}$ and binds to M2 muscarinic receptors, which downregulates adenylate cyclase activity (Figure 7).

There is some evidence for BK channels in the sympathetic and parasympathetic branches of the ANS. Reports indicate that BK currents are present in cardiac sympathetic nerves, as application of 20 nM IbTX to guinea pig sympathetic neurons caused a significant elongation (~13.5%) of action potential half-width (Ireland et al., 1998), and application of 500 μM TEA to guinea pig sympathetic neurons lengthened the action potential duration by 38% (Locknar et al., 2004). In parasympathetic neurons, BK channels are also implicated to regulate excitability, as 100 nM charybdotoxin (CTX) reduces K^+ current amplitude by 35% (Xu and Adams, 1992), and 50 nM IbTX increases the action potential duration by 22% in rat dorsal vagal neurons (Pedarzani et al., 2000). Furthermore, local application of 2 μM IbTX to vagal neurons in anesthetized rabbits increased stimulation-induced ACh release, suggesting that BK block could cause heart rate decreases by increasing vagal nerve ACh release (Kawada et al., 2010). Therefore, BK channels expressed in the ANS could act as a potential mechanism of heart rate regulation by PAX.

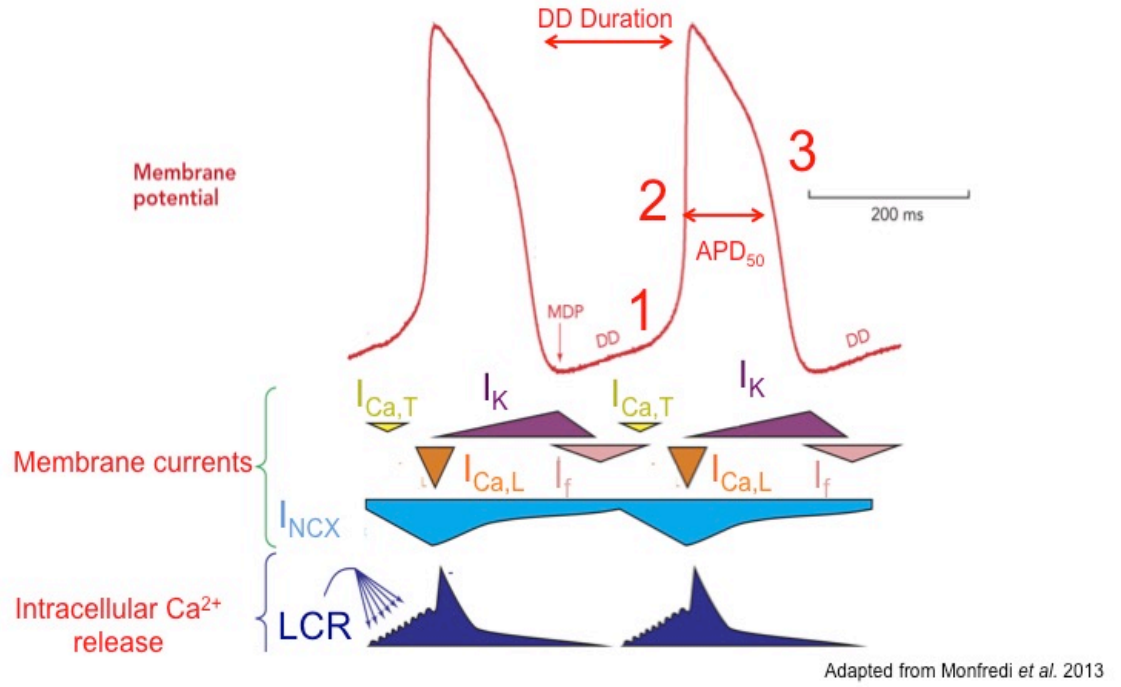

Figure 6: Simplified model of SANC automaticity

The SAN action potential consists of the diastolic depolarization (DD) (1), upstroke (2), and repolarization (3) phases. DD is initiated by I_f and local calcium release (LCR) from the sarcoplasmic reticulum (SR). LCRs activate I_{NCX}, which, along with I_f depolarize the membrane from the maximum diastolic potential (MDP) to the threshold potential. As the membrane depolarizes during DD, $I_{Ca,T}$ and $I_{Ca,L}$ currents activate, further depolarizing the membrane to the threshold potential. Upon reaching threshold, $I_{Ca,L}$ further activates, causing the upstroke of the action potential. During the upstroke, there is a large Ca^{2+} release from the SR. The upstroke of the action potential causes inactivation of $I_{Ca,L}$ and activation of I_K, which causes membrane repolarization. Membrane repolarization re-activates I_f, which restarts DD. When analyzing SANC action potentials, the duration of DD (DD duration), MDP, and action potential duration at 50% of the repolarization time (APD_{50}) were all measured. Figure adapted from Monfredi et al., 2013.

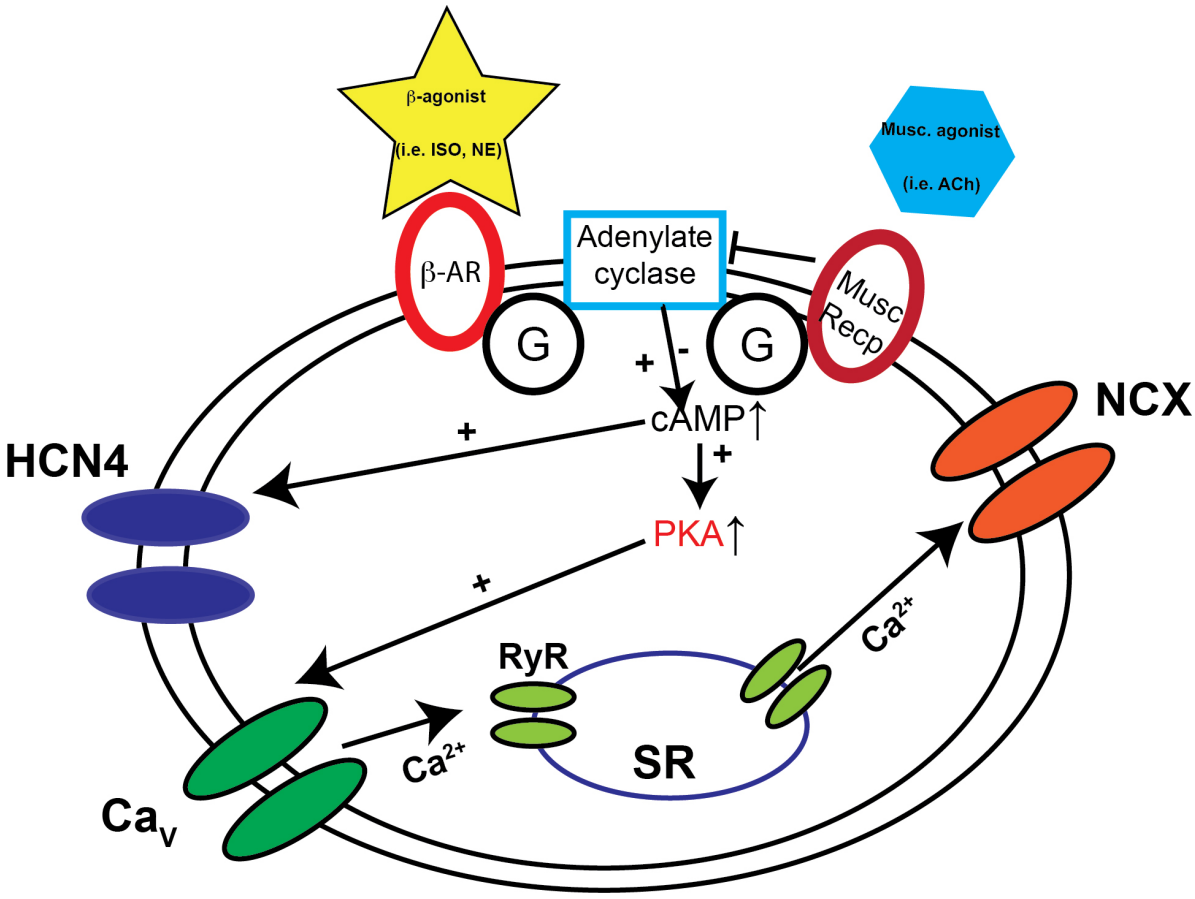

Figure 7: Autonomic regulation of DD in SANCs

Modulation of SANC firing is mediated by the sympathetic or parasympathetic nervous system. Norepinephrine (NE) or an agonist such as isoproterenol (ISO) activate β-adrenergic receptors and activate of adenylate cyclase (AC) through the G-protein coupled receptor pathway. AC facilitates production of cAMP, which promotes activation of HCN4 channels. cAMP also activates protein kinase A (PKA), which phosphorylates and promotes activation of voltage gated Ca^{2+} (Ca_V) channels. Ca^{2+} influx enhances Ca^{2+} release from ryanodine receptors (RyRs), which also activates the Na^{+}/Ca^{2+} exchanger (NCX). Increases in I_f, I_{Ca}, and I_{NCX} all increase the rate of DD, which leads to an increase in heart rate. Muscarinic receptor agonists slow AP firing by inhibiting cAMP production through the αG_i G-protein coupled receptors. Figure modified from Mangoni and Nargeot, 2008.

SANC action potential frequency is further controlled *in vivo* through the baroreflex, which is the homeostatic mechanism of maintaining arterial blood pressure through heart rate modulation (Lu et al., 2009). Increases in blood pressure stretch baroreceptors in the carotid sinus and aortic arch, which increases afferent neuronal firing towards the brain stem and causes elevation in vagal discharge (Fadel et al., 2003). This subsequently induces a decrease in both heart rate and blood pressure via increased parasympathetic tone. Conversely, reductions in blood pressure decrease stretch activation of baroreceptors, triggering catecholamine release in order to increase heart rate and blood pressure (Fadel et al., 2003).

Inhibition of BK channels with IbTX causes vasoconstriction and elevated vascular tone (Nelson et al., 1995), and mice with genetic deletions of the α or β1 subunit have elevated blood pressure (Brenner et al., 2000b; Sausbier et al., 2005); therefore, it could be hypothesized that pharmacological block of BK channels *in vivo* would cause increased vascular tone and blood pressure, and induce a compensational decrease in heart rate through the baroreflex. However, PAX did not cause a significant increase in blood pressure in WT mice (Imlach et al., 2010)(unpublished data), suggesting that the mechanism underlying BK inhibitor-induced reductions in heart rate is not through the baroreflex.

4.3 ***Materials and Methods***

4.3.1 Whole animal telemetry experiments and analysis

Wireless radio telemeters (ETA-F10, Data Sciences International, New Brighton, MN) were surgically implanted intraperitoneally or subcutaneously into one to four

month-old FVBN/J mice to record electrocardiograms (ECGs). Dr. Ling Chen of the Small Animal Physiology Core at the University of Maryland School of Medicine performed surgeries. Prior to surgeries, induction of anesthesia was performed in a sealed chamber using 2-3% isoflurane, with an oxygen flow-rate of 1-2 L/min. After induction of anesthesia, mice were transferred to a heated surgical platform and anesthesia was maintained using 1-3% isoflurane at a flow-rate of 0.5-1.5 L/min. To implant the transmitter, an incision was made through the skin on the neck, and surgical scissors were inserted into the incision to form a subcutaneous pocket using blunt dissection. The transmitter body was placed into the pocket with the leads oriented rostral in a Lead II configuration. The positive lead was capped using a piece of silicon tubing, and the lead was sutured to the surface of the abdomen, 1 cm to the right of the xiphoid process. The negative lead was also capped and sutured to the muscle wall above the right clavicle. The incision was sutured closed using 5-0 monofilament sutures, and further closed with staples. After the procedure, mice were removed from anesthesia and allowed to recover on a heated platform. Mice were given wetted food post-surgery and were injected subcutaneously with 0.05-0.1mg/kg of buprenorphine every 12 hours for a minimum of 72 hours post-operation, until the mice exhibited increased body mass and normal cage behavior. Transmitters were turned on to record vital signals (ECGs, cage activity) to ensure full recovery from the procedure prior to experiments, and to ensure that adequate data could be acquired from the transmitters.

To determine the effect of PAX on heart rate, ECGs were recorded continuously and 8mg/kg PAX (#2006, Tocris, Minneapolis, MN) or the equivalent volume of DMSO were injected intraperitoneally. PAX was administered between ZT 0 and 4 for each

experiment. Heart rate measurements were calculated using the averages of five 10-second segments during baseline (0.5 to 1 hour prior to PAX injection), and at denoted time intervals post injection. Measurements were conducted during periods of home-cage inactivity that were determined by the transmitter. ECG analysis was performed on 10-second segments of data collected when the mice were inactive at times representative of the baseline heart rate and the post-PAX injection heart rate. ECG interval analysis was performed manually using pClamp 10 (Axon Instruments) or Ponemah (Data Sciences International).

4.3.2 Mouse SANC isolation

Mouse SANCs were acutely isolated using a modified version of previously described methodology (Mangoni and Nargeot, 2001; Wu et al., 2009). After euthanasia, mouse hearts were excised and rinsed in normal Tyrode's solution containing (in mM): 140 NaCl, 5.4 KCl, 5 HEPES, 5.5 glucose, 1.8 $CaCl_2$, 1.0 $MgCl_2$, with the pH adjusted to 7.4 with NaOH. The right atrium was dissected, cut into strips, and rinsed in low-Ca^{2+} Tyrode's solution containing (in mM): 140 NaCl, 5.4 KCl, 5.5 HEPES, 5.5 glucose, 0.2 $CaCl_2$, 0.5 $MgCl_2$, 1.2 KH_2PO_4, 50 taurine, and 1mg/mL BSA with the pH adjusted to 6.9 with NaOH. Tissue strips were then digested at 35 °C in low-Ca^{2+} Tyrode's solution containing collagenase type II (LS004174, Worthington, Lakewood, NJ), elastase (LS002292, Worthington), and protease type XIV (P5174, Sigma-Aldrich, St. Louis, MO) for 25-30 minutes. Tissue was then rinsed three times in 35 °C kraft-bruhe (KB) solution, which contained (in mM): 100 potassium glutamate, 5.0 HEPES, 20 Glucose, 25 KCl, 10 potassium aspartate, 2 $MgSO_4$, 10 KH_2PO_4, 20 taurine, 5 creatine, 0.5 EGTA, and 1 mg/mL BSA, with pH adjusted to 7.2 with KOH. After the third rinse, strips were

tritrated using a wide-bore glass Pasteur pipette for 5-10 minutes until the strips became translucent and the KB solution became opaque. Cells were stored for up to 8 hours at 4°C. 10x stock solutions of normal Tyrode's and low-Ca^{2+} Tyrode's solution were kept at 4°C, while KB solution was stored in frozen aliquots at -20°C.

4.3.3 SANC electrophysiology

Electrophysiological experiments were performed as described (Lai et al., 2014). For SANC action potential recordings, cells were continuously perfused with Tyrode's solution at 0.7 mL/min at 35 ± 1°C. SANCs were identified by their characteristic morphology, spontaneous contractions, and ability to spontaneously fire action potentials. Perforated-patch action potential recordings were acquired in current-clamp mode at 20 kHz. Borosilicate glass pipettes (3-5 MΩ) were filled with (in mM): 130 potassium aspartate, 10 NaCl, 10 HEPES, 0.04 $CaCl_2$, 2 MgATP, 7 phosphocreatine, 0.1 NaGTP, and 240 μg/mL amphotericin B, with the pH adjusted to 7.2 with KOH. Stable perforations were obtained within 5-13 minutes, and only SANCs with stable baseline action potential firing patterns were analyzed. Frequency analysis was performed on one-minute segments of data using threshold-based detection methods, one minute after establishing stable perforation (baseline) or within 15 minutes after PAX application, at the time of the peak effect.

Action potential waveforms were analyzed according to the parameters previously described (Larson et al., 2013). Waveforms were analyzed in pClamp 10 (Axon Instruments). Four to six action potentials were analyzed at times where the firing rate was representative of the baseline firing rate, or the after-PAX firing rates. Action potentials and the derivative of the action potential waveform (dV/dt) were exported to

Microsoft Excel to determine specific intervals. The diastolic duration was defined as the time interval between the maximum diastolic potential and the threshold potential (V_{th}) for the next action potential. V_{th} was defined as the time at which 10% of the maximum dV/dt was reached. The action potential duration at 50% repolarization (APD_{50}) was defined as the time between V_{th} and the time at which 50% of the repolarization phase was reached.

Macroscopic BK current recordings were performed in the whole cell configuration at 30 ± 1°C during continuous perfusion of Tyrode's solution at 1.25 mL/min. Data were acquired in voltage-clamp mode at 20 kHz. Patch pipettes (1-3 MΩ) were filled with intracellular solution containing (in mM): 128 potassium aspartate, 6.6 sodium phosphocreatine, 7 KCl, 1 $MgCl_2$, 0.05 $CaCl_2$, 10 HEPES, 5 EGTA, and 4 Mg-ATP, with the pH adjusted to 7.2 with KOH. Macroscopic currents were evoked from a holding potential of -75 mV, followed by 50 ms voltage steps from -130 to +60 mV. All potentials were corrected for liquid junction potential (14.9 mV). Currents were averaged from 4-5 voltage families at baseline and after 3 μM PAX application. Series resistance was compensated at 60%, and only recordings where access resistance was < 10MΩ and changed less than 15% over the course of the experiment were used for analysis. SANCs were distinguished from atrial cells based on the presence of I_f, which was evoked by 500 ms hyperpolarizing voltage steps from -65 to -145 mV in the presence of 1 mM Ba^{2+}, which blocks $I_{K,ir}$ (Cho et al., 2003; Liao et al., 2010). Atrial cells had no I_f currents. For representative I_f currents, the time-independent leak current was subtracted from the current evoked by hyperpolarizing voltage steps.

4.3.4 Immunocytochemistry

Immunocytochemistry was performed as described (Lai et al., 2014). Mouse SANCs were fixed for 20 minutes with 2% paraformaldehyde, and then permeabilized and blocked with PBS containing 2 mg/mL BSA and 0.075% Triton-X100. Cells were incubated overnight at 4°C in blocking solution containing 1:100 dilutions of mouse α-HCN4 (N114/10, Neuromab, Davis, CA) and rabbit α-BK (APC-021, Alamone Labs, Jerusalem, Israel), washed in blocking solution, and incubated with 1:1000 dilutions of mouse Alexa 488 and rabbit Alexa 568 secondary antibodies (Life Technologies, Grand Island, NY) for two hours at room temperature. Following PBS washes, cells were mounted onto glass slides using Vectashield (Vector Laboratories, Burlingame, CA). Images were collected at 40X using a LSM 5 Live confocal microscope (Zeiss, Jena, Germany). SANCs were identified by positive HCN4 expression. Fluorescence intensity measurements were performed blind of genotype and analyzed using Zen 2009 Software (Zeiss). Cell perimeters were outlined using the DIC image, and the average raw pixel intensity of each fluorophore was calculated within this area. Acquisition was identical for all cells (gain = 700).

BK channel protein detection was amplified using a tyramide signal amplification kit (Cat. # T20932 or #T20934, Life Technologies). Mouse SANCs were fixed for 20 minutes with 2% paraformaldehyde, washed with PBS, and then permeabilized with PBS containing 2 mg/mL BSA and 0.075% Triton-X100. Cells were treated with a biotin blocking kit (E-21390, Life Technologies). Endogenous peroxidases were then quenched by incubating cells with 3% H_2O_2 for 30 minutes. Cells were washed and then blocked for one hour using the kit blocking reagent. Cells were incubated at 4°C overnight in

1:1000 α-BK and 1:100 α-HCN4 antibodies. Cells were washed 3x in PBS, and then incubated with 1:1000 tyramide-labeled Alexa Fluor 568 (BK) and Alexa Fluor 488 (HCN4) antibodies (Life Technologies). Following 3 PBS washes, cells were mounted onto glass slides using Vectashield, and imaged as described above.

4.3.5 RT-PCR and BK channel cloning from SANCs

RT-PCR was performed by Joshua Whitt as previously described (Lai et al., 2014). RNA was isolated from individual WT or *Kcnma1*$^{-/-}$ cells pooled from the SAN region using cell lysis buffer (Signosis, Santa Clara, Ca). RT-PCR was conducted on total RNA using the MyTaq One-Step RT-PCR kit (Bioline, Taunton, MA) and with gene specific primers according to the manufacturers protocol. Reactions were performed on a PTC-200 Cycler, and BK and HCN4 PCR products (206 and 337 bp, respectively) were visualized on a 1.5% ethidium bromide-stained gel by electrophoresis.

RT-PCR product isolation and subcloning was performed by Bing Jiang (Bioinnovatise, Rockville, MD) as described below. To clone BK channels from SANCs, individual SANCs were identified after perfusion with 35ºC Tyrode's solution, and at least 20 cells were pooled for lysis and RNA extraction. BK channel cDNAs covering splice sites 1-4 (Shelley et al., 2013) were amplified via RT-PCR using the following sequences: (Reverse transcriptase primers) 5' TCTGTAAACCATTTCTTTTCT 3' and 5' GCCGCTCTTCCTGAACGTACTT 3'; and PCR primers (both variants) (F) 5' GAGTACAAGTCTGCCAACAG 3' and (R) 5' TCACCAGGGTCCGTATTAGG 3'. Products were gel-purified, subcloned, and two full-length products were obtained and sequenced– BK_{VYR} (GenBank accession #KF530042) and BK_{QEERL} (GenBank accession

#KF530043). Sequences were subcloned into pcDNA3.1 for expression in HEK293T cells.

4.3.6 HEK cell electrophysiology

To record macroscopic BK currents evoked from the cloned BK channels, BK_{VYR} and BK_{QEERL} cDNA was transiently transfected into HEK293T cells as described in Chapter 3. For whole-cell recordings, the internal and external solutions, and voltage protocols were identical to those used with native SANCs. For inside-out patch recordings, the internal (bath) solution was identical to that used for native SANC recordings, while the external (pipette) solution consisted of normal Tyrode's solution excluding Ca^{2+}. The total Ca^{2+} concentration required to reach the desired free Ca^{2+} concentration for inside-out patch recordings was determined using WebMaxC, and solutions were buffered using 5 mM HEDTA. For inside-out patch recordings, currents were evoked from a holding potential of -75mV, followed by 50 ms depolarizing voltage steps from -130 mV to +110 mV, followed by a hyperpolarizing voltage step back to -75 mV. Experiments using HEK293T cells were performed at room temperature.

I_f current recordings from HEK cells were performed on HEK293 cells stably expressing HCN4, the channel underlying I_f in SANCs. Cells were provided by Dr. Cathy Proenza at the University of Colorado. Cells were passaged and grown under selection with 100 μg/mL hygromycin. Currents were evoked using 3 s hyperpolarizing voltage steps from -50 mV to -160 mV.

4.3.7 Statistics

Data analysis was performed using pClamp 10 (Axon Instruments). Significance was determined at $P < 0.05$ at the indicated tests. Graphs were generated in Prism 5.0 (GraphPad), and statistical analysis was performed using Origin Lab 8.5 (Origin Lab). Data are presented as means ± SEM.

4.4 ***Results***

4.4.1 BK inhibitors reduce heart rate in vivo by slowing cardiac pacing

To determine the mechanism by which PAX slows heart rate *in vivo* in mice, we recorded heart rates and electrocardiograms (ECGs) from mice using wireless telemetry transmitters before and after injection of 8mg/kg PAX. PAX is a lipophilic, membrane-permeable compound that inhibits BK channels by stabilizing the channel in a closed state (Sanchez and McManus, 1996; Zhou and Lingle, 2014). 8 mg/kg PAX was utilized because of its previous use in experiments examining the role of BK channels in heart rate regulation (Imlach et al., 2010), and because 8 mg/kg PAX was demonstrated to cause impairment in motor function, a phenotype that is typically observed in *Kcnma1*$^{-/-}$ mice (Imlach et al., 2008). Additional information on PAX can be found in Section 1.4.

Similar to the results of previous studies (Imlach et al., 2010), injection of PAX induced a significant reduction in heart rate in WT mice within two hours of PAX injection (Figure 8B). Heart rate did not decrease when injecting WT mice with dimethyl sulfoxide (DMSO), the vehicle for PAX, or when injecting *Kcnma1*$^{-/-}$ mice with PAX (Figure 8B). These results suggest that the reduction in heart rate observed after PAX

injection in WT mice is due to BK channel inhibition, rather than off-target effects of PAX or DMSO.

Next, to identify the mechanism by which PAX alters cardiac conduction *in vivo*, we analyzed mouse ECGs before and after PAX injection. We examined specific intervals that provide insight on changes in cardiac conduction; the P-P interval (sinus rhythm), the R-R interval (interbeat interval), the P-R interval (conduction through the atrioventricular (AV) node, the Q-T interval (ventricular depolarization and repolarization), and the T-P interval (interval between ventricular repolarization and initiation of atrial depolarization). Significant increases in the P-P, R-R, Q-T, and T-P intervals were observed after PAX injection (Figure 8C), suggesting that PAX could reduce heart rate by slowing cardiac pacing (P-P, T-P) and elongating ventricular depolarization and repolarization (Q-T). The P-R interval was not significantly longer after PAX injection, indicating that AV conduction block did not contribute to the PAX-induced heart rate reduction.

Next, we quantified the components of the cardiac conduction cycle that accounted for the PAX-induced heart rate reduction to determine what the reduction in heart rate was most attributed to. To do this, we calculated the difference in each interval after PAX injection as a percent of the total change in the R-R interval. The increase in P-P interval was after PAX injection was almost identical to the increase in the R-R interval after PAX, suggesting that the PAX-induced heart rate reduction was due to slowing of the sinus rhythm. The increase in T-P after PAX injection accounted for 56.5% of the total increase in R-R interval, also indicating that inhibition of BK channels slows the sinus rhythm. The increase in Q-T interval after PAX injection only accounted

for 35.7% of the total increase in the R-R interval, suggesting that although PAX may affect ventricular repolarization, it is not the predominant cause of the PAX-induced heart rate decrease. The remaining 7.8% of the increase in R-R interval after PAX injection was due to the increase in P-R interval. ECG intervals were not significantly different in *Kcnma1*$^{-/-}$ mice at baseline, indicating that genetic deletion of BK channels did not affect cardiac conduction. In combination, because of the increase in both P-P and T-P intervals after PAX injection, our data suggests that PAX reduces mouse heart rates *in vivo* by slowing the sinus rhythm of the heart.

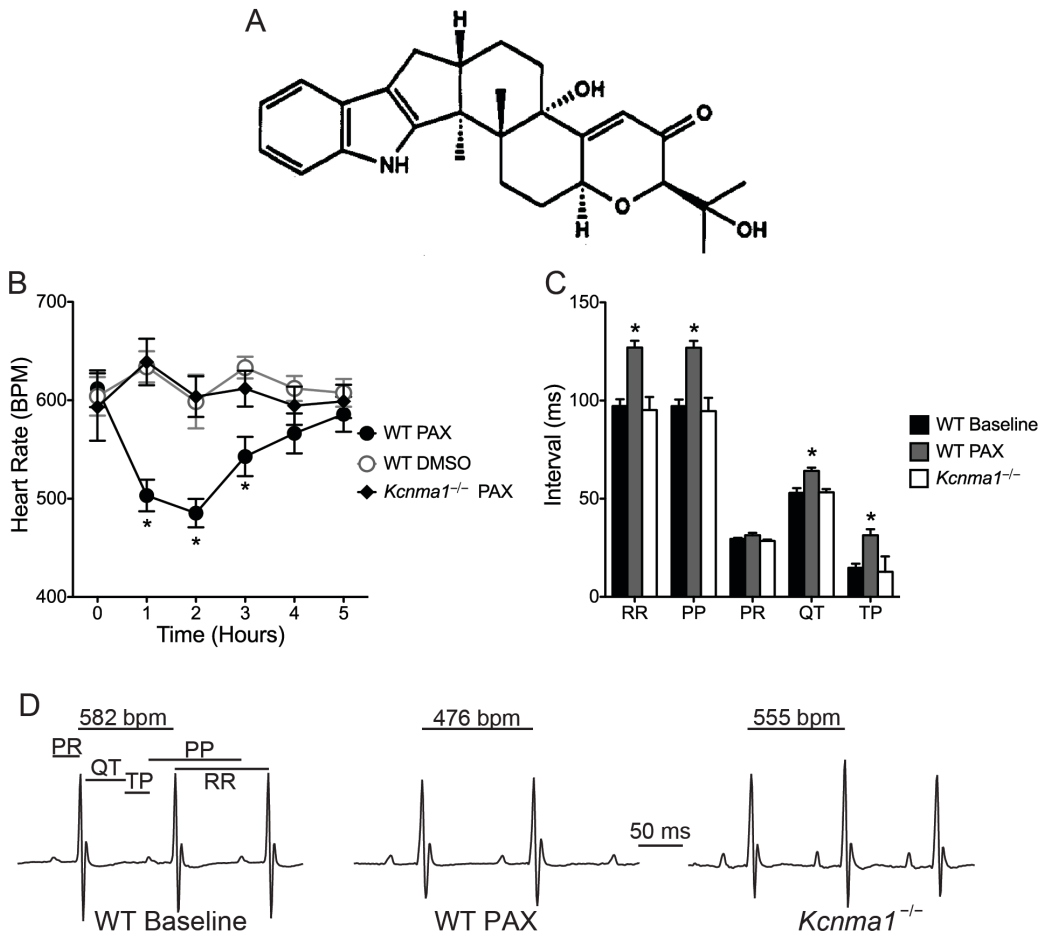

Figure 8: PAX decreases heart rates of WT but not *Kcnma1*$^{-/-}$ mice

(A) Structure of paxilline (Knaus et al., 1994). PAX is a lipophilic BK channel inhibitor that stabilizies BK channels in a closed conformation. (B) ECG waveforms were obtained from awake, freely moving animals using surgically implanted telemetry transmitters. Heart rates were recorded at baseline and after intraperitoneal injection of 8 mg/kg PAX or DMSO vehicle. Heart rate was decreased in PAX-injected WT mice (n = 13), but not *Kcnma1*$^{-/-}$ (n = 7) or WT mice treated with DMSO (n = 9, $P = 10^{-9}$, factorial ANOVA). *Bonferroni post-hocs (WT PAX vs WT DMSO), 1 hr ($P = 10^{-5}$), 2 hr ($P = 10^{-4}$), and 3 hr (P = 0.003) post-injection. (C) Intervals from ECG waveforms of WT mice at baseline (n = 8), 2 hrs after PAX injection (n = 8), and *Kcnma1*$^{-/-}$ at baseline (n = 3). PAX-induced slowed heart rate is indicated by the elongated RR interval after PAX ($P = 10^{-5}$, one-way ANOVA; *Bonferroni post-hoc, baseline vs PAX, $P = 10^{-5}$). The PP sinus rhythm was longer after PAX injection, but not in *Kcnma1*$^{-/-}$ mice ($P = 10^{-5}$, one-way ANOVA; *Bonferroni post-hoc, baseline vs PAX, $P = 10^{-5}$). The PR interval (atrioventricular node conduction) was not different after PAX injection or in *Kcnma1*$^{-/-}$ mice (P = 0.18, one-way ANOVA). (D) Representative ECG recordings from a WT or *Kcnma1*$^{-/-}$ mouse during baseline conditions or after PAX injection. R-R intervals indicated above traces are the average heart rate values for each representative mouse.

4.4.2 Abolishment of BK channel function slows isolated mouse SANC firing rates

Because the predominant mechanism by which PAX decreases heart rate *in vivo* is a slowed the sinus rhythm, we hypothesized that BK channel inhibitors slow the firing rate of SANCs. To test this hypothesis, we recorded action potentials from mouse SANCs in the presence of BK channel inhibitors and from *Kcnma1*$^{-/-}$ mouse SANCs. A significant reduction in SANC firing rates occurred in the presence of 3 μM PAX (Figure 9F). This result was consistent with the PAX-induced slowing of cardiac pacing *in vivo* (Figure 8C), and further suggests that acute inhibition of BK channels slows heart rate by disrupting SANC firing rates.

To identify the mechanism by which PAX slowed the firing rate of SANCs, we analyzed the SANC action potential waveforms. For this analysis, we examined diastolic depolarization duration (DD duration), the action potential duration at 50% repolarization (APD_{50}), and the maximum diastolic potential (MDP) (Larson et al., 2013). Interestingly, DD was elongated after application of PAX, as the DD duration was almost two times longer after PAX application (Figure 9G). In contrast, the APD_{50} and MDP were not significantly different (Figure 9H, Figure 9I). These results suggest that rather than regulating SANC action potential frequency by altering the repolarization phase of the action potential like other K^+ currents in SANCs (Clark et al., 2004; Kodama et al., 1999), BK channels modulate SANC firing frequency by affecting the DD phase of the SANC action potential.

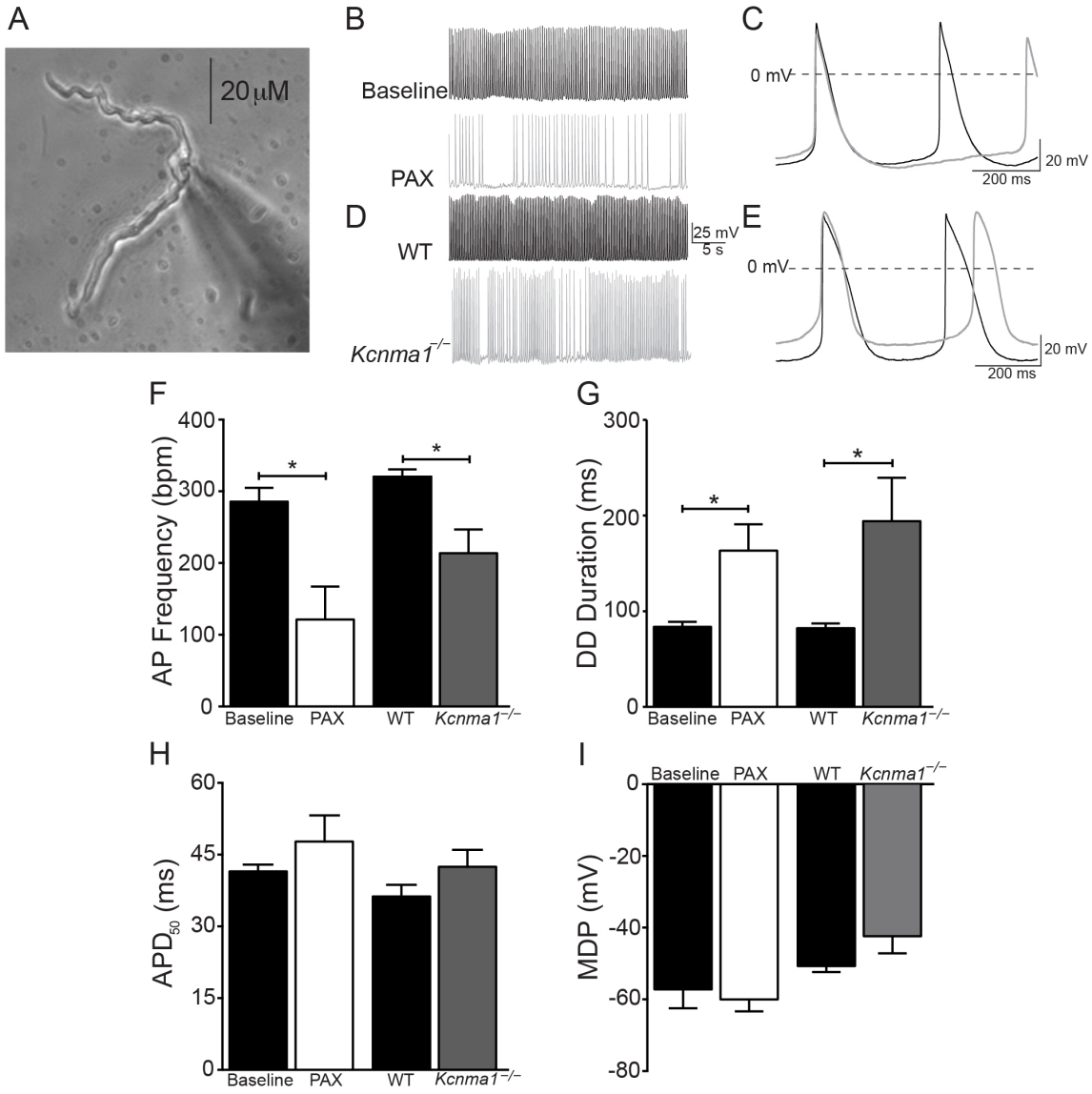

Figure 9: PAX decreases SANC action potential firing frequency

(A) Isolated mouse SANC in a perforated-patch configuration. (B-D) Representative action potentials from a WT SANC during baseline conditions and after application of 3 μM PAX (gray trace) (B, C), and WT and *Kcnma1*$^{-/-}$ (gray trace) SANCs during baseline conditions (D, E). (F) Average action potential frequencies for WT SANCs during baseline recording conditions and during the peak effect of PAX (n = 7; P = 0.024, Paired t-test), and WT (n = 12) and *Kcnma1*$^{-/-}$ (n = 11) SANCs under baseline conditions (P = 0.012, Mann-Whitney). Bpm (beats per minute), number of action potentials in one minute. (G) Diastolic depolarization (DD) durations for WT SANCs during baseline conditions and during the peak effect of PAX (n = 6, P = 0.018, Paired t – test), and WT

(n = 12) and *Kcnma1*$^{-/-}$ (n = 11) SANCs under baseline conditions (P = 0.012, Mann-Whitney). (H) Action potential duration at half maximum (APD_{50}) measurements (baseline vs PAX, P = 0.262, Paired t – test; WT vs *Kcnma1*$^{-/-}$, P = 0.157, unpaired t - test). (I) Maximum diastolic depolarization (MDP) (baseline vs PAX, P = 0.93, Mann-Whitney; WT vs *Kcnma1*$^{-/-}$, P = 0.101, unpaired t - test). PAX experiments were conducted on SANCs isolated from FVB/NJ background mice, while WT and *Kcnma1*$^{-/-}$ SANCs were obtained from C57BL/6J background mice. Action potential parameters used for analysis can be found in Figure 6.

To determine whether the effects of PAX on SANC firing were not due to off-target effects of PAX on intracellular Ca^{2+} cycling proteins crucial to SANC automaticity, such as SERCA (Bilmen et al., 2002), we next tested the effect of 230 nM IbTX on SANC firing rates. Because IbTX inhibits BK channels from the extracellular face and is membrane-impermeable (Candia et al., 1992; Giangiacomo et al., 1992), it can only inhibit plasma membrane-bound BK channels; therefore, effects of IbTX on action potential frequency would suggest that BK channels are on the plasma membrane of SANCs. Perfusion of 230 nM IbTX induced a 29% reduction in WT SANC firing frequency (Figure 10A). Correlating well with the PAX data, IbTX also elongated the DD duration but did not significantly alter the MDP or APD_{50} (Figure 10). This result provides further evidence that BK channels regulate the firing rate of mouse SANCs, and suggests that BK channels on the plasma membrane regulate SANC excitability.

To further demonstrate that abolishment of BK currents reduces SANC firing rates, we examined the action potential frequencies of *Kcnma1*$^{-/-}$ mouse SANCs (Figure 9D). Surprisingly, although *Kcnma1*$^{-/-}$ SANCs have baseline heart rates similar to WT mice *in vivo* (Imlach et al., 2010; Sausbier et al., 2005)(Figure 8B), we found that *Kcnma1*$^{-/-}$ SANCs had lower baseline firing rates compared to WT SANCs (Figure 9F), and that the reduced firing rate was also associated with a longer DD duration compared to WT mice (Figure 9G). This data was acquired in collaboration with Yuejin Wu, an expert in mouse SANC electrophysiology at the University of Iowa. This data provides further evidence that BK channels are essential for regulating SANC action potential frequencies, and suggests that additional factors may provide heart rate compensation in *Kcnma1*$^{-/-}$ mice *in vivo* that allow them to have normal heart rates.

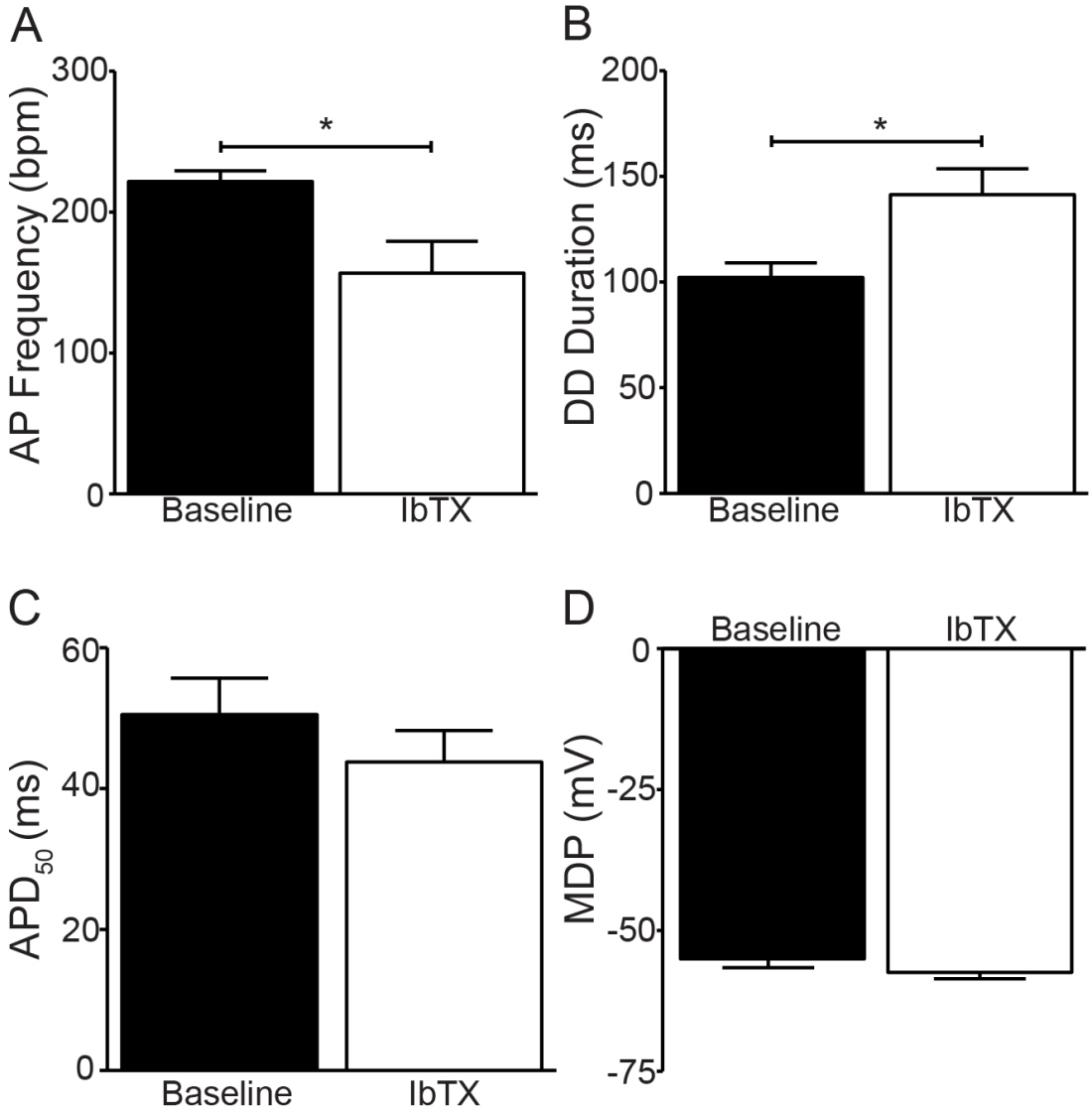

Figure 10: Iberiotoxin decreases SANC firing rate

(A) Average SANC firing frequency recorded in perforated-patch configuration during baseline conditions and after application of 230 nM IbTX (n = 9, P = 0.026, Paired t-test). (B) DD duration measurements during baseline conditions and after application of IBTX (n = 8, P = 0.041, Paired t - test). (C) APD_{50} measurements during baseline conditions and after application of IBTX (n = 8, P = 0.18, Paired t - test). (D) MDP measurements during baseline conditions and after application of IBTX (n = 8, P = 0.075, Paired t – test).

4.4.3 Elevated activation of β-adrenergic receptor pathway precludes the effects of BK channel ablation on SANC firing

In vivo, heart rate is determined not only by the intrinsic firing rate of SANCs, but also by autonomic nervous system regulation of SANC excitability. One mechanism that could cause *Kcnma1*$^{-/-}$ mice to have similar heart rates to WT mice is elevated sympathetic tone. We tested the hypothesis that *Kcnma1*$^{-/-}$ mice may have normal heart rates *in vivo* due to elevated sympathetic tone by determining whether the PAX-induced reduction in SANC firing could be recovered by isoproterenol (ISO), a β-adrenergic receptor agonist. In these experiments, baseline firing rates from WT SANCs were paced with 1 nM ISO, followed by co-application of 1 nM ISO and 3 μM PAX (Figure 11A). 3μM PAX caused a significant reduction in the action potential frequency, suggesting that even under β-adrenergic signaling, BK channel inhibition causes a reduction in SANC firing (Figure 11C). 3 μM PAX also increased the DD duration in the presence of 1 nM ISO without affecting the APD_{50} or MDP (Figure 11D).

Next, cells were treated with 3 μM PAX combined with a saturating dose (1 μM) of ISO (Wu et al., 2009) to determine whether saturating β-adrenergic receptor stimulation could reverse the PAX-induced reduction in firing. 1 μM ISO induced a complete recovery in the action potential frequency within 5 minutes (Figure 11C), as well as a reduction in DD duration to back baseline levels (Figure 11D). In combination, these results suggest that the reduction in SANC action potential frequency caused by BK channel elimination may be functionally compensated for in *Kcnma1*$^{-/-}$ mice *in vivo* through increased sympathetic tone.

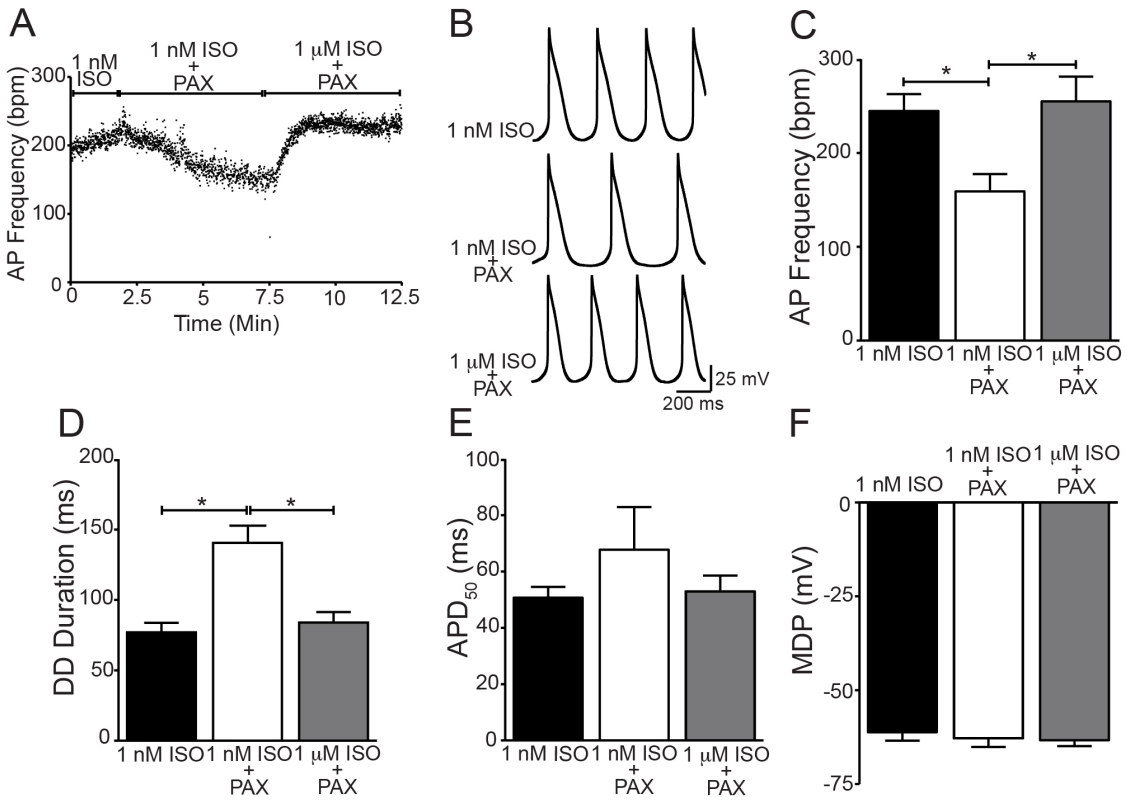

Figure 11: ISO compensates for the PAX-induced reduction in SANC firing rate

(A) Representative experiment showing SANC action potential firing rate over time at baseline pacing (1 nM ISO), after application of 3 μM PAX to reduce firing rate, and after elevating ISO to 1 μM to recover firing rate. (B) Representative action potential waveforms from *A*. (*C*) Average action potential frequencies ($n = 7$, $P < 10^{-4}$, one-way repeated measures ANOVA, *Bonferroni post-hoc, 1 nM ISO vs 1nM ISO + PAX, $P = 0.003$; 1nM ISO + PAX vs 1 μM ISO + PAX, $P = 0.001$). (D) DD duration ($P < 10^{-5}$, one-way repeated measures ANOVA, *Bonferroni post-hoc, 1 nM ISO vs 1nM ISO + PAX, $P = 10^{-4}$; 1nM ISO + PAX vs 1 μM ISO + PAX, $P = 10^{-4}$). (E) APD_{50} ($P > 0.05$, one-way repeated measures ANOVA). (F) MDP ($P > 0.05$, one-way repeated measures ANOVA, *Bonferroni post-hoc, 1 nM ISO vs 1nM ISO + PAX, $P = 0.435$; 1nM ISO + PAX vs 1 μM ISO + PAX, $P = 0.99$).

4.4.4 Characterization of BK currents from mouse SANCs

Our results suggest that the BK channels that regulate SANC firing are expressed on SANC plasma membrane, leading us to hypothesize that BK currents could be recorded from SANCs. We tested this hypothesis by performing whole-cell voltage-clamp recordings from SANCs in physiological solutions. To isolate the BK current component of the initial total outward current (Figure 12A), we perfused 3 μM PAX onto SANCs for 2 minutes, and subtracted the residual current (Figure 12B) from the initial current to obtain the PAX-sensitive (BK) current (Figure 12B - inset). I_f currents were recorded at the end of each experiment to identify the cell as an SANC (Figure 12C), since I_f is not present in atrial cells at the applied voltage steps (Marger et al., 2011).

A voltage- and PAX-sensitive current was detected in 5 out of 6 SANCs (Figure 12D). The PAX-sensitive current had a peak amplitude of 1.4 ± 0.3 pA/pF (Figure 12D). To verify that current rundown did not contaminate the PAX-sensitive current, currents were recorded on additional cells in the presence of the vehicle (DMSO or Tyrode's). No vehicle-sensitive current was observed in these cells (Figure 12E), further suggesting that the PAX-sensitive current in SANCs was actually a BK current.

I_f, which is evoked by HCN4 channels, is an essential inward current that initiates DD (DiFrancesco, 2006), and inhibition of I_f causes a reduction in SANC firing rates (Baruscotti et al., 2011). To determine whether PAX-induced elongation of DD was not due to inhibition of I_f, we tested the effect of PAX on I_f in both native mouse SANCs, and in HEK293 cells stably expressing HCN4 channels. 3 μM PAX did not reduce I_f currents in either SANCs or HCN4-expressing HEK293 cells (Figure 13). These results demonstrate that PAX does not prolong DD through off-target effects on I_f.

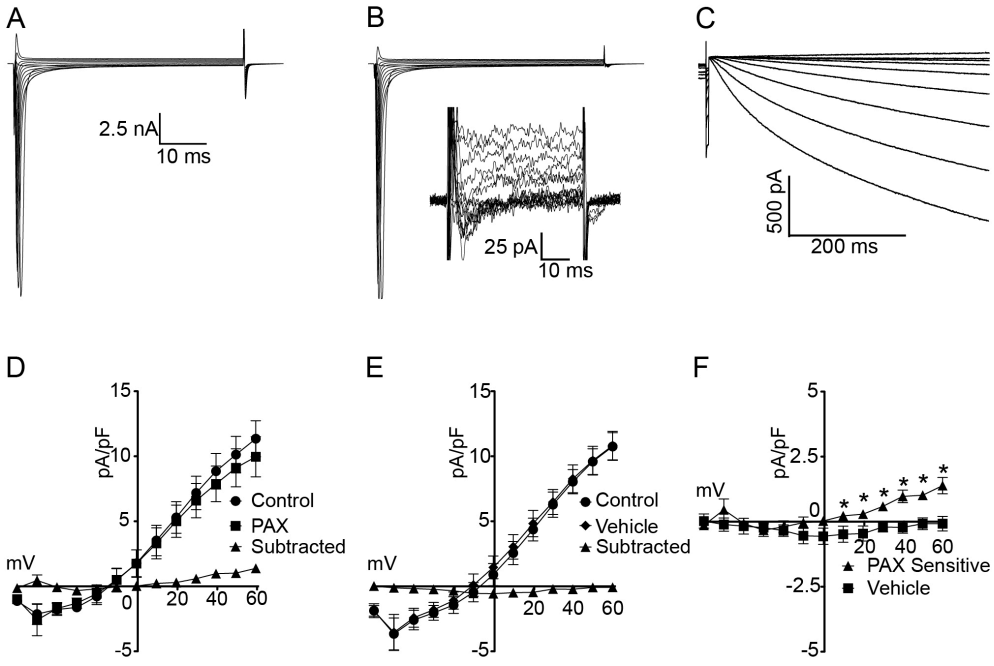

Figure 12: PAX-sensitive currents in SANCs

(A, B) Whole cell macroscopic currents were evoked from SANCs from a holding potential of -75 mV (with 5 mM EGTA in the intracellular pipette solution). Representative currents from baseline (A) and after 3 μM PAX (B). Inset in (B) is the PAX-subtracted current. (C) I_f current from the same cell. I_f currents (D) Average current density versus voltage for baseline currents (circles), after PAX (squares), and PAX-sensitive component (triangles). Current values were obtained from steady-state levels at the end of the voltage step to prevent contamination from the initial inward current ($n = 5$ cells). Currents were normalized to cell capacitance (40.2 ± 4.6 pF, $n = 6$). (E) Average current density for the vehicle-sensitive control current ($n = 6$ cells). (F) The PAX-sensitive current increases with voltage, but the control current is negligible (Control vs PAX-sensitive current $P = 10^{-5}$, repeated measures ANOVA, *Unpaired t-test, $P < 0.05$ from +10 to +60 mV).

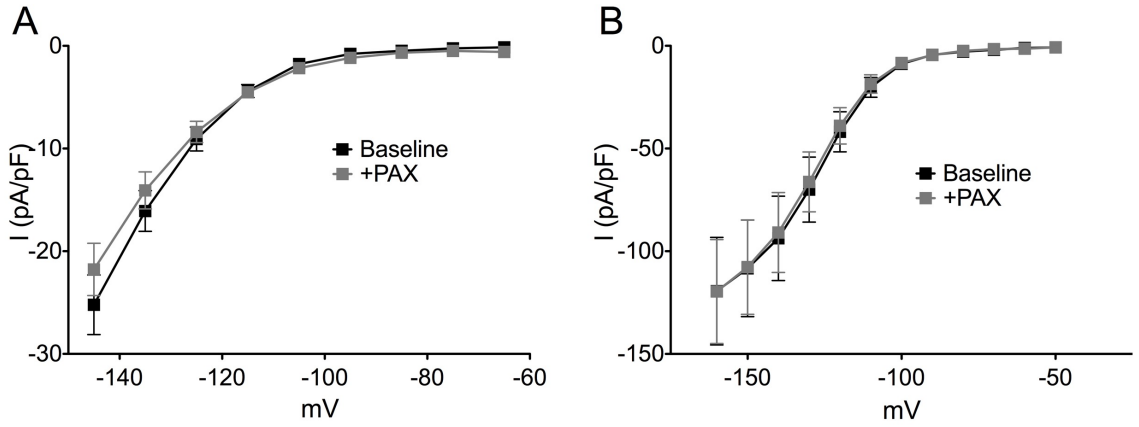

Figure 13: PAX does not inhibit I_f

Normalized current-voltage relationships for I_f currents recorded under baseline conditions and after application of PAX from SANCs (A) and HEK293 cells stably expressing HCN4 channels (B). HEK293 cells were provided by Cathy Proenza. I_f was evoked in a whole-cell patch configuration using 500 ms hyperpolarizing voltage steps in SANCs, and 3s hyperpolarizing voltage steps in HCN4-expressing HEK293 cells. I-V relationships in the +PAX condition were obtained 2 minutes post PAX perfusion. $n = 5$ cells for each data set. Data are means ± SEM.

4.4.5 BK channel expression in mouse SAN

To characterize BK channel expression in SANCs, we performed reverse-transcriptase PCR (RT-PCR) and immunocytochemistry to determine BK channel transcript and protein levels, respectively. First, RT-PCR was performed on WT and *Kcnma1*$^{-/-}$ mouse SANCs by Joshua Whitt. BK channel RNA was positively identified from SANCs by designing primers that specifically flanked regions of the channel that were deleted *Kcnma1*$^{-/-}$ mice. HCN4 was amplified as a control to demonstrate that isolated cells were SANCs. BK channel RT-PCR products were detected from WT SANCs, but not *Kcnma1*$^{-/-}$ SANCs or WT SANCs in the absence of reverse transcriptase (Figure 14A). This result indicates that BK channel transcripts are present in SANCs.

Next, to visualize BK channel expression in SANCs, conventional immunocytochemistry was utilized on isolated WT and *Kcnma1*$^{-/-}$ mouse SANCs. Cells were co-labeled with a rabbit polyclonal BK channel antibody that recognizes the intracellular –COOH terminus of the BK α-subunit, and a mouse monoclonal antibody against HCN4 channels to positively identify SANCs (Figure 14B). BK channel expression levels were quantified in SANCs by calculating the average pixel intensity for BK and HCN4 fluorescence for each cell. WT SANCs exhibited higher BK signal intensities than cells isolated from *Kcnma1*$^{-/-}$ mice, indicating that BK channel protein is expressed in SANCs (Figure 14C). BK expression was also found to overlap with HCN4 expression (Figure 14B), suggesting that BK expression occurs on SANC plasma membranes.

Although BK channel signal intensity was appreciably higher in WT SANCs compared to *Kcnma1*$^{-/-}$ cells, the signal intensity still relatively low. To amplify the BK

expression signal intensity for better visualization, a tyramide signal amplification (TSA) kit was used, which amplifies the signal through a catalytic reaction between horseradish peroxidase (HRP) and a tyramide-labeled secondary antibody that becomes activated upon treatment with H_2O_2. The signal intensity in WT cells treated with primary BK channel antibody was significantly higher than the intensity of WT cells treated only with the secondary antibody (Figure 14E). These results further demonstrate that BK channels are expressed in SANCs.

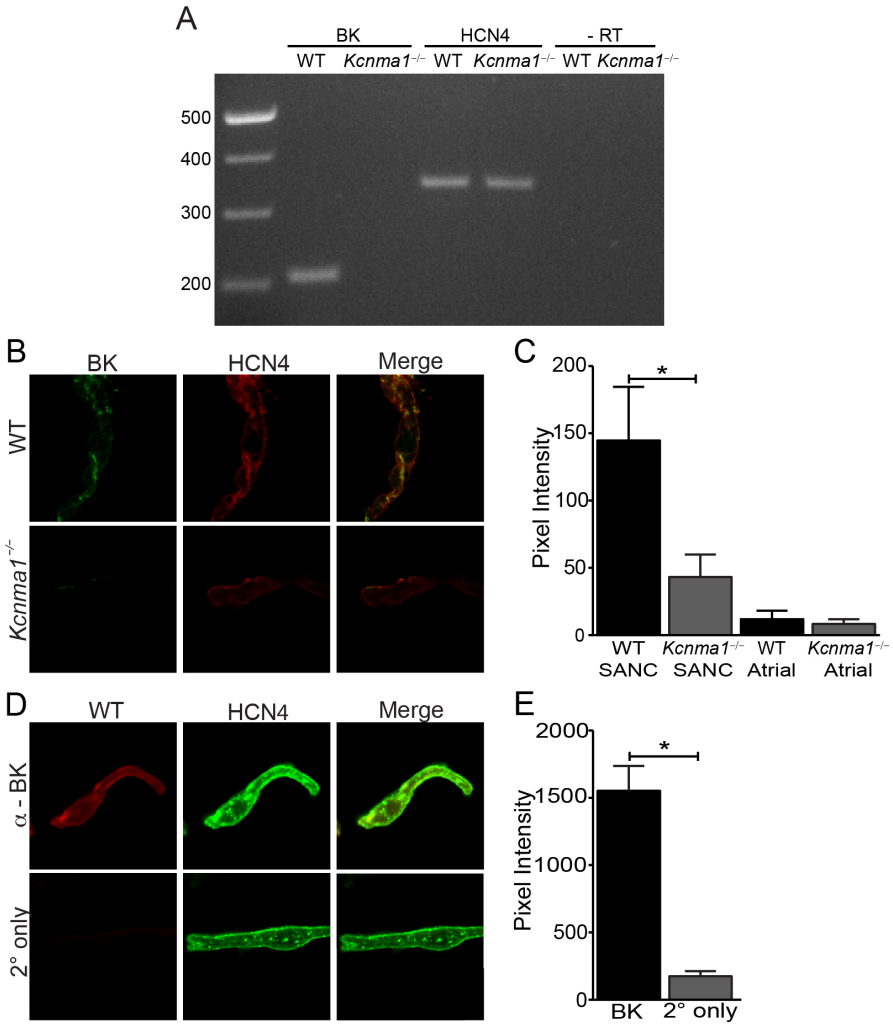

Figure 14: Detection of BK channels in SANCs

(A) RT-PCR from WT and *Kcnma1*$^{-/-}$ SAN (performed by Joshua Whitt). The specificity of BK expression was verified using N-terminal primers located within the deleted *Kcnma1*$^{-/-}$ sequence. A 206 bp product was amplified from WT SAN, while no product was amplified from *Kcnma1*$^{-/-}$ SAN (n = 2). HCN4 was amplified from both WT and *Kcnma1*$^{-/-}$ SAN (337 bp). (B) Confocal images from WT and *Kcnma1*$^{-/-}$ SANCs incubated with α-BK (green) and α-HCN4 (red) antibodies. Images collected under equivalent gain settings. (C) Average pixel intensity values for α-BK fluorescence in SANCs (WT, n = 5 cells and *Kcnma1*$^{-/-}$, n = 5) and atria (WT, n = 4 cells and *Kcnma1*$^{-/-}$, n = 3). In SANCs, WT BK expression was increased compared to *Kcnma1*$^{-/-}$ (P = 0.04, unpaired t- test). (D) Tyramide signal amplification of BK signal (red) from WT SANCs. HCN4 (green) immunofluorescence was performed as in *B*. (E) Average pixel intensity values for BK signal (n = 21 cells) versus no primary control (n = 20; P =10^{-8}, Mann-Whitney).

4.4.6 Characterization of currents evoked by BK channels cloned from mouse SANCs

Since we could not characterize Ca^{2+}-dependent activation from native SANCs because we could not increase the intracellular Ca^{2+}, we characterized current properties of BK channels cloned from SANCs. We first identified the BK channel splice variants expressed in SANCs by amplifying BK channel transcripts from single SANCs by RT-PCR, and then characterized BK currents after expressing the resulting BK channel cDNAs in HEK293T cells. Two cDNA products were obtained from SANCs that lacked alternative exons at splice sites 1-3, but differed in the alternative exon at splice site 4 (–QEERL and -VYR). These constructs were identical to constructs previously cloned by our lab from brain (Shelley et al., 2013) and bladder (unpublished data)**.**

First, we determined whether BK_{QEERL} and BK_{VYR} currents exhibited similar properties to the native BK current recorded from SANCs. HEK293T cells were transfected with BK_{QEERL} or BK_{VYR} variants tagged with a yellow fluorescent protein (YFP) to positively identify cells with BK expression, and BK currents were recorded in whole-cell patch configuration. Both BK_{QEERL} and BK_{VYR} currents had similar I-V relationships to native BK currents from SANCs (Figure 15C). This result suggests that native SANC BK currents were small and activated at more positive potentials than expected due to the high concentration of EGTA (5 mM), and low resulting Ca^{2+} concentration (1.9 nM) in the internal pipette solution.

Next, to further characterize the properties of currents evoked by BK_{QEERL} and BK_{VYR} channels, we recorded BK currents at nominal, 1 μM, and 50 μM Ca^{2+} in an inside-out patch configuration. The normalized I-V relationship for both BK_{QEERL} and BK_{VYR} currents became left-shifted as the intracellular Ca^{2+} was increased, but the

voltage at half maximal activation ($V_{1/2}$) for both constructs were similar at each Ca^{2+} concentration (Figure 15B). Although these variants contained different alternative exons at the COOH-terminus, it was not surprising that the BK_{QEERL} and BK_{VYR} currents exhibited similar properties in physiological K^+ solutions, as other studies performed in symmetrical K^+ solutions suggest that BK_{QEERL} and BK_{VYR} have similar G-V relationships, activation and deactivation kinetics in multiple Ca^{2+} concentrations (Joshua Whitt, unpublished data).

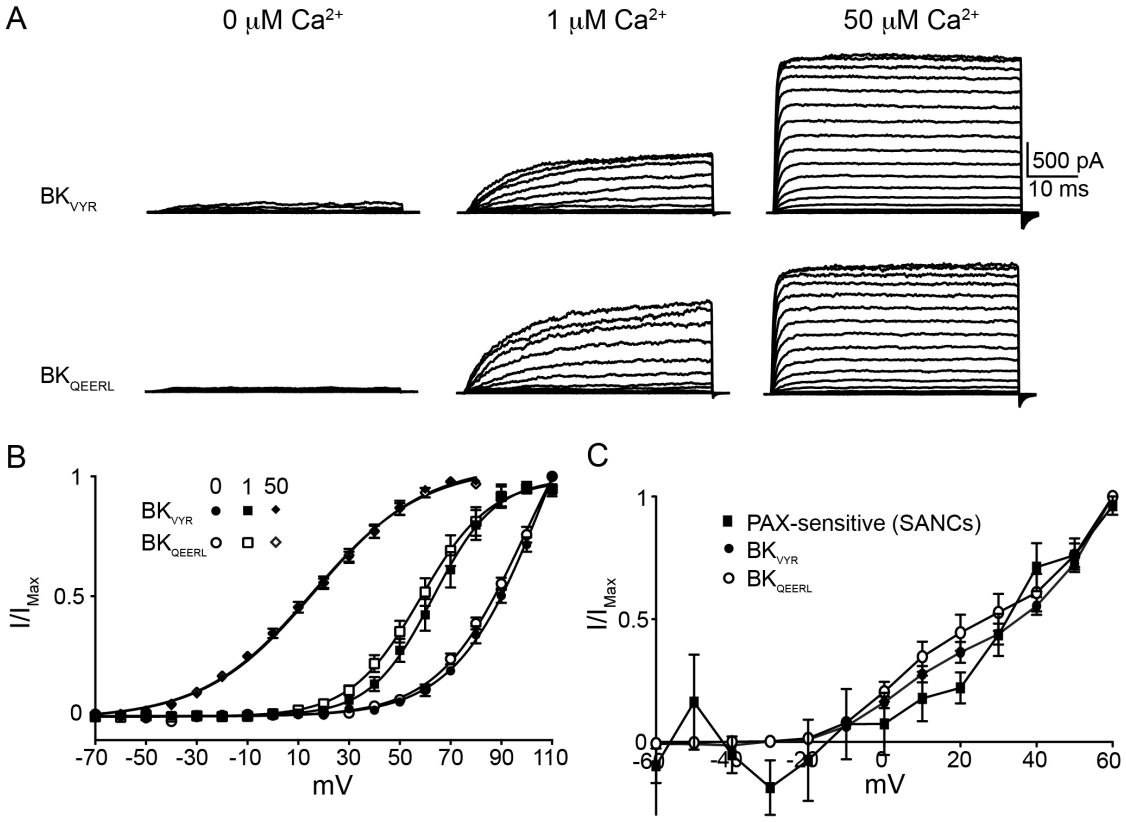

Figure 15: Characterization of currents produced by BK channel variants cloned from SANCs

Macroscopic currents were evoked from HEK293T cells expressing BK_{VYR} or BK_{QEERL} cDNAs. Recordings were performed in physiological K^+ (5.4 mM external/135 mM internal). (A) Representative current traces from inside-out patches at nominal, 1 μM, and 50 μM free Ca^{2+}. Currents were recorded using 50 ms depolarizing voltage steps from -130 mV to +110 mV. (B) Average normalized I-V relationships from inside-out patch recordings from BK_{VYR} and BK_{QEERL} channel variants ($I/I_{max[+110mV]}$). *n* = 6-9 patches per condition. Current amplitudes were obtained from the end of the steady-state current at the end of the depolarizing voltage step. (C) Average normalized I-V relationships ($I/I_{max[+60mV]}$) recorded in whole-cell configuration with the same intracellular and bath solutions used for SANCs in Figure 12. BK_{VYR} and BK_{QEERL}, *n* = 9-10 cells for each channel variant. The PAX-sensitive current from SANCs in Figure 12 was replotted as I/I_{max} for comparison (*n* = 5 SANCs). The voltage protocol was identical to that used in native SANCs.

4.5 ***Discussion***

In the heart, BK channels mediate cardioprotection against ischemic injury (Bentzen et al., 2009; Singh et al., 2013; Xu et al., 2002), and regulate heart rate in rodents (Imlach et al., 2010) . However, roles for BK channels in regulating cardiac cell excitability had not been reported prior to this work. This chapter describes a novel role for BK channels in mediating the automaticity of SANCs, the primary cardiac pacemaking cells (Lai et al., 2014). We demonstrate that: 1) pharmacological inhibition of BK channels *in vivo* reduces heart rate in mice (Figure 8), 2) BK channel inhibitors and genetic deletion of BK channels reduce the spontaneous firing rate of isolated SANCs (Figure 9, Figure 10), 3) β-adrenergic receptor agonists can recover the reduction in firing rate caused by PAX (Figure 11), 4) BK channel transcripts and protein can be detected from SANCs (Figure 14), and 5) BK currents can be detected from native SANCs (Figure 12). We also characterized properties of BK currents evoked by channels cloned from SANCs and found that they exhibit similar I-V relationships to the native SANC BK current (Figure 15). In combination, these results support the hypothesis that BK channels regulate heart rate by mediating the firing rate of SANCs.

4.5.1 Is heart rate compensated for in Kcnma1$^{-/-}$ mice?

Although PAX caused a reduction in heart rate in WT mice, the baseline heart rates of *Kcnma1*$^{-/-}$ were similar to those of WT mice (Figure 8). This result is consistent with others that reported the heart rates of *Kcnma1*$^{-/-}$ mice (Imlach et al., 2010; Sausbier et al., 2005). Interestingly, *Kcnma1*$^{-/-}$ SANCs had lower intrinsic firing rates compared to WT cells, which suggests that the heart rates of *Kcnma1*$^{-/-}$ mice may be compensated for *in vivo*. Other mice with genetic deletions of channels known to regulate SANC

automaticity, such as $Ca_V1.3$ or HCN4, have similar heart rates to WT mice when sympathetic tone is increased pharmacologically or through activity (Herrmann et al., 2007; Platzer et al., 2000). This suggests that *Kcnma1*$^{-/-}$ mice could potentially have normal heart rates due to elevated sympathetic tone. Our data correlate well with this hypothesis, as a saturating concentration of ISO can recover the detrimental effect of PAX on SANC action potential frequency (Figure 11). Further experiments, such as catecholamine measurements, could help further determine whether sympathetic tone is elevated in *Kcnma1*$^{-/-}$ mice.

4.5.2 BK current inhibition reduces excitability in SANCs

Interestingly, the reduction in SANC firing observed after BK current inhibition contradicts the general result of BK current abolishment in smooth muscle and neurons, which is an increase in excitability (Heppner et al., 1997; Meredith et al., 2004; 2006; Nelson et al., 1995). Previous reports indicate that BK currents can have multiple effects on cell excitability, as expression of gain-of-function BK channels can both enhance and reduce neuronal excitability, and pharmacological inhibition of BK currents can suppress excitability in a mouse seizure model (Montgomery and Meredith, 2012; Shruti et al., 2008). Our results are consistent with the reduction in excitability observed in other cardiac pacemaking cells after block of Ca^{2+}-activated K^+ channels, such as intermediate-conductance (IK) and small-conductance (SK) channels (Chen et al., 2013; Weisbrod et al., 2013).

Diastolic depolarization (DD) is heavily dependent on synergy between both voltage- and Ca^{2+}-clock mechanisms. The phenotype observed with inhibition of other Ca^{2+}-activated K^+ channels in cardiac pacemaker cell types, which is a reduction of

excitability due to elongation of DD, is consistent with our results. In previous studies, inhibition of IK currents causes MDP depolarization. This decreases pacemaker cell excitability by reducing the hyperpolarizing drive that activates I_f at the beginning of DD, which precludes activation of currents that participate in late DD, such as $I_{Ca,L}$ (Weisbrod et al., 2013). Interestingly, DD was elongated after genetic or pharmacological inhibition of BK currents, even though we did not observe a significant depolarization of MDP. BK currents are activated in other cell types by coupling to Ca^{2+} sourced from Ca_V channels or SR Ca^{2+} release (Berkefeld et al., 2006; Nelson et al., 1995), both of which play prominent roles in DD. Therefore, inhibition of BK currents that activate during DD, which would depolarize the membrane, may facilitate inactivation of currents that are prevalent during DD, such as I_{Na} or I_{Ca} (Kodama et al., 1997; Lei et al., 2004). Alternatively, BK currents could be activated by the bulk Ca^{2+} transient that occurs during the upstroke of the action potential. Therefore, inhibition of BK currents could potentially affect the rate of membrane hyperpolarization that activates I_f, which subsequently could reduce excitability by reducing the rate of DD.

4.5.3 Characterization of native BK currents from SANCs

Characterizing the properties of native BK currents, such as the voltage-dependence of activation at increasing Ca^{2+}, was not possible because of the high concentration of intracellular EGTA (5 mM) required to maintain recording integrity (Figure 15). 5 mM EGTA would chelate internal Ca^{2+} to a calculated concentration of 1.9 nM, which would not be sufficient to activate BK currents at physiological DD potentials based on our cloned channel BK current recordings (Figure 15B). Attempts at recording BK currents with reduced EGTA concentrations or elevated intracellular Ca^{2+}

were unsuccessful. We addressed this issue by characterizing BK currents evoked by cloned BK channels. We first demonstrated that cloned BK channels with at 1.9 nM intracellular Ca^{2+} exhibited a similar I-V to native SANC BK currents (Figure 15C), indicating that the native BK current, despite being small and activating at positive potentials, was actually a BK current. At elevated Ca^{2+} (50 μM), which is a potential local Ca^{2+} concentration at Ca^{2+} spark sites or adjacent to voltage-gated Ca^{2+} channels (Berkefeld et al., 2006; Fakler and Adelman, 2008; Perez et al., 2001), BK currents began to activate at the hyperpolarized potentials that occur during DD (Figure 15B). This data suggests that BK currents in SANCs could be activated during DD by Ca^{2+} from either through voltage-gated Ca^{2+} channels or RyRs. Future experiments could be designed to determine the Ca^{2+} source that activates BK currents during DD (Section 4.6).

4.5.4 BK currents may regulate ventricular myocyte excitability

BK expression has previously been reported in ventricular myocytes (Singh et al., 2013; Xu et al., 2002), but these reports do no implicate BK channels in regulating ventricular myocyte excitability. IbTX was previously reported to not to affect rat ventricular myocyte action potentials (Takamatsu et al., 2003). Our ECG data suggests that BK channel inhibition does affect ventricular myocyte excitability, as the Q-T interval was prolonged by PAX (Figure 8C). A potential explanation for the conflicting data may be β4-subunit expression, as β4 has been detected in the heart (Behrens et al., 2000; Brenner et al., 2000a; Meera et al., 2000) and conveys IbTX-resistance to BK channels at 100 nM (Meera et al., 2000; Takamatsu et al., 2003). A more thorough molecular and electrophysiological characterization of BK channels in ventricular

myoctyes would be required in order to understand the mechanism by which PAX elongates the Q-T interval.

4.5.5 Model of BK current regulation of SANC firing

Our data indicates that eliminating BK currents reduces SANC excitability and cardiac pacing *in vivo* by elongating the DD duration. This finding contradicts the general phenotype observed with abolishment of BK channel function, as pharmacological inhibition and genetic ablation of BK currents generally increases cell excitability (Heppner et al., 1997; Meredith et al., 2004; 2006; Nelson et al., 1995). BK currents in neurons, and cells such as urinary bladder smooth muscle cells, usually contribute to the repolarization and afterhyperpolarization phases of the action potential. In SANCs, repolarization is mediated by fast ($I_{K,r}$) and slow ($I_{K,s}$) delayed rectifier K^+ currents and the transient outward ($I_{T,o}$) K^+ current. Pharmacological inhibition of these K^+ currents causes elongation of the APD_{50} and depolarization of the MDP, which are hypothesized to reduce excitability by reducing I_f (Boyett et al., 1998; Clark et al., 2004; Kodama et al., 1999; Ono et al., 2000). Although ablating BK channel function reduces the action potential frequency of SANCs, only a modest increase in the APD_{50} was observed, which was not statistically significant (Figure 9H). This finding suggests that BK currents may not be heavily involved in regulating SANC repolarization, and indicates that BK channels regulate SANC excitability by affecting a different phase of the action potential.

BK current inhibition does not induced depolarization of the MDP (Figure 9I), which suggests that BK currents would not regulate the initial phases of DD that are mediated primarily by I_f. Following the MDP, membrane hyperpolarization, such as that

caused by BK currents, is required to facilitate I_f activation and recovery from inactivation of I_{Ca} and I_{Na}. Based on our recordings obtained from BK channels cloned from SANCs, BK activation at the membrane potentials that encompass DD would require elevation of intracellular Ca^{2+} (Figure 15B). Two potential Ca^{2+} sources that could couple to BK channels and are active during the later stages of DD are membrane-bound voltage-gated Ca^{2+} channels and local Ca^{2+} release from the SR (Figure 6). Since BK currents would hyperpolarize the membrane, it might be expected that inhibition of BK currents that activate during the later stages of DD due to elevation of Ca^{2+} would cause membrane depolarization. This could potentially prevent recovery of inactivation of I_{Ca} or I_{Na}, as well as reduce the hyperpolarizing force that would activate I_f after the initiation of DD, and subsequently cause a reduction in SANC excitability.

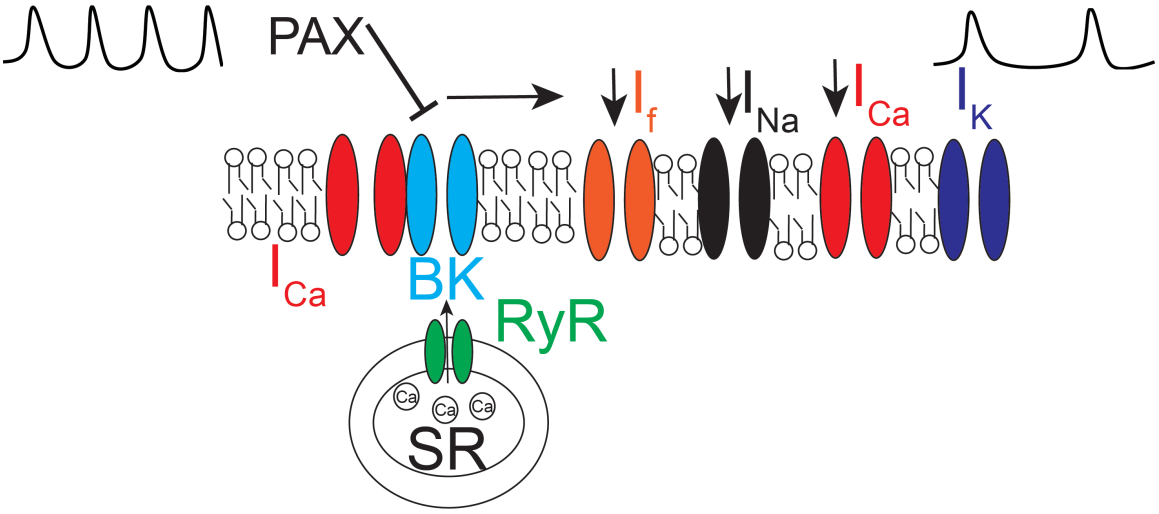

Figure 16: Proposed model of BK current regulation of SANC automaticity

BK current inhibition reduces SANC excitability by increasing the DD duration. Our data from BK channels cloned from SANCs suggests that coupling of BK channels to Ca_V and/or RyR is required for BK channel activation during DD. Inhibition of BK currents with PAX may facilitate an increase in the DD duration by subsequently reducing I_f current, or preventing I_{Ca} or I_{Na} from recovering from inactivation, all of which would reduce the available inward current required to initiate DD.

4.6 ***Future Studies***

Our data suggests that BK channels regulate the DD phase of the action potential, but the mechanism is still unclear. To determine the Ca^{2+} sources that activate BK channels during DD, it would be interesting to record BK currents in a perforated patch configuration in the presence of L-type Ca^{2+} channel inhibitor isradipine (Mangoni et al., 2006), or ryanodine, which blocks SR Ca^{2+} release from RyRs and would subsequently preclude BK current activation (Nelson et al., 1995; Vinogradova et al., 2002). Recording currents in perforated patch would allow for intracellular Ca^{2+} cycling to be maintained during experiments. By determining whether BK currents are abolished in the presence of either Ca^{2+} source inhibitor, we could determine the mechanism by which BK currents are activated.

Another future study would be to determine whether BK channels other than on the plasma membrane in SANCs regulate action potential frequency. The magnitude of PAX-effect on SANC firing was greater (57%) than the effect of IbTX (29%), suggesting that BK channels localized in other areas besides the plasma membrane, such as in mitochondria (Singh et al., 2013), may regulate SANC automaticity. It is unknown whether BK channels are expressed in the mitochondria of SANCs, so further characterization of SANC mitochondria would be required. If BK channels were found in SANC mitochondria, to test whether they regulate SANC firing, IbTX could be applied to SANCs first to block plasma membrane-bound BK channels, followed by PAX application to block intracellular BK channels. A further reduction after PAX application would suggest that intracellular BK channels regulate SANC automaticity.

A third future study would be to explore the role of BK β-subunits in SANC function. β-subunits, such as β4, have been detected in cardiac tissue and are generally linked with increases in Ca^{2+} sensitivity (Brenner et al., 2000a; Meera et al., 2000). In our experiments, BK currents evoked by the α-subunit alone begin to activate at the potentials that encompass DD at high Ca^{2+} (50 μM), and β-subunit co-expression may cause BK current activation to become more robust in this potential range. Furthermore, β4-subunit expression may contribute to reduced effect of IbTX on SANC firing compared to PAX. Future experiments may consist of characterizing BK_{QEERL} and BK_{VYR} in physiological solutions while co-expressed with β-subunits, as well as characterizing β-subunit expression in isolated SANCs.

4.7 ***Summary***

In this chapter, we identified BK channels as novel regulators of SAN function. Inhibition of BK channels was demonstrated to reduce cardiac pacing in mice *in vivo,* and decrease the firing rates of isolated mouse SANCs. BK channel protein and transcripts were identified in isolated SANCs, and the native BK current properties obtained from SANCs were similar to those of currents recorded from BK channels cloned from SANCs and expressed in HEK293 cells. Our findings indicate that BK channels are essential regulators of intrinsic SANC automaticity, and that BK channels modulate SANC firing by altering DD, the phase of the SANC action potential that initiates intrinsic excitability.

Chapter 5: Regulation of BK currents by single nucleotide polymorphisms

5.1 *Introduction*

Diversity of BK current properties can be attributed to multiple factors, including alternative splicing and auxiliary subunits. However, the effect of single-nucleotide polymorphisms (SNPs) on BK current properties has not been extensively studied. SNPs are a type of genetic variation that cause approximately 90% of human sequence variations (Collins et al., 1998), and SNPs in ion channels have previously been associated with conditions such as epilepsy (Klassen et al., 2011), schizophrenia (Lee et al., 2013), sinus node dysfunction (Baig et al., 2010), and obesity (Jiao et al., 2011).

There are 155 SNPs in the human *KCNMA1* sequence; however, only approximately 63% (99/155) of these are non-synonymous SNPs, or SNPs that affect the encoded amino acid sequence. Furthermore, only two polymorphisms have been characterized or linked to pathological conditions. The first polymorphism (D434G) is associated with epilepsy and dyskinesia in humans (Du et al., 2005). D434G, which is the RCK1 domain in the BK channel C-terminus, causes a +100 mV negative shift in the conductance-voltage (G-V) relationship and significantly increases the single channel open probability of the channel (Du et al., 2005; Yang et al., 2010). The second SNP (A138V) is in the intracellular S0-S1 linker region and has been linked with autism. Although a cell line isolated from a patient with the A138V SNP had a 70% reduction in BK current compared to control patients (Laumonnier et al., 2006), the properties of the A138V BK current, such as the voltage-dependence, Ca^{2+} sensitivity, or current kinetics were not reported. Therefore, the link between the A138V SNP and autism is still unclear.

Because *KCNMA1* SNPs have been linked to epilepsy and autism, and there are 98 non-synonymous SNPs in *KCNMA1* that have not been characterized, we predicted that SNPs may regulate BK current properties. We hypothesized that SNPs linked with pathophysiological conditions or located in domains of the C-terminus previously demonstrated to regulate Ca^{2+}-dependent activation would alter BK current properties. To test this hypothesis, we assembled a list of all known SNPs in *KCNMA1*, and identified SNPs that were disease-linked or in regions of the C-terminus reported to regulate BK current properties. Next, we characterized BK currents evoked from BK channels containing SNPs in symmetrical and physiological K^+ solutions. Then, to identify the effect that SNPs may have on BK currents elicited by physiological stimuli, we measured the amplitudes of currents evoked from BK channels containing SNPs in response to different action potential waveform commands.

5.2 ***Methodology***

5.2.1 Synthesis of human BK (hBK) channel variant

For experiments involving SNPs, we used the human BK (hBK) channel clone, which does not contain alternative exons at splice sites one through three (S1-S3), and contains a residue sequence that ends in –QEERL at splice site four (S4, Table 2). This variant was chosen due to its expression in multiple tissues, including vascular smooth muscle and brain (Dworetzky et al., 1994; McCobb et al., 1995). To construct a "humanized" clone for expression in HEK cells with this particular exon combination, referred to as "hBK" throughout this study, we first converted an existing mouse clone (mBK_{Zero}) to a human clone (hBK_{Zero}) by replacing 8 amino acids that differ in the mouse sequence with the human sequence (Table 3). Next, we subcloned the mouse cDNA

fragment ($mBK_{QEERL,}$ F4) into hBK_{Zero} to create a clone with the indicated exon combination (hBK, Table 3, Figure 17). Upon constructing hBK, further site directed mutagenesis (P1158Q) was performed to complete humanization of hBK (Table 3).

Construct	S1	S2	S3	S4
mBK_{QEERL}	_	_	_	-KYVQEERL
hBK_{Zero}	_	_	-AKPGKLPLVSVNQ EKNSGTHILMITEL-	-NRKEMVYR
hBK_{SRKR}	- SRKR -	_	-AKPGKLPLVSVNQ EKNSGTHILMITEL-	-NRKEMVYR
hBK	_	_	_	-KYVQEERL

Table 2: List of BK channel variants used and the amino acid sequences at each alternative splice site

mBK_{QEERL} and hBK sequences were identified by Jessica Lu. hBK_{Zero} and hBK_{SRKR} were derived from mouse constructs that were identified in our lab's previous publication (Shelley et al., 2013).

Residue #	mBK_{Zero} Amino Acid	hBK_{Zero} Amino Acid	Original Codon (mouse)	Revised Codon (human)
21	G	S	GGC	AGC
23	G	_	GGT	_
42	_	S	_	AGC
151	V	A	GTG	GCG
684	V	I	GTC	ATC
696	R	K	AGG	AAG
704	P	S	CCA	TCA
1158	P	Q	CCG	CAG

Table 3: Amino acid differences between mBK_{Zero} and hBK_{Zero}

Table 3 describes the residue variation between mouse and human BK_{Zero} channel variants (identified by Jessica Lu), and the base pair substitution required to generate the human amino acid.

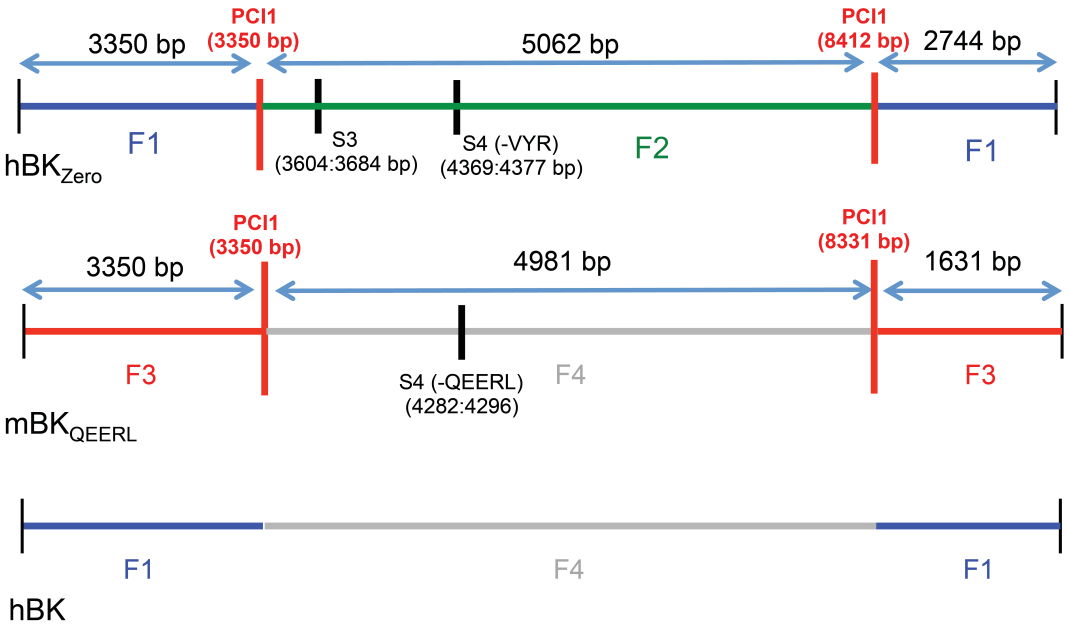

Figure 17: Strategy for constructing hBK channel variant

To generate hBK, we first generated the hBK$_{Zero}$ clone. hBK$_{Zero}$ was generated by aligning a consensus human BK channel sequence with the mouse BK$_{Zero}$ (mBK$_{Zero}$) clone (Shelley et al., 2013). Mouse and human BK channel sequence variance was determined by Jessica Lu. Eight amino acid differences were identified between the consensus human BK channel sequence and mBK$_{Zero}$. These residues were mutated in mBK$_{Zero}$ via site-directed mutatgenesis in order to generate hBK$_{Zero}$ (Table 2). Upon synthesis of the hBK$_{Zero}$ variant, hBK$_{Zero}$ sequence was then aligned with other human BK channel sequences found in GenBank and described in other publications to identify the sequence most frequently occurring in human tissue. This sequence was most similar to our lab's mBK$_{QEERL}$ construct (Figure 17), which contains no alternate exon at S3, and contains the residue sequence at S4 ending in –QEERL. Base pairs 3351 – 8331 (F4) were ligated from mBK$_{QEERL}$ into hBK$_{Zero}$, replacing base pairs 3351 – 8412 (F2) to synthesize a construct with an appropriate alternate exon combination, which is the hBK construct. Additional site-directed mutatgensis (P1158Q) was then performed due to mouse/human variation (Table 3) to generate the final hBK construct to be used for experiments.

5.2.2 Identification of SNPs that regulate BK current properties

Human *KCNMA1* SNPs predicted to affect BK current properties were chosen from a table of known SNPs constructed by Jessica Lu. SNPs chosen for experiments were evaluated based upon: 1) proximity of SNP to residues previously identified to regulate BK current properties, 2) the magnitude of change in amino acid properties introduced by the SNP, 3) association of the SNP to disease, and 4) the predicted effect of the SNP on protein function using the software algorithms MutPred and NetPhos.

MutPred is a freely-available computational model based on protein sequence that models changes in structure and function. While earlier computational modeling programs, such as SIFT (Ng and Henikoff, 2003) and PolyPhen (Ramensky et al., 2002), predict deleterious effects of amino acid mutations using sequence homology and structural information from protein databases, MutPred is unique because it is trained on five databases of known protein mutations and generates a hypothesis for the molecular mechanism underlying a deleterious effect on protein function (Li et al., 2009). To evaluate a mutation as deleterious, MutPred assigns the mutation a general score from 0 (nondeleterious) to 1 (deleterious). Additionally, MutPred provides a hypothesis, if possible, for the mechanism underlying the deleterious effect of mutations on protein function. For this study, we were most interested in mutations with a MutPred general score ≥ 0.5 that had actionable hypotheses.

As a control to determine the ability of MutPred to identify SNPs that would alter BK current properties, we determined the MutPred score for mutations previously identified to alter BK current properties (Table 5). These 'control' mutations were a

mutation in the Ca^{2+} bowl (D959A), the Ca^{2+} sensing site in RCK1 (D434A), and voltage sensor (R272Q).

NetPhos was used to predict whether SNPs would affect phosphorylation of specific residues in hBK. NetPhos is an algorithm that predicts phosphorylation by comparing a given sequence with hundreds of known phosphorylatable sequences (Blom et al., 1999). Our lab used NetPhos to predict phosphorylation of S642, as previously described (Shelley et al., 2013). We used NetPhos on the hBK before and after introducing SNPs to hBK to predict whether specific residues might be phosphorylated after introduction of SNPs. To evaluate if a mutation affected residue phosphorylation, NetPhos would assign each serine, tyrosine, and threonine a score between 0 (not phosphorylated) and 1 (phosphorylated). SNPs that either introduced or eliminated a residue with a NetPhos score of > 0.5 were considered for experiments.

5.2.3 HEK cell culture and electrophysiology

HEK293T cells were cultured and transfected as described in Chapter 3. For symmetrical K^+ experiments, macroscopic BK currents were recorded in an inside-out patch configuration from HEK293T cells transfected with the construct of interest. Recordings were acquired at 50 kHz. Thin-walled glass capillaries with resistances, after fire-polishing, between 1.5 and 3 MΩ were used for experiments. The internal (bath) solution contained (in mM): 140 $KMeSO_3$, 2 KCl, and 20 HEPES, while the external (pipette) solution contained: 140 $KMeSO_3$, 2 KCl, 1 $MgCl_2$, and 20 HEPES. The solutions were set to a pH of 7.2 using KOH, as setting the pH of intracellular solutions with NaOH was found to cause voltage-dependent block in the outward currents above +100 mV (Figure 36). Total Ca^{2+} concentrations required to obtained the desired free

Ca^{2+} concentration were calculated using WebMaxC as described in Chapter 3. Solutions were buffered with either EGTA (0 μM Ca^{2+}) or HEDTA (1 and 10 μM Ca^{2+}). For calculations with WebMaxC, the temperature was 20 °C and the ionic value was 0.16.

In symmetrical K^+, BK currents were evoked from a holding potential of -100 mV, using 20 ms voltage steps from -150 mV to 300 mV, followed by a 10 ms hyperpolarizing step back to -80 mV to generate tail currents. G-V analysis was conducted at 200 μs after the peak tail current as previously described (Brenner et al., 2000a), to minimize contamination by the capacitive transient. Activation kinetics were determined by fitting the rising phase of the outward currents to single exponential functions. To measure deactivation kinetics, patches were subjected to a 20 ms voltage step to +200 mV, followed by 10 ms voltage steps from -200 mV to -50 mV. Deactivation kinetics were measured by fitting tail currents with single exponential functions. Leak currents were subtracted using a P/5 protocol with a subsweep holding potential of -120 mV as previously described (Shelley et al., 2013).

In physiological K^+, macroscopic BK currents were elicited in an inside-out patch configuration. The external (pipette) solution contained (in mM): 134 NaCl, 6 KCl, 1 $MgCl_2$, 10 glucose, and 10 HEPES. The pH was adjusted to 7.4 with NaOH. The internal (bath) solution contained: 110 K-aspartate, 10 NaCl, 30 KCl, 10 HEPES, 1 $MgCl_2$, 5 HEDTA and 10 μM free-Ca^{2+}. The pH was adjusted to 7.2 with KOH. To generate the G-V relationship, currents were evoked by holding patches at -100mV, followed by 20 ms square voltage steps from -150 mV to +150 mV, followed by a 10 ms tail step to -150 mV. G-V analysis was performed on the tail currents as described above.

G-V relationships were generated for all patches subjected to action potential voltage commands.

Following square waveform current recordings, we recorded BK currents in response to action potential waveforms. The peak current elicited by each action potential voltage command was normalized to the peak steady state current evoked by square waveforms when determining the G-V relationship. The peak steady-state current for each patch occurred between +90 and +120 mV. Four action potential commands were used for experiments; two representative action potentials from a mouse suprachiasmatic nucleus (SCN) neuron during the circadian day (SCN_{Day}) or night (SCN_{Night}) (Shelley et al., 2013), representative action potentials from a mouse SANC (Lai et al., 2014), and a representative action potential evoked from a mouse urinary bladder smooth muscle cell. SCN action potentials were obtained from whole-cell recordings from mouse SCN neurons. Mouse SANC action potentials were obtained from mouse SANCs in a perforated patch configuration (Lai et al., 2014). Mouse bladder action potential waveforms were extracted using Dagra (Blue Leaf Software, Hamilton, New Zealand) from an image obtained from Dr. Tom Heppner at the University of Vermont. The voltage command waveform used for each experiment can be found in Figure 27.

5.2.4 Statistics and Data Analysis

Data analysis was performed using pClamp 10 (Axon Instruments). Graphs were generated in Prism 5.0 (GraphPad), and statistical analysis was performed using Origin Lab 8.5 (Origin Lab). Prism 5.0 was used for two-way repeated-measure ANOVAs when analyzing BK current kinetics. Data are presented as means ± SEM.

5.3 ***Results***

5.3.1 Characterization of mouse and human BK constructs

To determine whether the eight amino acids introduced to humanize mBK_{QEERL} altered BK currents (Table 3), we characterized macroscopic current recordings from both hBK and mBK_{QEERL}. hBK and mBK_{QEERL} have identical exons and residue combinations (Table 2). hBK and mBK_{QEERL} had similar $V_{1/2}$ values, activation, and deactivation kinetics except when noted (Figure 18, Figure 19, Table 4), suggesting that the 8 amino acid substitutions generally did not affect BK current properties.

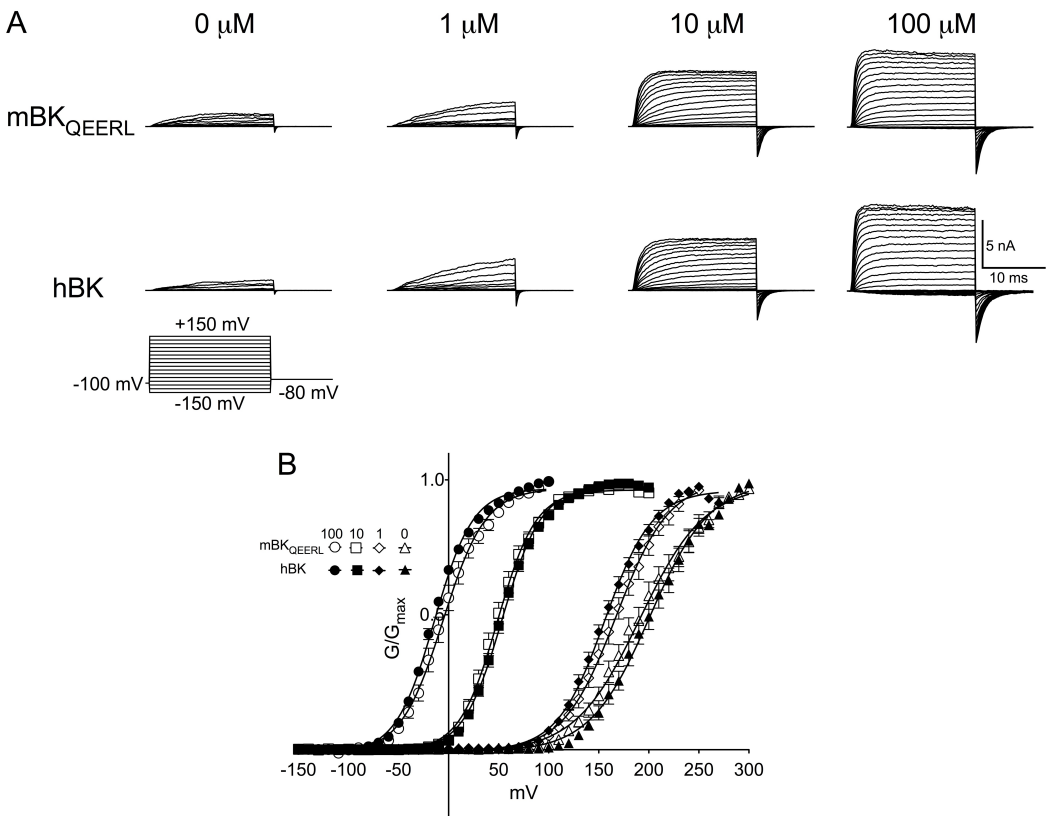

Figure 18: Characterization of mBK$_{QEERL}$ and hBK currents

(A) Representative macroscopic BK currents recorded at indicated Ca^{2+} concentration from inside-out patches in response to depolarizing voltage steps. Currents were recorded from separate patches. (B) Normalized conductance-voltage (G-V) relationship for BK currents at indicated Ca^{2+} concentrations. $V_{1/2}$ values for each variant at indicated Ca^{2+} concentration, and number of patches used for analysis is listed in Table 4.

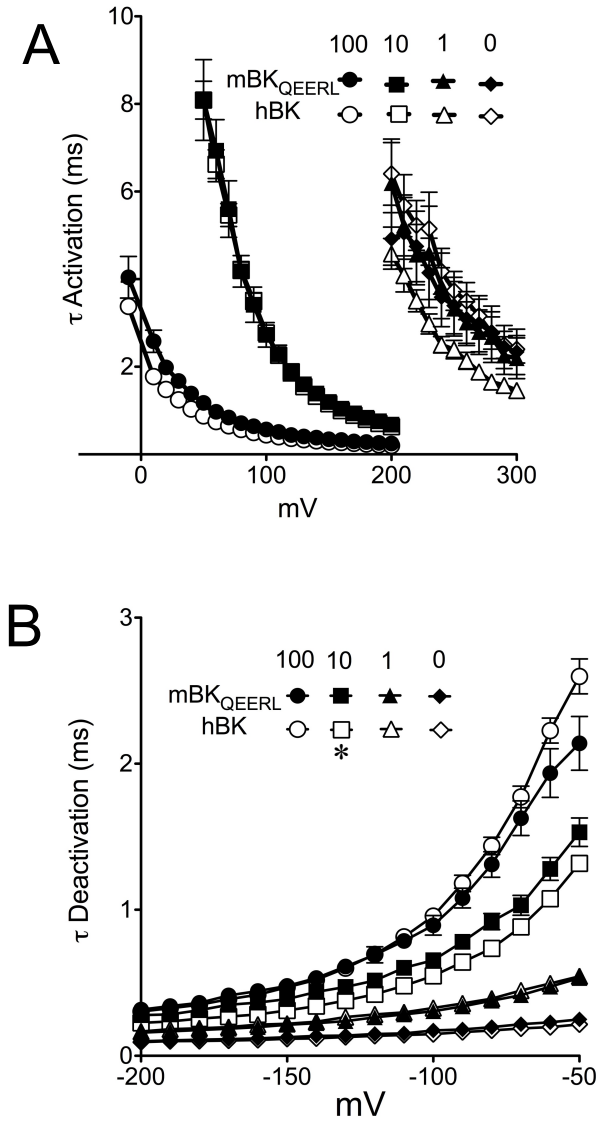

Figure 19: Activation and deactivation kinetics for mBK$_{QEERL}$ and hBK

(A) Activation time constants were determined by fitting the rising phase of the outward currents to single exponential functions. Constructs had significantly different activation kinetics at 100 μM Ca^{2+} (P = 0.002). (B) Deactivation time constants were determined by fitting tail currents to single exponential functions, following voltage steps to +200 mV. Constructs had significantly different deactivation kinetics at 10 μM Ca^{2+} (P = 0.005). Significance was tested using a repeated-measures two-way ANOVA.

Construct	$V_{1/2}$ (mV)			
	100 μM Ca^{2+}	**10 μM Ca^{2+}**	**1 μM Ca^{2+}**	**0 μM Ca^{2+}**
mBK_{QEERL}	-4 ± 4 (11)	49 ± 3 (10)	165 ± 5 (11)	193 ± 7 (15)
hBK	-14 ± 1 (18) * P = 0.01	53 ± 2 (28)	152 ± 3 (14) * P = 0.04	203 ± 7 (10)

Table 4: $V_{1/2}$ values for mBK_{QEERL} and hBK currents

Number of patches used for analysis is listed in parentheses. Significance (*, $P < 0.05$) was tested at each Ca^{2+} concentration using an unpaired *t*-test. Exact P value listed if $P < 0.05$.

5.3.2 Identification of four SNPs that regulate BK current properties

From a comprehensive table of known human *KCNMA1* SNPs (assembled by Jessica Lu), we predicted four SNPs that could potentially alter BK current properties. For this study we limited the SNPs chosen to ones that were linked with disease or in the gating ring (C-terminus) of the BK α-subunit, since the gating ring regulates of Ca^{2+}-dependent activation (Jiang et al., 2002; Xia et al., 2002; Yusifov et al., 2008; Zhang et al., 2010). We performed an extensive literature search to identify non-synonymous SNPs in functional domains of the C-terminus that regulate BK current properties, and to identify SNPs throughout the α-subunit implicated in pathophysiological conditions. Furthermore, we utilized MutPred and NetPhos to predict SNPs that would have a deleterious effect on protein function, or alter phosphorylation. Through this search, we identified four SNPs (A138V, C495G, N599D, and R800W) for further study (Figure 20).

A138V was chosen based on previous data identifying this SNP in a data set of 117 autistic patients (Laumonnier et al., 2006). In this study, whole-cell BK currents were isolated from lymphoblastoid cell lines isolated from one autistic patient and control patients, and it was found that BK currents from the autistic patient cell line were approximately 70% smaller than those of the control cells. Additionally, the resting membrane potential was significantly more depolarized (4.8 mV)(Laumonnier et al., 2006). These results suggest that A138V reduces current amplitude and may alter excitability, although the mechanism is unclear. The A138V mutation SNP had a MutPred score of 0.310, suggesting that there is a low probability that A138V has a deleterious effect on protein function. However, MutPred has limited predictive value on

some BK control mutations; for example, the mD959A mutation in the Ca^{2+} bowl causes a + 80 mV shift in the voltage at half of the maximum conductance as derived from the G-V Boltzmann fit ($V_{1/2}$) (Bao, 2004), even though the mutation has a low MutPred score (0.343).

C495G was chosen for experiments based on relevance of this residue in previous work (Zhang and Horrigan, 2005; Zhang et al., 2006), its position in a conserved linker region in RCK1 known to regulate the G-V relationship (Zhang and Horrigan, 2005), and because glycine residues convey flexibility to protein structures. In previous studies, C495A (mBK_{C430A}) inhibited the effect of cysteine-modifying reagents, which normally cause a negative-shift in the G-V relationship (Zhang and Horrigan, 2005). Additionally, mBK_{C430A} currents exhibited right-shifted $V_{1/2}$ values at low (≤1 μM) Ca^{2+} compared to WT channels (Zhang and Horrigan, 2005). In the context of hBK used in this study, MutPred predicted that C495G would have a deleterious effect on protein function (0.568), and the actionable hypothesis for C495G was a gain of disorder.

The third SNP chosen for this study was N599D. N599D was chosen because the SNP introduces a negatively-charged aspartic acid directly adjacent to E600 (mBK_{E535}), a residue critical to the Ca^{2+} sensing site in RCK1 (Zhang et al., 2010). $mBK_{E535,}$ along with $mBK_{D362/D367}$, are essential to the RCK1 Ca^{2+} sensing site. mBK_{E535A} caused a +100mV shift in the $\Delta V_{1/2}$, where $\Delta V_{1/2} = V_{1/2}$ (0 uM Ca^{2+}) – $V_{1/2}$ (100 uM Ca^{2+}), compared to the +200 mV shift in $\Delta V_{1/2}$ for WT channels. This indicates mBK_{E535A} reduces the Ca^{2+} sensitivity of BK channels, and that mBK_{E535} is essential for activation of BK channels by Ca^{2+}. Additionally, N599D was chosen because of its MutPred score of 0.713, although there were no actionable hypotheses associated with this mutation.

Because N599D (asparagine to aspartic acid) mutation is a non-conservative mutation that introduces a negatively-charged residue into the RCK1 Ca^{2+} sensing site, we hypothesized that N599D may alter the structure of the RCK1 Ca^{2+}-sensing site, which would affect Ca^{2+} sensing and subsequently alter the G-V relationship and kinetics of BK currents.

R800W, located within RCK2, was the fourth SNP chosen for experiments. R800W was chosen due to its vicinity to G798 and N801, two residues implicated in regulating the interface between RCK1 and RCK2 (Kim et al., 2008). Also, R800W is a non-conservative amino acid substitution, as the mutation increases the size of the residue and eliminates a positive charge. Furthermore, the R800W received a MutPred score of 0.706, with an actionable hypothesis for being a loss of methylation at R800.

G798 and N801 (G803 and N806 in the rat BK (rBK) sequence) are two residues thought to regulate the flexible interface that governs interaction between RCK1 and RCK2 (Kim et al., 2008). rBK_{G803D} caused a hyperpolarizing shift in the G-V relationship at multiple Ca^{2+} concentrations, while N806K caused a +45 mV hyperpolarizing shift. Furthermore, mutating rBK_{G803} to other residues introduced either hyperpolarizing (P, D, E, C, A), depolarizing (K), or no change to the $V_{1/2.}$ Because this data was performed on rBK, which contains a residue sequence at splice site 3, it is unknown whether G798 mutations would alter the structure and function of the hBK variant, which lacks the S3 exon. However, assuming that G798D alters hBK and rBK current properties through similar mechanisms, and because of R800W introduces a large, bulky tryptophan residue to the interface, we predict that R800W may alter the flexible interface between RCK1 and RCK2 and therefore affect current properties.

SNP	Location	Previous experiments	Nature of substitution	MutPred Score
A138V	S0-S1 Linker	• Linked with autism • Reduced current amplitude in autistic patient	Conservative	0.310
C495G	RCK1	• Mediates effects of MTS reagents • Affects current rundown due to oxidation	Introduction of glycine (flexibility)	0.568
N599D	RCK1	E600 regulates RCK1 Ca^{2+} sensing site	Introduction of negative charge	0.713
R800W	RCK2	G798 and N801 regulate RCK1/RCK2 flexible interface	Elimination of positive charge, introduction of bulky residue	0.706
Control Mutations	**Location**	**Effect**	**Nature of substitution**	**MutPred Score**
R272Q	S4	• Enhances voltage-dependence of activation • Leftshift in G-V Relationship	Deletion of positive charge	0.885
D434G	RCK1	• Enhances voltage-dependence of activation • Leftshift in G-V	Deletion of negative charge	0.570
D959A	RCK2	• Decreases voltage-dependence of activation • Right-shift in G-V in presence of Ca^{2+}	Deletion of negative charge	0.343

Table 5: Summary of the properties of SNPs chosen for experiments

hBK SNPs chosen for experiments are listed, along with their location in the channel structure. The rationale for each SNP, including previous work at or near the residues of interest, the nature of the amino acid substitution, and MutPred score are also listed. Mutations previously determined to affect BK current properties were used as controls to determine the ability of MutPred to predict deleterious mutations in protein function.

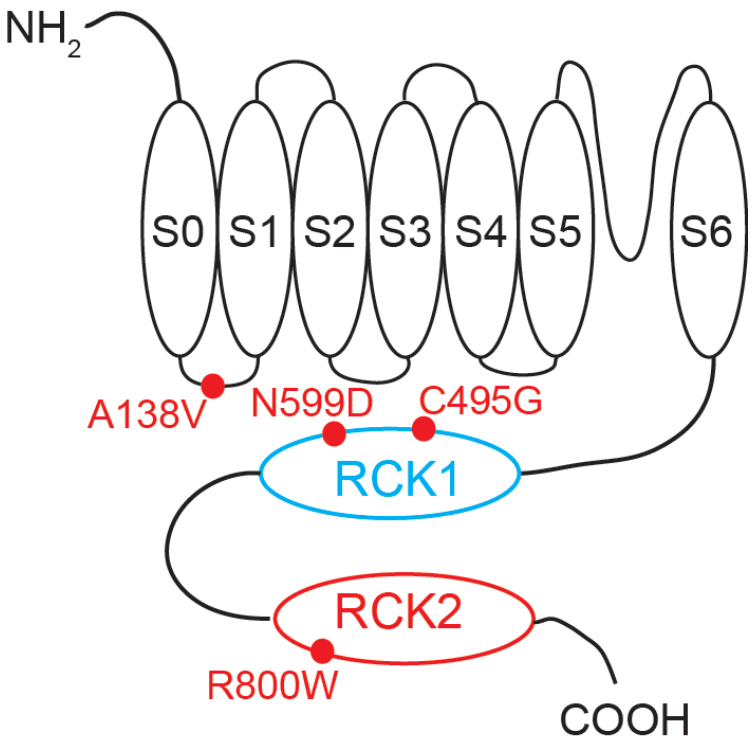

Figure 20: Location of *KCNMA1* SNPs used in this study

Schematic of one BK channel α-subunit. SNPs chosen for this study are denoted by red circles.

5.3.3 C495G, N599D, and R800W regulate steady state current properties

To investigate the effect of SNPs on steady-state BK current properties, we first expressed SNP-containing BK channels in HEK293T cells and recorded macroscopic BK currents in an inside-out patch configuration in symmetrical K^+ at 0, 1, 10, and 100 μM intracellular Ca^{2+} (Figure 21). The effects of SNPs on BK current G-V relationships, activation, and deactivation kinetics varied depending on the Ca^{2+} concentration used for recordings. At 100 μM Ca^{2+}, the G-V relationship for A138V, C495G, N599D, and R800W were all significantly right-shifted compared to hBK (Figure 22) as the $V_{1/2}$ for hBK was 11 to 18 mV more depolarized than the $V_{1/2}$ for each SNP (Table 6). Accompanying the right-shift in G-V relationship, we found that A138V, C495G, N599D and R800W currents all also exhibited slower time constants of activation (τ_{Act}, Figure 23) and faster time constants of deactivation (τ_{Deact}, Figure 24).

At 10 μM Ca^{2+}, the G-V relationship of C495G currents was significantly left-shifted compared to hBK, suggesting that C495G enables BK channels to open more easily at 10 μM Ca^{2+} (Figure 22B). Correlating with the depolarized G-V relationship, C495G currents also exhibited slightly faster τ_{Act} (Figure 23B) and slower τ_{Deact} (Figure 24B), than hBK currents. Interestingly at 10 μM Ca^{2+}, R800W currents had $V_{1/2}$ values that were significantly more positive compared to hBK, and R800W currents exhibited slower τ_{Act} (Figure 23D) and faster τ_{Deact} (Figure 24D). This suggests that R800W channels open less-easily compared to hBK at 10 μM Ca^{2+}. Unlike C495G and R800W, which demonstrated different $V_{1/2}$ and kinetic properties at 10 μM Ca^{2+}, the $V_{1/2}$ values for A138V and N599D were not significantly different from hBK at 10 μM Ca^{2+} (Table 6). Also, τ_{Act} and τ_{Deact} were similar between A138V, N599D, and hBK (Figure 23,

Figure 24), further suggesting that these mutant constructs behaved similarly to hBK at 10 μM Ca^{2+}.

At 1 μM Ca^{2+}, the effects of SNPs on steady-state current properties were complex. The leftward shift in G-V and faster activation kinetics compared to hBK exhibited by C495G at 10 μM Ca^{2+} was also observed at 1 μM Ca^{2+}, as C495G currents demonstrated an 8 mV, albeit not statistically significant, hyperpolarizing shift in the $V_{1/2}$ compared to hBK (Table 6), as well as faster τ_{Act} (Figure 23B). The G-V relationship of R800W currents, similar to what occurred at 100 and 10 μM Ca^{2+}, was approximately 20 mV right-shifted compared to hBK (Figure 22D). The right-shift in G-V relationship was accompanied by slower τ_{Act} and faster τ_{Deact} (Figure 23D, Figure 24D). This suggests that R800W causes BK channels to open less easily in 1 μM Ca^{2+}. Interestingly, N599D currents, which did not cause a significant shift in $V_{1/2}$ at 10 μM Ca^{2+}, induced a 20mV depolarizing shift in $V_{1/2}$ compared to hBK (Figure 22C, Table 6) and N599D currents exhibited slower τ_{Act} (Figure 23C), suggesting that the N599D mutation causes BK channels to open less easily at low Ca^{2+} concentrations compared to the hBK. The G-V relationship, activation and deactivation time constants for A138V currents at 1 μM Ca^{2+} were not significantly different from hBK (Figure 22A, Figure 23A, Figure 24A).

Lastly at 0 μM Ca^{2+}, we found no significant differences in the G-V relationship, activation and deactivation time constants between hBK and A138V, C495G, and N599D currents (Figure 22, Figure 23, Figure 24). Although the G-V relationship and τ_{Deact} at 0 μM Ca^{2+} were not different between R800W and hBK (Figure 22D, Figure 24D, Table 6), surprisingly we found that R800W currents still demonstrated slower τ_{Act} (Figure 23D). Because the primary effects of these SNPs on BK current properties only in the

presence of low (1 μM), intermediate (10 μM), or saturating (100 μM) Ca^{2+} rather than under Ca^{2+}-free conditions, this data suggests that the SNPs we investigated primarily regulate BK current properties by altering BK channels' ability to be gated by Ca^{2+}.

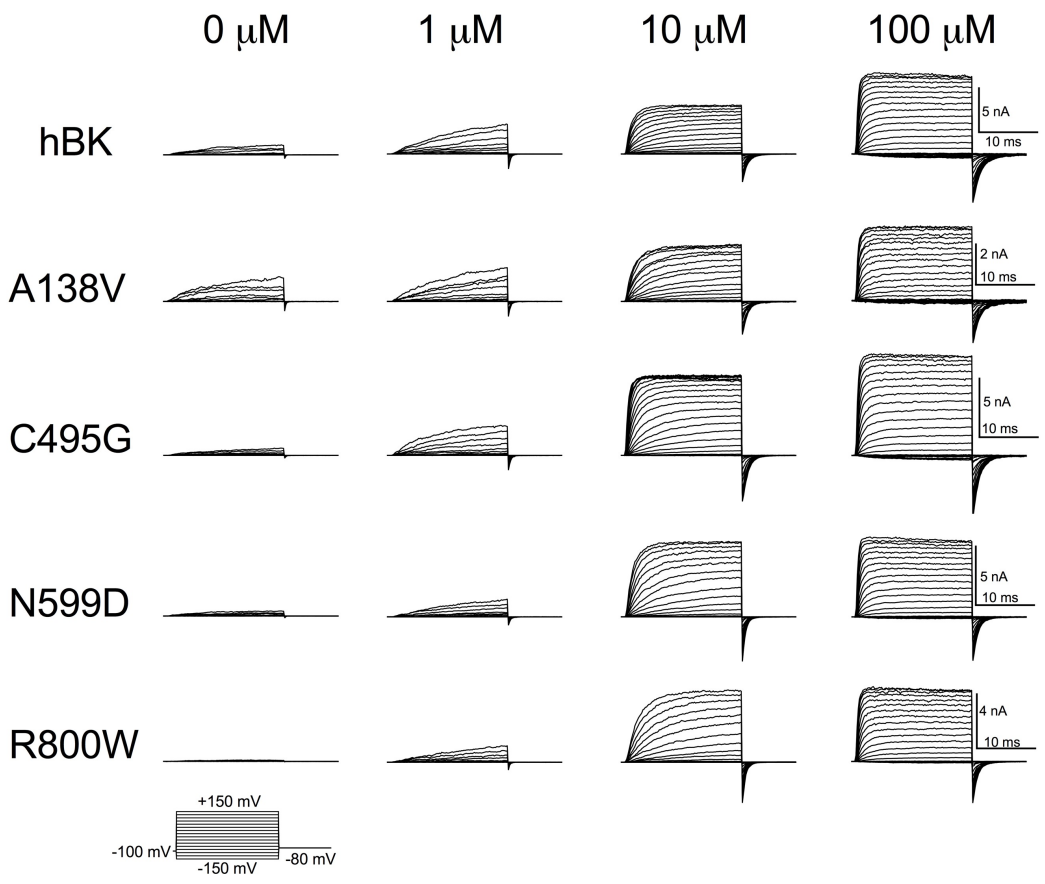

Figure 21: hBK and hBK SNP currents in symmetrical K^+

Representative macroscopic BK current traces recorded at the indicated Ca^{2+} concentration from inside-out patches from hBK and hBK SNPs. Currents were recorded from individual patches at each Ca^{2+} concentration.

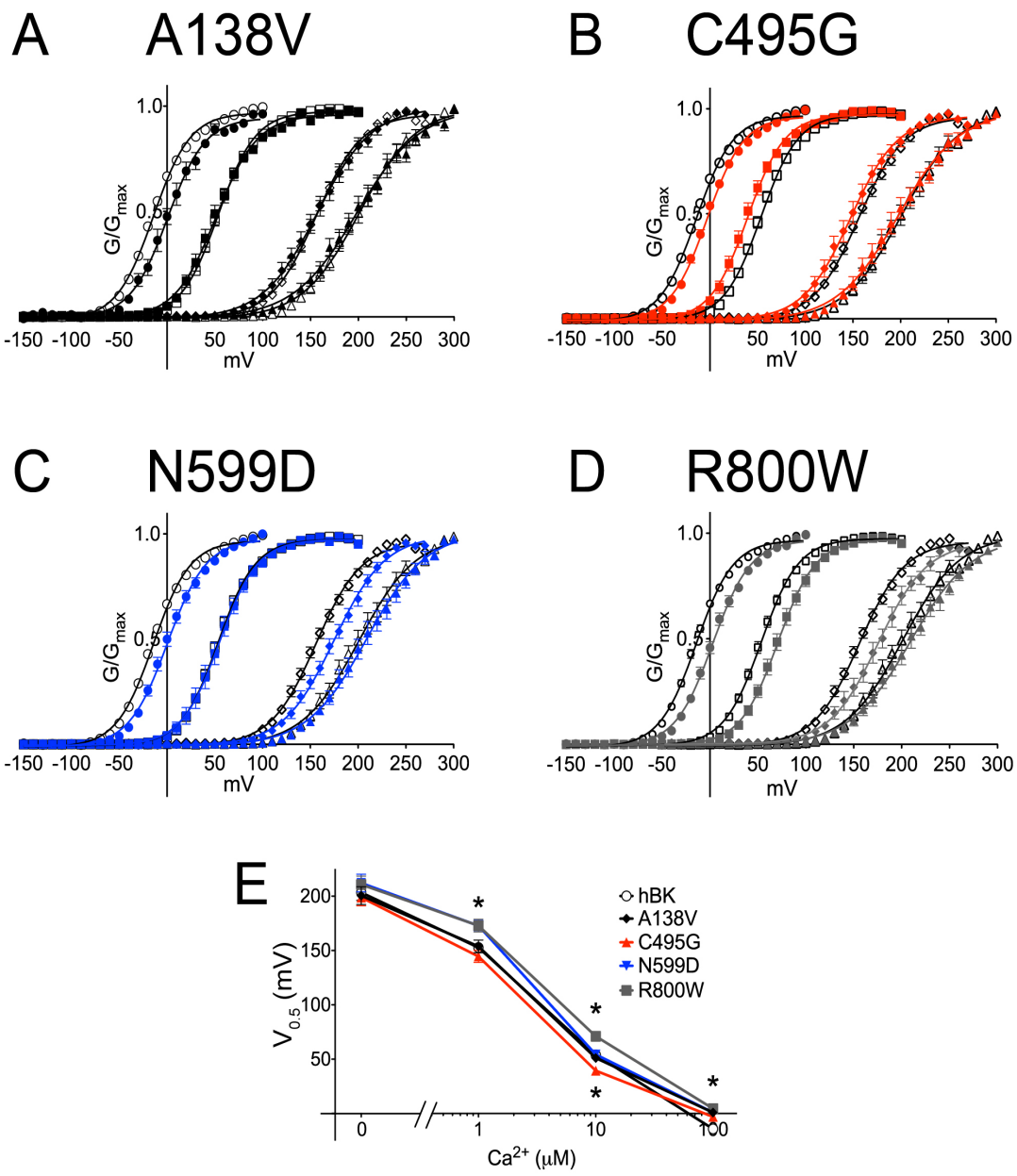

Figure 22: G-V relationship of hBK SNP currents in symmetrical K^+

(A-D) G-V relationships between hBK and A138V, C495G, N599D, and R800W currents. hBK is denoted by open symbols and hBK SNPs are denoted by shaded symbols at 100 (circles), 10 (squares), 1 (diamonds), 0 μM (triangles) Ca^{2+}. (E) Plot of $V_{1/2}$ versus Ca^{2+} exemplifying differences in the voltage-dependence of activation between hBK and BK channel SNPs at each Ca^{2+} concentration. Significance (*, $P < 0.05$) was tested within each Ca^{2+} concentration using a one-way ANOVA. $V_{1/2}$, P values, and number of patches analyzed at each Ca^{2+} concentration are listed in Table 6.

Construct	$V_{1/2}$ (mV)			
	100 μM Ca^{2+}	**10 μM Ca^{2+}**	**1 μM Ca^{2+}**	**0 μM Ca^{2+}**
hBK	-14 ± 1 (18)	53 ± 2 (28)	152 ± 3 (14)	203 ± 7 (10)
A138V	0 ± 3 (9) * P = 0.001	51 ± 3 (8)	153 ± 5 (9)	200 ± 8 (8)
C495G	-3 ± 1 (15) * P = 0.009	39 ± 3 (10) * P = 0.019	144 ± 5 (10)	198 ± 7 (10)
N599D	0 ± 2 (15) * P = 1×10^{-4}	54 ± 4 (12)	172 ± 4 (11) * P = 0.029	212 ± 8 (11)
R800W	3 ± 2 (19) * P = 1×10^{-6}	71 ± 3 (16) * P = 2×10^{-4}	172 ± 5 (10) * P = 0.035	210 ± 7 (11)

Table 6: $V_{1/2}$ values for hBK and hBK SNP currents

Number of patches used to acquire data at each Ca^{2+} concentration is denoted in parenthesis. Significance (*, $P < 0.05$) was tested using a one-way ANOVA within each Ca^{2+} concentration. P value is listed if $P < 0.05$.

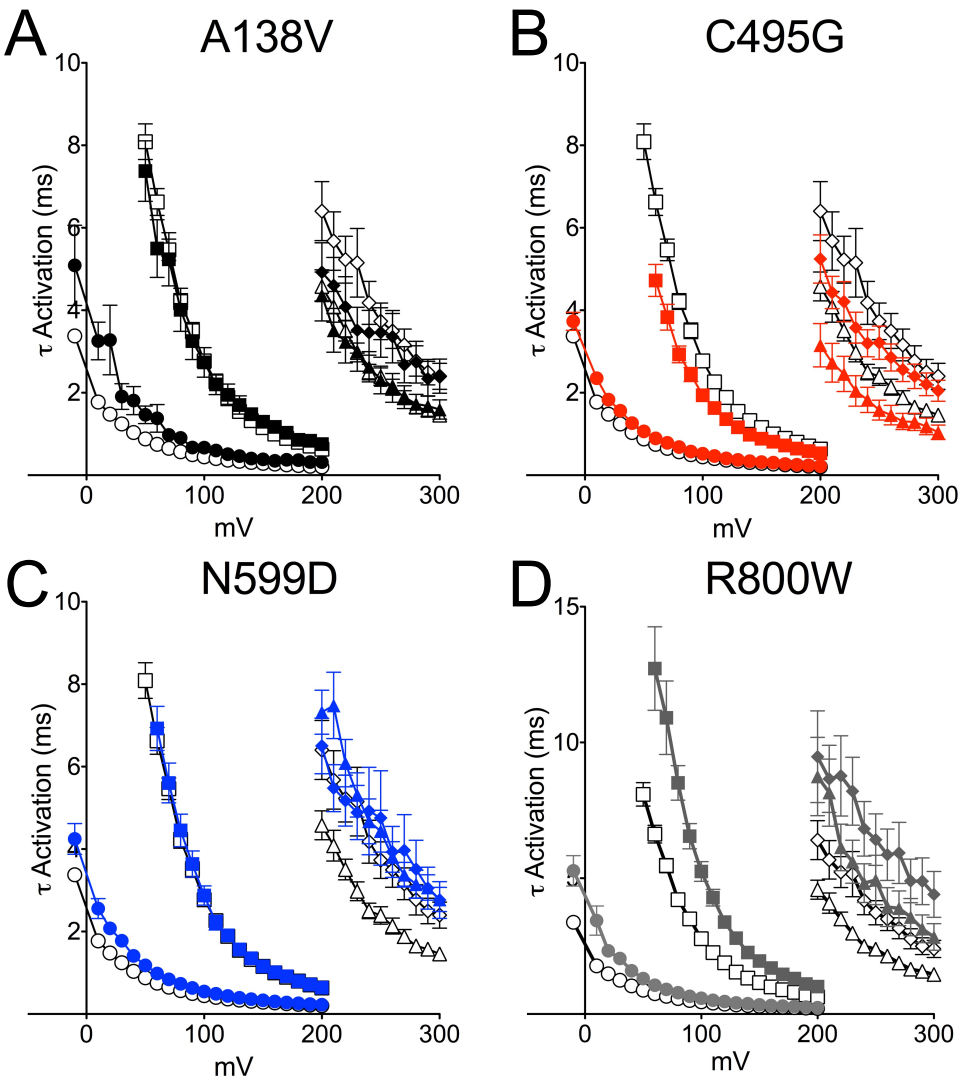

Figure 23: Activation kinetics for hBK SNPs in symmetrical K^+

Activation kinetics were determined by fitting the rising phase of hBK (open symbol) and hBK SNP (closed symbols) currents to single exponential functions at 0 (diamond), 1 (triangle), 10 (square), and 100 (circle) μM Ca^{2+}. Significant differences in activation kinetics were found at 100 μM (A138V, $P < 0.001$; C495G, $P < 0.001$; N599D, $P = 0.001$; R800W, $P < 0.001$), 10 μM (C495G, $P = 0.002$; R800W, $P < 0.001$), 1 μM (C495G, $P = 0.032$; N599D, $P < 0.001$; R800W, $P = 0.001$), and 0 μM Ca^{2+} (R800W, $P = 0.028$). Significance ($P < 0.05$) was tested using a two-way repeated measures ANOVA.

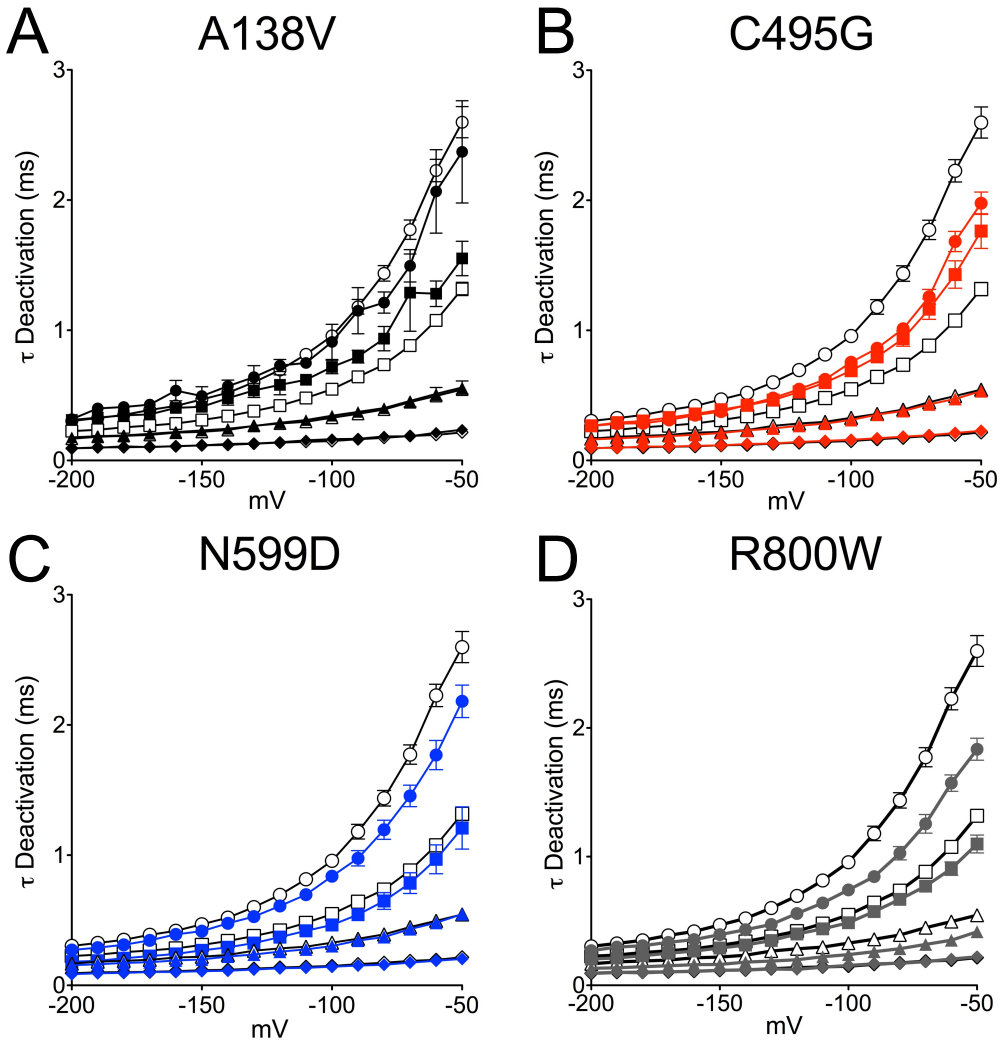

Figure 24: Deactivation kinetics for hBK SNPs in symmetrical K^+

Deactivation kinetics were determined by fitting tail currents of hBK (open symbol) and hBK SNP (closed symbols) currents to single exponential functions at 0 (diamond), 1 (triangle), 10 (square), and 100 (circle) μM Ca^{2+}. Significant differences in deactivation kinetics were found between hBK and hBK SNPs at 100 μM (C495G, $P < 0.001$; N599D, $P = 0.016$; R800W, $P < 0.001$), 10 μM (A138V, $P = 0.002$; C495G, $P < 0.001$), and 1 μM Ca^{2+} (R800W, $P < 0.001$). Significance ($P < 0.05$) was tested using a two-way repeated measures ANOVA.

5.3.4 C495G and R800W alter BK current activation kinetics in physiological solutions

To determine whether the altered G-V relationships and current kinetics caused by BK channel SNPs would still occur under physiological conditions, we next recorded macroscopic BK currents in a physiological K^+ gradient. We recorded currents in physiological concentrations of Na^+ (10 mM internal/134 mM external) and K^+ (140 mM internal/6 mM external)(Herrera et al., 2002). Although an extensive amount of work has examined the effect of C-terminal mutations on BK current properties (Kim et al., 2008; Yang et al., 2010; Zhang and Horrigan, 2005; Zhang et al., 2010), few studies examine the properties of BK currents evoked in physiological K^+. Because C495G and R800W currents exhibited altered G-V relationships and current kinetics in symmetrical K^+, we hypothesized that C495G and R800W would also affect these BK current properties in physiological K^+.

To test the hypothesis that C495G and R800W regulate BK current properties in physiological K^+, we first recorded macroscopic BK currents evoked by square voltage steps in an inside-out patch configuration. These experiments were performed with 10 μM intracellular Ca^{2+}, as 10 μM Ca^{2+} is a physiologically-relevant Ca^{2+} concentration that activates BK currents at both Ca^{2+} spark sites and in Ca_V channel/BK channel nanodomain complexes (Berkefeld et al., 2006; Fakler and Adelman, 2008; Perez et al., 2001). Additionally, we chose 10 μM Ca^{2+} because C495G and R800W altered the G-V and current kinetics at 10 μM Ca^{2+} in symmetrical K^+ solutions. Interestingly, although we observed left and right-shifts in the G-V relationship with C495G and R800W, respectively in symmetrical K^+ (Figure 22, Table 6), we did not observe significant shifts in the G-V relationship with either C495G or R800W currents (Figure 25B). However,

C495G currents still had faster τ_{Act}, and R800W currents had slower τ_{Act} compared to hBK currents (Figure 25C), which mimicked the trend observed in symmetrical K^+ solutions. Deactivation kinetics between hBK, C495G, and R800W currents were not significantly different (Figure 25D). Similar to our results in symmetrical K^+, A138V and N599D currents exhibited similar G-V relationships and τ_{Act} compared to hBK currents in physiological K^+ solutions (Figure 25).

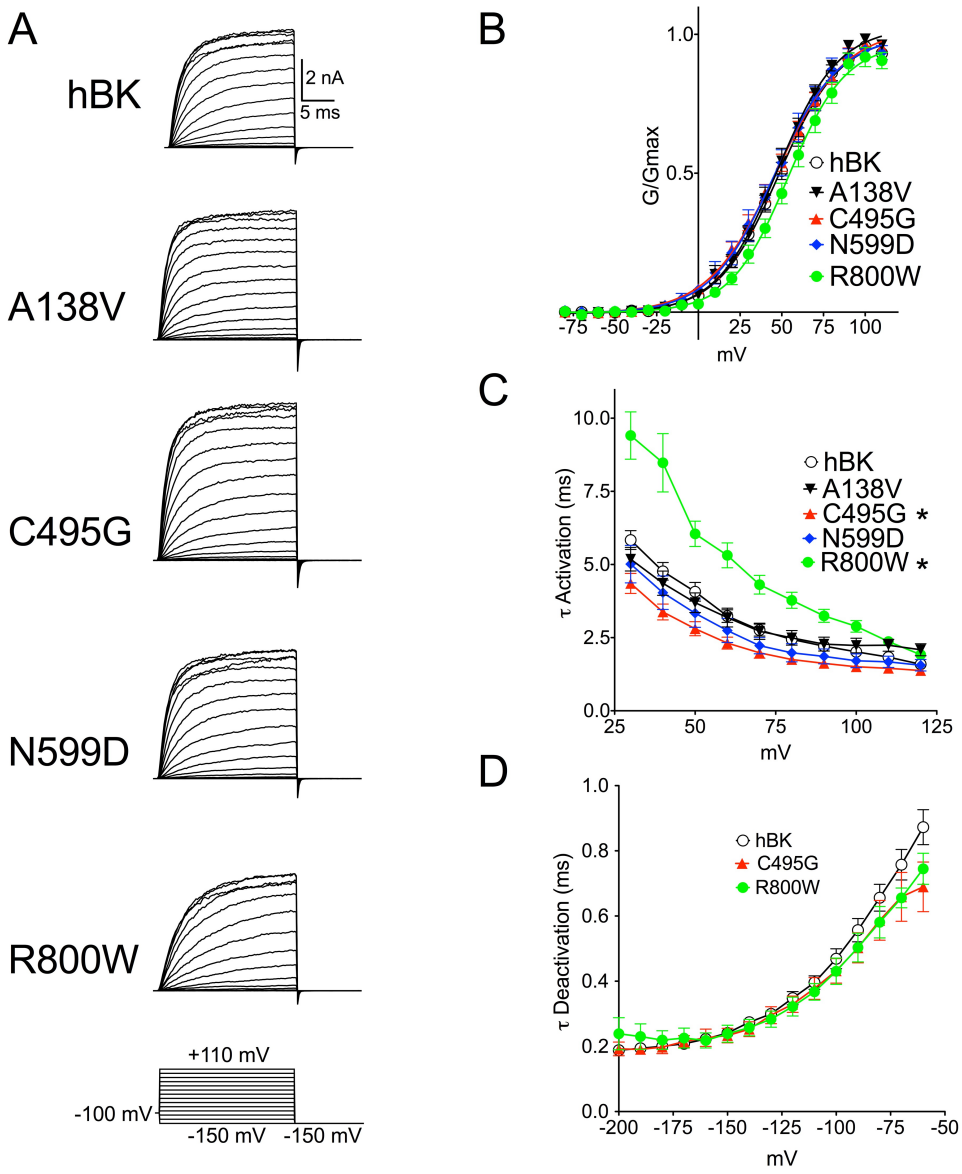

Figure 25: Characterization of hBK SNPs in physiological K^+

(A) Representative macroscopic current traces from hBK and hBK SNPs at 10 μM intracellular Ca^{2+}. (B) G-V relationship between hBK and hBK SNPs. (C) Activation time constants for hBK SNP currents. Time constants were determined by fitting the rising phase of the currents to single exponential functions. (D) Deactivation time constants for hBK, C495G, and R800W currents. Time constants were determined by fitting tail currents to single exponential functions. Significant differences in activation kinetics were found between hBK and C495G ($P = 0.004$) and R800W ($P < 0.001$). Statistical significance with activation/deactivation kinetics was tested using a two-way repeated measures ANOVA with Bonferroni post-hoc test. $n = 9 – 18$ patches analyzed per BK channel variant.

5.3.5 C495G and R800W regulate BK currents evoked by action potentials

To test the hypothesis that *KCNMA1* SNPs alter BK currents evoked under physiological conditions, we measured peak BK current amplitudes evoked by action potential waveforms obtained from mouse SCN neurons, mouse urinary bladder cells, and mouse SANCs. These cell types were chosen because BK currents regulate the excitability of each of these cells, and these action potentials exhibit a range of driving forces and depolarization rates (Heppner et al., 1997; Lai et al., 2014; Shelley et al., 2013). Because the G-V relationships and deactivation kinetics for each SNP were similar in physiological K^+, we predicted that the currents amplitudes elicited by C495G and R800W channels may differ compared to hBK currents due to altered activation kinetics.

We predicted that SNP-induced changes in activation kinetics would alter the action potential-evoked current amplitude because of the depolarization rate of the utilized action potentials. The peak current is a function of the current activation kinetics, since currents with slower τ_{Act} require more time to reach a maximally "activated" state than currents with faster τ_{Act}. Therefore, action potentials with longer depolarization rates, such as the SANC action potential, will enable BK currents more time to reach a maximally activated state than action potentials with shorter depolarization rates, such as the SCN neuron action potentials (Figure 26A). Example action potential evoked currents from each action potential stimulus is provided in Figure 26B.

After recording macroscopic currents in response to square voltage steps from each patch, the patch was subjected to the four action potential waveforms to evoke BK currents. To compare hBK current amplitudes with BK-SNP current amplitudes, the

action potential-evoked current was normalized to the maximum outward current evoked from each patch using the square voltage step protocol. When comparing the peak normalized current evoked by SCN_{Day} action potentials, we found that C495G currents were significantly larger than hBK currents, while R800W currents were significantly reduced compared to hBK currents (Figure 27A). The amplitudes of A138V and N599D currents evoked by SCN_{Day} were not significantly different than hBK currents (Figure 27A). When utilizing the SCN_{Night} action potential, which has a more depolarized resting membrane potential, slower upstroke velocity, longer half-width, and less depolarized peak potential compared to SCN_{Day} (Figure 27B), we found that C495G currents trended towards having larger currents, while R800W normalized currents were significantly smaller compared to hBK currents (Figure 27B). The amplitudes of the currents evoked by SCN_{Day} and SCN_{Night} correlate well with the activation kinetics observed with C495G and R800W patches in physiological K^+, since C495G currents had more rapid τ_{Act} and R800W currents had slower τ_{Act} (Figure 25C). As expected based on the symmetrical K^+ data at 10 μM Ca^{2+} (Figure 22-24), and the lack of difference in G-V relationship, or activation kinetics in physiological K^+ (Figure 25), A138V and N599D did not exhibit significantly altered normalized peak-current amplitudes with either the SCN_{Day} or SCN_{Night} action potentials (Figure 27A, Figure 27B).

Next, we examined BK currents evoked by bladder smooth muscle cell and mouse SANC action potential waveforms. Utilizing the bladder smooth muscle action potential, C495G currents trended towards being larger than hBK currents and R800W currents trended towards being smaller than hBK currents (Figure 27C). A138V and N599D currents were not statistically different than hBK currents (Figure 27C). When

analyzing currents evoked by SANC action potentials, which had the longest duration and largest peak amplitude of the action potentials used for experiments, we found that R800W normalized currents were significantly reduced compared to hBK currents (Figure 27D). A138V, C495G, N599D did not significantly affect the peak current evoked by a SANC action potential (Figure 27D). Interestingly, the difference in peak current amplitudes between C495G and R800W with hBK was less when evoking currents with the SANC action potentials and bladder action potentials, which were appreciably longer, than with SCN_{Day} or SCN_{Night} action potentials. This data suggests that BK current activation kinetics play an essential role in determining the peak amplitude of BK currents evoked by a physiological stimulus in physiological K^+, and that this trend becomes less apparent with longer depolarizing stimuli that allow BK currents to fully activate.

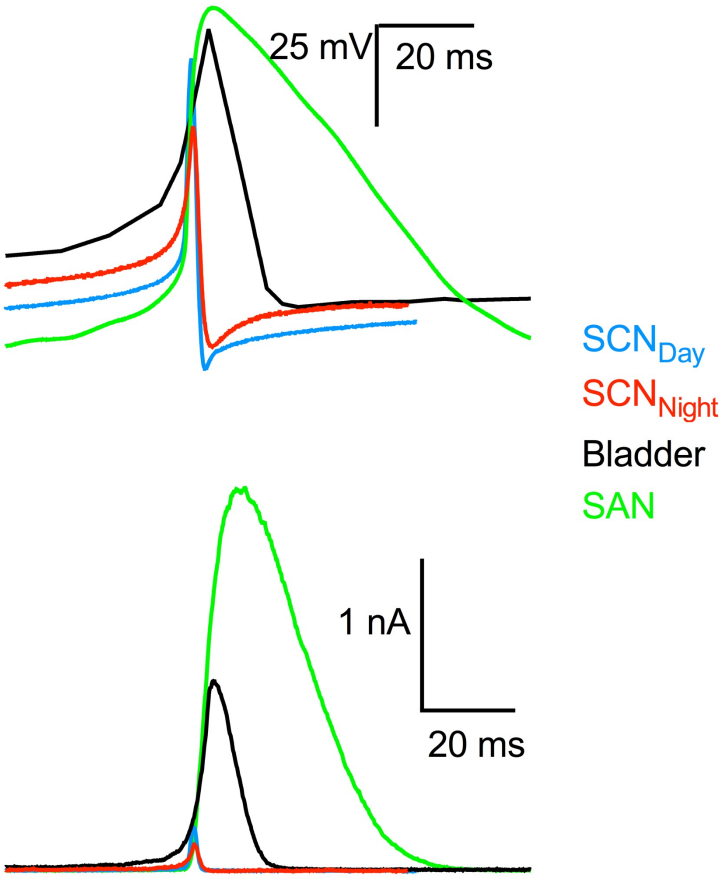

Figure 26: Action potential waveforms used for recordings and corresponding evoked currents

(A) Schematic of representative action potential waveforms (A) and corresponding evoked BK currents (B). Evoked currents were recorded from a single patch expressing hBK channels subjected to all four action potential voltage commands.

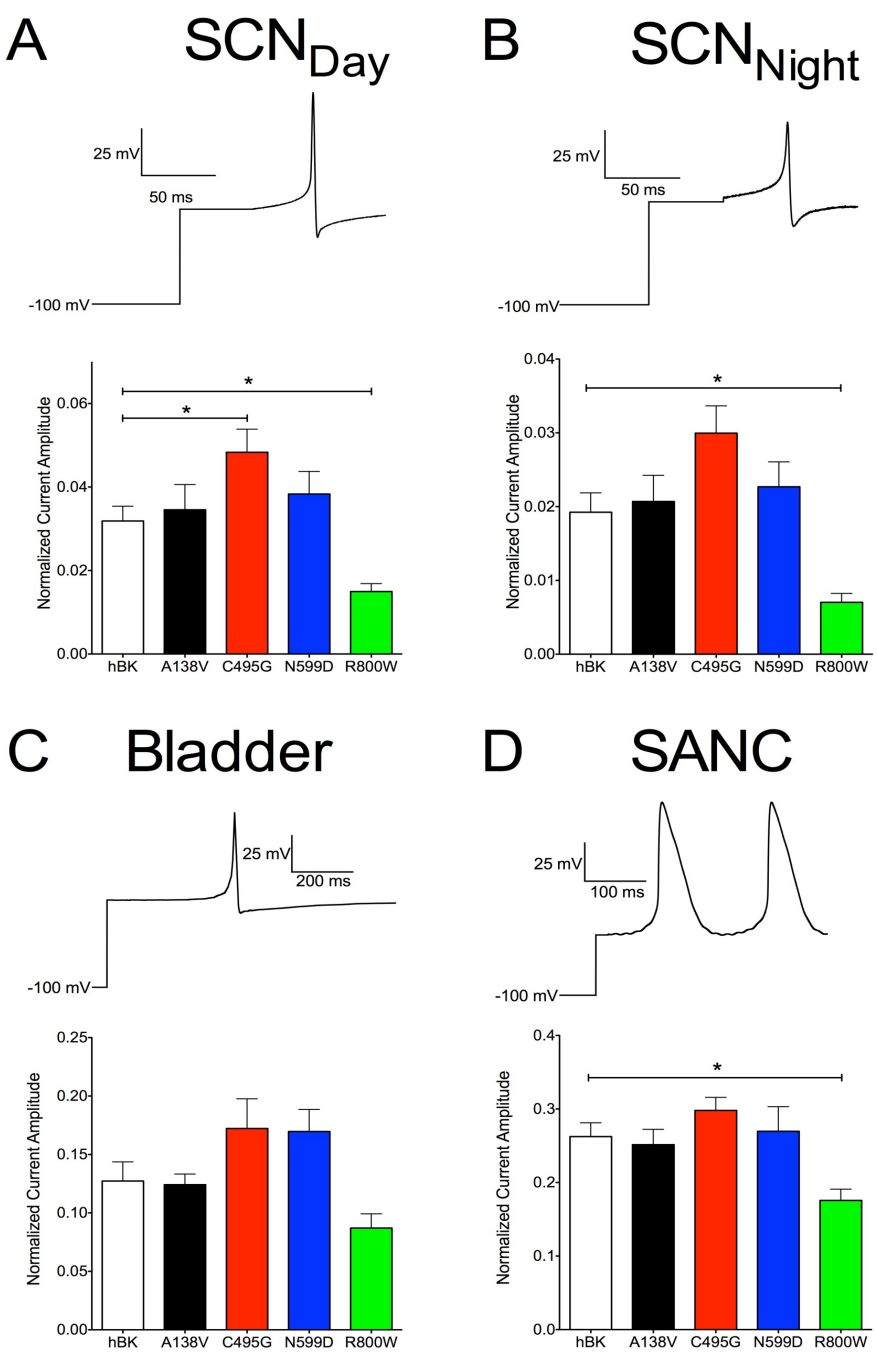

Figure 27: Normalized BK current amplitudes evoked by action potentials

Action potential voltage commands and corresponding normalized current amplitudes evoked by SCN_{Day} (A), SCN_{Night} (B), bladder cell (C), and SANC (D) action potentials. The current amplitudes evoked by the SAN action potential (D) were measured from the current evoked by the second action potential. Asterisks denote significance where $P < 0.05$. Significance was tested using a one-way ANOVA. Number of patches per experiment and exact P values are listed in Table 7.

Construct	Normalized Current Amplitude			
	SCN_{Day}	**SCN_{Night}**	**Bladder**	**SAN**
hBK	0.031 ± 0.003 (18)	0.019 ± 0.002 (18)	0.127 ± 0.016 (11)	0.262 ± 0.018 (18)
A138V	0.034 ± 0.006 (10)	0.020 ± 0.003 (10)	0.124 ± 0.009 (6)	0.251 ± 0.020 (10)
C495G	0.048 ± 0.005 (17) * P = 0.049	0.029 ± 0.003 (17)	0.172 ± 0.025 (9)	0.298 ± 0.017 (17)
N599D	0.038 ± 0.005 (8)	0.022 ± 0.003 (8)	0.169 ± 0.018 (5)	0.269 ± 0.033 (8)
R800W	0.019 ± 0.006 (17) * P = 0.039	0.007 ± 0.001 (17) * P = 0.017	0.087 ± 0.012 (9)	0.175 ± 0.015 (17) * P = 0.009

Table 7: Normalized current amplitudes in response to action potential waveforms

Normalized current amplitudes of BK currents evoked by action potential waveforms. Numbers in parenthesis indicate the number of patches analyzed per condition. Asterisks denote statistical significance ($P < 0.05$) from hBK using a one-way ANOVA.

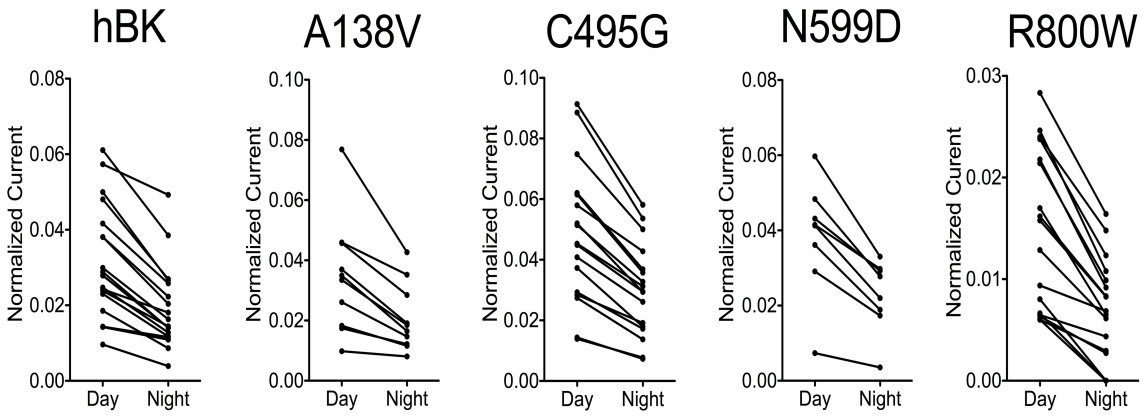

Figure 28: Paired normalized current amplitudes evoked by BK channels in response to SCN action potentials

Because three out of 17 R800W patches did not evoke current in response to SCN_{Night} action potentials, we verified that all patches evoked current in response to SCN_{Day} action potentials. Normalized currents evoked by SCN_{Night} action potentials were always lower than currents evoked by SCN_{Day} action potentials, suggesting that differences in current properties, and differences in the amplitude of the action potential are essential in determining the amplitude of the peak BK current evoked by action potentials.

5.4 ***Discussion***

BK current properties are determined by multiple factors, such as phosphorylation (Yan et al., 2008), alternative splicing (Johnson et al., 2011; Shelley et al., 2013; Xie and McCobb, 1998), and auxiliary subunits (Brenner et al., 2000a; 2005; Yan and Aldrich, 2010), but few studies have addressed *KCNMA1* SNPs or the effect of SNPs on BK current properties (Du et al., 2005; Jiao et al., 2011; Klassen et al., 2011; Laumonnier et al., 2006). In this study, we identified that SNPs can modulate BK current properties, and that SNP-induced changes in BK current properties may affect the amplitude of BK currents evoked by action potentials. This data suggests that SNPs in *KCNMA1* are an under-investigated mechanism of BK current diversity.

5.4.1 SNPs alter BK current properties in symmetrical K^+

A138V, which is linked with autism, is one of the few BK SNPs that has been linked with disease (Laumonnier et al., 2006). Although we hypothesized that autism may be linked with differences in BK current properties, interestingly we found that BK current properties were not affected by A138V in symmetrical K^+. In the previous report, BK currents recorded from a cell line obtained from an autistic patient with the A138V SNP were smaller than BK currents from control patient cells. Interestingly, we found that A138V expression was lower visually compared to hBK and other hBK SNPs (Figure 29), and although current properties were not greatly affected, the magnitude of currents evoked by A138V channels trended lower than the amplitudes of hBK currents (data not shown). Previous analysis of this sequence suggests that this substitution creates a splice donor site in the second exon, which could potentially affect A138V channel expression (Guglielmi et al., 2015; Laumonnier et al., 2006). Combined, this

suggests that the lower current density in A138V patient cells may be due to differences in channel expression and trafficking, rather than changes in current properties.

C495G induced different effects on the G-V relationship compared to other studies that examined the effect of mutations at C495. C495 (mBK_{C430}) is within a series of 8 amino acids in RCK1 that links an α-helix and β-sheet, and this linker is conserved among BK channels but not other K^+ channels (Zhang and Horrigan, 2005). Because deletion of the linker causes a left-shift in the G-V relationship, it suggests that modifications of mBK_{C430} disrupt the linker or the linker's interactions with other residues in the gating ring (Zhang and Horrigan, 2005). Interestingly, BK currents evoked from C495G-containing channels at 1 and 10 μM exhibited "gain-of-function" properties, as the G-V relationship was shifted to more hyperpolarized potentials (Figure 22), and C495G currents exhibited faster τ_{Act} compared to hBK currents (Figure 23B). Based on the previous studies and our findings, our results suggest that the C495G SNP may influence the structure the αD-βD linker in RCK1 and its interaction with surrounding residues. Potentially, the glycine residue causes the αD-βD linker to become more flexible and alters the structure of the gating ring in the presence of Ca^{2+}. Further studies, such as recording currents when C495 is mutated to residues that convey less flexibility, would be required to test this hypothesis.

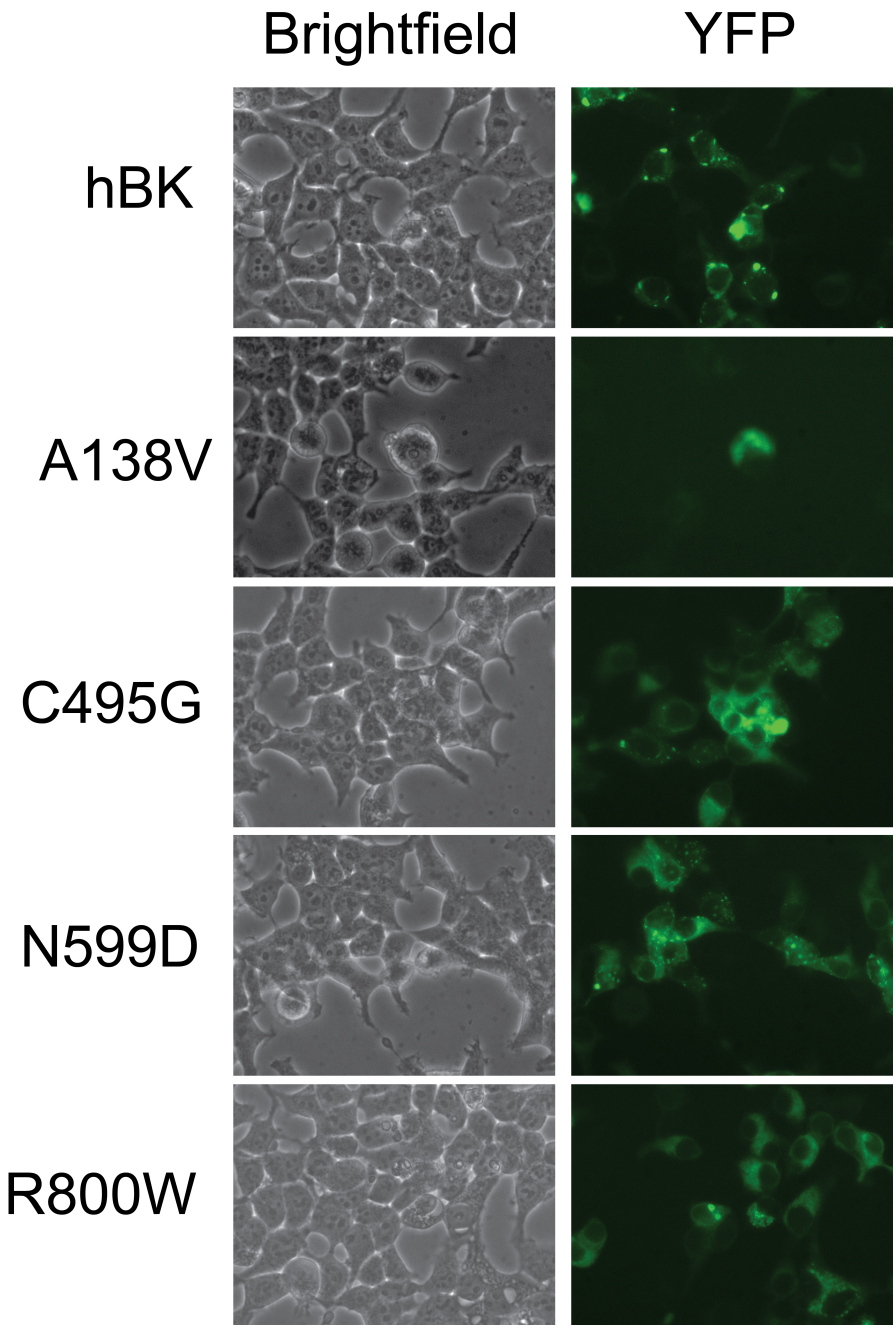

Figure 29: Expression of hBK and hBK SNPs in HEK293T cells

Representative images acquired of HEK293T cells expressing hBK channel constructs. Transfections were performed using TransIt LT-1 transfection reagent. Images were acquired at 40x magnification.

The effects of N599D on BK current properties were also complex. Previous mutations of N599 (mBK_{N534A}) cause a relatively small effect on the G-V relationship compared to mutations at E600 (mBK_{E535A}), a residue critical in RCK1 Ca^{2+} sensing (Zhang et al., 2010). We hypothesized that N599D may alter the structure of the RCK1 Ca^{2+} sensing site in the presence of Ca^{2+}, since the SNP introduces a negatively charged residue directly next to E600. Based on our data in low intracellular Ca^{2+} (1 μM Ca^{2+}), the negative charge introduced by N599D may disrupt the interaction of the RCK1 Ca^{2+} sensing site with other residues within the gating ring, and therefore alter the G-V relationship and activation kinetics. It is unknown how N599D would affect the way Ca^{2+} ions interact with the high-affinity Ca^{2+} sensing site in RCK1, since crystal structures of the gating ring lack Ca^{2+} ions at the RCK1 Ca^{2+} sensing site (Yuan et al., 2011). Therefore, further studies would be required to understand the structural mechanism that enables N599D to regulate BK current properties in low Ca^{2+} conditions.

R800W caused the most consistent effect on BK current properties, as R800W currents generally exhibited loss-of-function properties. R800W is located near a proposed flexible interface between RCK1 and RCK2, and mutations of residues in the vicinity of R800W in the rat BK channel (rBK_{G803D}) cause a negative shift in the G-V relationship, and an increase in the single channel P_O (Kim et al., 2008). Because R800 itself was not mutated in this study and is not the focus of any previous crystal structure studies, the role of R800 in regulating the G-V or the rate at which the pore opens is unclear. It can be hypothesized that elimination of the positive charge and addition of a large, bulky tryptophan residue may disrupt the RCK1/RCK2 interface, therefore affecting the structural change in the gating ring that occurs in the presence of Ca^{2+}.

We did not observe any change in G-V relationship with any of the SNPs we analyzed at 0 μM Ca^{2+} (Figure 22, Table 6). Because previous studies that delete or mutate residues directly involved in Ca^{2+} coordination do not have a significant effect on the G-V relationship or $V_{1/2}$ values in 0 μM Ca^{2+} conditions (Xia et al., 2002; Zhang et al., 2010), it was not surprising that we did not find significant differences in the G-V or $V_{1/2}$ values between hBK and hBK-SNP channels. Similar to what occurred in the presence of Ca^{2+}, R800W caused an increase in the τ_{Act} at 0 μM Ca^{2+} (Figure 23), indicating that R800W currents activate slower compared to hBK currents under Ca^{2+}-free conditions. Further studies, especially ones that examine the crystal structure around this residue, would be necessary in order to understand the mechanism underlying R800W's effects on current activation kinetics under nominal Ca^{2+} conditions.

5.4.2 SNPs alter BK current activation kinetics in physiological K^+ solutions

Unexpectedly, the effects of SNPs on current properties were different in symmetrical and physiological K^+ solutions. We found that the shifts in G-V relationship observed in symmetrical K^+ due to BK SNPs were not present in physiological K^+, but the changes in activation kinetics were maintained (Figure 25C). It is unknown how physiological solutions would affect the structure of the C-terminus or Ca^{2+}-dependent activation of BK currents. However, differing results in G-V relationships in symmetrical and physiological K^+ solutions have been previously reported (Jaffe et al., 2011; Wang et al., 2009; 2014). It could be speculated that the ionic environment created by physiological solutions alters the coupling between the voltage-sensor, pore, and gating ring. We did observe block of BK currents by Na^+ in physiological solutions at potentials greater than +120 mV (data not shown), but it is unknown whether Na^+

precluded any affects on the G-V. Further experiments, would be required to understand the mechanism underlying why SNPs have differing effects on G-V relationships in symmetrical and physiological K^+ solutions. Additionally, further experiments could be performed at different intracellular Ca^{2+} concentrations to identify if shifts in the G-V relationship occur in physiological solutions at different Ca^{2+} concentrations.

5.4.3 BK channel SNPs alter the amplitude of currents evoked by physiological stimuli

Despite SNPs not affecting BK current G-V relationships in physiological K^+, the current amplitudes evoked by action potential waveforms did exhibit differences. Our data suggests that a potential mechanism underlying the altered action potential-induced peak current amplitudes is changes in current activation kinetics. Shorter action potentials such as the SCN_{Day} action potential enhanced the effect of differences in activation kinetics on BK current amplitudes. For example, faster activating currents evoked by C495G-channels were 54% larger than hBK, whereas slower-activating currents evoked by R800W-channels were 51% smaller than hBK currents. However, as the action potential depolarization phase became longer, the magnitude of difference between hBK and hBK-SNP currents was reduced, presumably because the longer depolarization phases enabled increased current recruitment and reduced the influence of activation kinetics. This was evident when comparing current amplitudes evoked by the SAN action potential, as C495G-currents were only 13% larger than hBK currents, while R800W-currents were only 33% smaller than hBK (Figure 27D).

The differences in BK current properties induced by SNPs may also have important physiological implications, as BK currents regulate excitability in multiple tissues, including the brain (Meredith et al., 2006), urinary bladder (Heppner et al., 1997),

and sinoatrial node (Lai et al., 2014). Because the difference in BK current amplitude caused by SNPs is more apparent with shorter action potentials, it could be expected that the effects of BK channel SNPs on cellular excitability may vary depending on the cell type. Furthermore, because SNPs in *KCNMA1* induced a range of differences in current properties, this data suggests that SNPs may be another mechanism of introducing BK current diversity in physiological conditions.

5.5 ***Future Studies***

Our data provides evidence that non-synonymous SNPs can affect BK current properties. However, we only characterized four of the 99 identified non-synonymous polymorphisms, meaning that there may be several more polymorphisms that affect BK current properties. BK channels are extensively alternatively spliced and its been shown by our lab and others (Johnson et al., 2011; Shelley et al., 2013; Xie and McCobb, 1998) that the exon combination in the C-terminus can alter the current properties, or preclude the effects of exons on current kinetics. Therefore, there are a seemingly infinite number of SNP/splice variant channels to record current properties from, and it would be interesting to determine whether the mutations we characterized would have identical effects on current properties on a different splice variant background.

Additionally, our action potential waveform command experiments were performed at a single Ca^{2+} concentration (10 μM). Physiologically, the Ca^{2+} sources that activate BK currents, which include voltage-gated Ca^{2+} channels (Berkefeld et al., 2006; Herrera and Nelson, 2002) and ryanodine receptors (Brenner et al., 2000b; Nelson et al., 1995; Sausbier et al., 2005) are dynamically activated by changes in membrane potential or influx of Ca^{2+}, meaning that intracellular Ca^{2+} is also dynamically changing. Our

experiments were performed at a single Ca^{2+} concentration (10 μM Ca^{2+}), a feasible Ca^{2+} concentration near a Ca^{2+} spark site or in a Ca^{2+} channel nano-domain complex with BK channels (Berkefeld et al., 2006; Fakler and Adelman, 2008; Perez et al., 2001). It would be interesting to record action potential-evoked currents from *KCNMA1* SNPs at a range of Ca^{2+} concentrations in order to determine whether the SNPs we used for experiments affect BK current properties at Ca^{2+} concentrations other than 10 μM Ca^{2+} in physiological solutions.

Furthermore, under physiological conditions, the α-subunit of the channel is co-expressed with auxiliary subunits, such as β1 in smooth muscle (Brenner et al., 2000b; McCobb et al., 1995), β4 subunit in neuronal tissue (Brenner et al., 2000a; Meera et al., 2000), or γ1 subunits in the salivary glands and prostate (Yan and Aldrich, 2012). These subunits affect multiple properties of BK currents, including their voltage-dependence of activation, Ca^{2+}-sensitivity, activation and deactivation kinetics, and sensitivity to toxins (Brenner et al., 2000a; 2005; McCobb et al., 1995; Meera et al., 2000; Yan and Aldrich, 2010). It has previously been demonstrated that β4 subunits have opposite effects on current G-V relationships in physiological K^+ gradient compared to symmetrical K^+ (Wang et al., 2014), and similarly, we found shifts in G-V relationship induced by C495G and R800W in symmetrical K^+ were not observed in physiological K^+ solutions. It would be interesting to determine whether these SNPs, which affect the activation and deactivation kinetics of BK currents in both symmetrical K^+ and physiological solutions, would still have the same effects when co-expressed with β- or γ-subunits.

5.6 ***Summary***

The work performed in this chapter identifies that SNPs in *KCNMA1* can modulate BK current properties. The SNPs chosen for this work were either disease-linked, or in domains of the BK channel C-terminus that regulate Ca^{2+}-dependent activation. We found that the effects of SNPs on BK current properties were Ca^{2+} concentration-dependent. Also, we found that SNP-induced changes in current properties regulate the amplitudes of BK currents evoked by action potential waveforms. These results suggest that *KCNMA1* SNPs can increase the diversity of BK currents evoked by physiological stimuli.

Chapter 6. Conclusions

Although BK channels regulate several different cardiovascular functions, no previous studies have indicated that BK channels regulate cardiomyocyte excitability. The work presented in the first Specific Aim is the first to identify that BK channels regulate the excitability of SANCs, the heart's predominant pacemaking cells. We identified that abolishment of BK channel function slows heart rate by reducing the firing rate of SANCs. The role that BK currents play in the excitability of SANCs contradicts the general role of BK currents play in other smooth muscle cells and neurons, since eliminating BK currents generally causes an increase in excitability. This work not only identifies a novel excitatory role for BK currents, but also identifies another channel important in the intrinsic excitability of SANCs.

Identification of all ion channels that regulate cardiac pacing is essential when developing therapies for cardiac arrhythmias. Mutations of ion channels known to regulate the intrinsic excitability of SANCs, such as Na^+ and Ca^{2+} channels can lead to sinus node dysfunction (Baig et al., 2010; Lei et al., 2008), and several drugs designed to combat arrhythmias work by targeting ion channels (Sanguinetti and Bennett, 2003). Our work contributes to the understanding of the ionic mechanisms that underlie the intrinsic excitability of SANCs, which will aid in the development of therapies designed to treat cardiac arrhythmias. Also, this work identifies BK channels as a novel therapeutic target for treating sinus rhythm disorders.

The second aim of this work identifies that SNPs are an under-investigated mechanism that creates BK current diversity in physiological conditions. SNPs had profound effects on BK current activation kinetics, which may influence the amplitude of

BK currents evoked by action potential waveforms. The effect of SNPs on BK current amplitudes was also dependent on the type of physiological stimulus applied to the channels, suggesting that the effect of SNPs on BK currents may vary in different tissues. Future work should focus on continuing to characterize other SNPs in *KCNMA1*. Because BK channels are expressed throughout the cardiovascular system, and SNPs can affect BK current properties, our work suggests that SNPs in *KCNMA1* can greatly diversify BK currents in physiological conditions, and could potentially serve as a marker for cardiovascular disease.

Chapter 7. Appendix

The results of several experiments were not included in the main results sections in Chapters 3 and 4. The appendix serves as a place for these results.

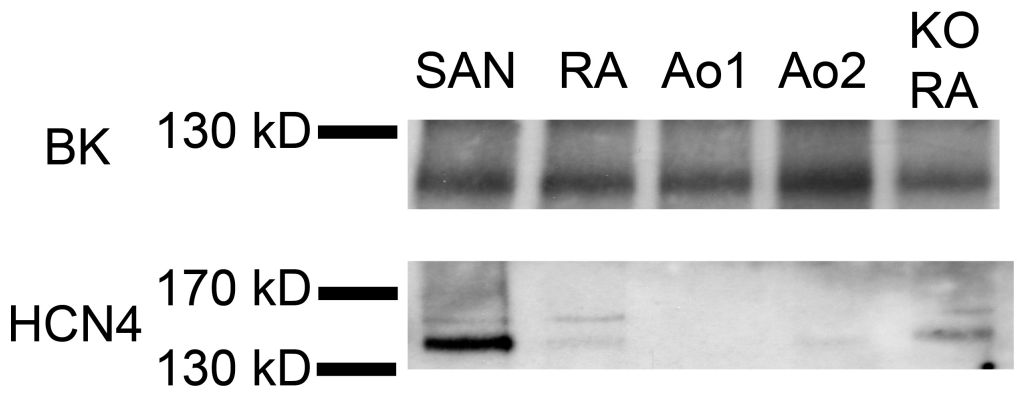

Figure 30: Detection of BK channel protein via immunoprecipitation

Example immunoprecipitation blot demonstrating BK channel protein detection in the SAN. Protein was obtained from WT SAN, right atria (RA), two aorta samples (Ao1 and Ao2) and *Kcnma1*$^{-/-}$ (KO) RA. As a control for SAN tissue, the non-specific protein samples from the immunoprecipitation were probed for HCN4 expression. 30 μg of protein was loaded per well.

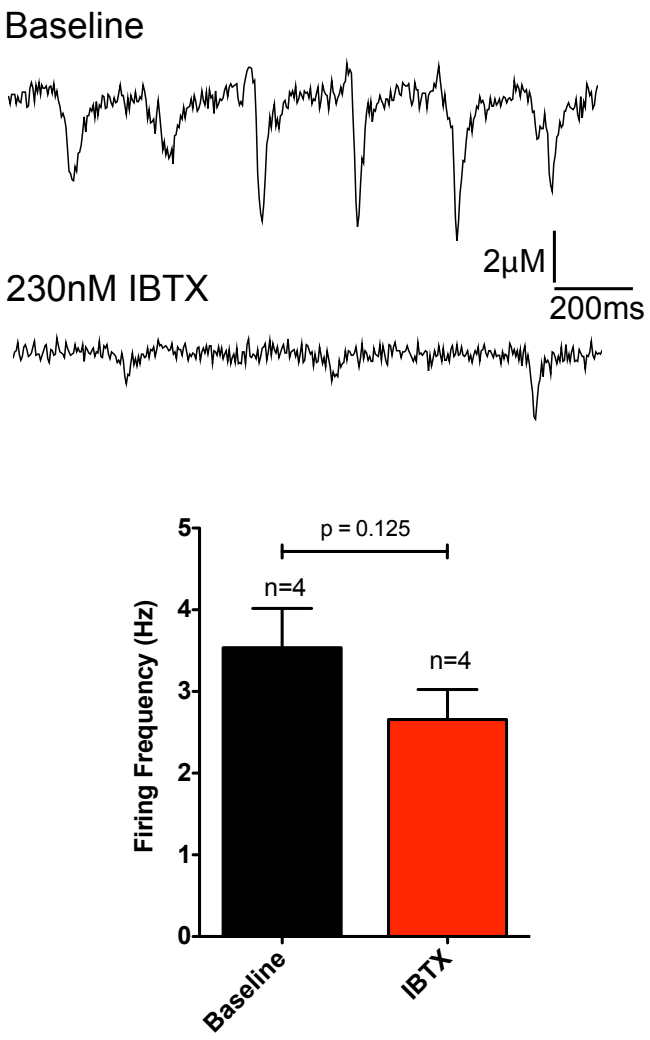

Figure 31: Effect of IbTX on the spontaneous contraction rate of mouse SANCs

(A) Representative contractions from one mouse SAN cell during baseline conditions and after application of 230nM IbTX. IbTX is a highly potent, membrane impermeable BK channel blocker. Contractions were measured using optical edge detection software. (B) IbTX causes a reduction in the average contraction rate of SAN cells. p=0.125, significance tested using a Wilcoxon matched-pairs signed rank test.

Parameter	WT Baseline (n = 7-8)	WT – TAC (n = 7-8)	TgPer1^{R207Q} Baseline (n = 2)	TgPer1^{R207Q}-TAC (n = 2)
Mass (g)	26.45 ±6 0.81	32.65 ± 1.15	32.75 ± 0.55	40.45 ± 2.8
Heart rate (bpm)	366 ± 11.88	414.4 ± 26.32	413 ± 55	369.5 ± 65.5
LVDs (mm)	2.65 ± 0.17	3.32 ± 0.10	3.12 ± 0.40	3.56 ± 0.24
LVDd (mm)	3.78 ± 0.11	4.11 ± 0.11	4.57 ± 0.43	4.72 ± 0.14
LVPWs (mm)	1.00 ± 0.06	1.15 ± 0.11	1.13 ± 0.15	1.18 ± 0.12
LVPWd (mm)	0.67 ± 0.03	0.80 ± 0.04	0.74 ± 0.03	0.80 ± 0.11
IVSs (mm)	0.96 ± 0.06	1.01 ± 0.02	1.12 ± 0.06	0.99 ± 0.15
IVSd (mm)	0.64 ± 0.04	0.76 ± 0.03	0.84 ± 0.05	0.66 ± 0.23
Aortic diameter (mm)	1.44 ± 0.02	1.75 ± 0.05	1.7 ± 0.02	1.77 ± 0.02
E_{max} (mm/s)	590.2 ± 45.3	536.1 ± 37.62	551.3 ± 72.3	632 ± 28.1
A_{max} (mm/s)	312.5 ± 25.05	356.9 ± 49.6	387.3 ± 49.65	376.6 ± 37.7
E/A	1.90 ± 0.09	1.7 ± 0.20	1.425 ± 0.00	1.68 ± 0.09
FS LVD (%)	30.18 ± 2.82	19.13 ± 0.83	32.08 ± 2.32	24.67 ± 2.89
LVEF (%)	57.46 ± 4.42	39.78 ±1.51	60.25 ± 3.65	48.8 ± 4.80
LV mass (g)	0.96 ± 0.01	1.03 ± 0.01	1.04 ± 0.00	1.005 ± 0.09
Normalized LV Mass	0.03 ± 0.00	0.03 ± 0.00	0.03 ± 0.00	0.02 ± 0.00
SV (µL)	34.6 ± 2.34	29.88 ± 2.06	57.9 ± 9.38	50.28 ± 1.42
Normalized Cardiac Output	0.68 ± 0.09	0.60 ± 0.06	0.53 ± 0.06	0.46 ± 0.14

Table 8: Heart parameters via echocardiography

Mouse echocardiogram measurements were performed on wild-type (WT) and transgenic mice expressing a gain-of-function BK channel (*TgPer1*^{R207Q}) before and after transverse aortic constriction (TAC). BK channels regulate vasodilation, and TAC is a well established model of pressure-induced hypertrophy of the heart (Rockman et al., 1994). We hypothesized that gain of function BK channels would promote vasodilation, and therefore prevent cardiac hypertrophy, which was determined by the left ventricular (LV) mass. TAC experiments did not yield the expected increase in LV mass, suggesting that the aortic banding was not stringent enough. Abbreviations used for cardiac parameters are: LV diameter during systole (LVDs) and diastole (LVDd), LV posterior wall during systole (LVPWs) and diastole (LVPWd), intraventrcular septal wall thickness during systole (LVSs) and diastole (LVSd), fractional shortening of the LV diameter (FS LVD), LV ejection fraction (LVEF), and stroke volume (SV).

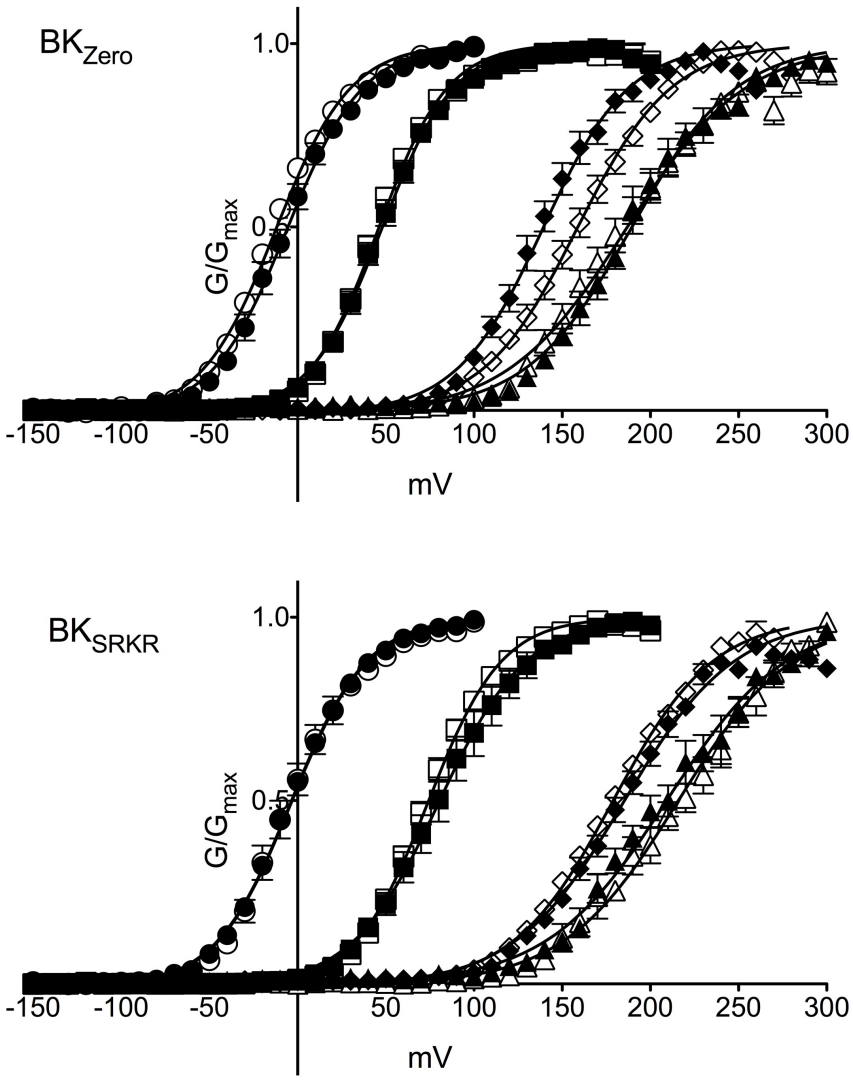

Figure 32: G-V relationships of BK_{Zero} and BK_{SRKR} currents

Macroscopic BK currents were recorded from human (closed symbols) and mouse (open symbols) BK_{Zero} and BK_{SRKR} channels at 0 (triangle), 1 (diamond), 10 (square) and 100 (circle) μM Ca^{2+}. $V_{1/2}$ values and number of patches used per variant for analysis are listed in Table 9.

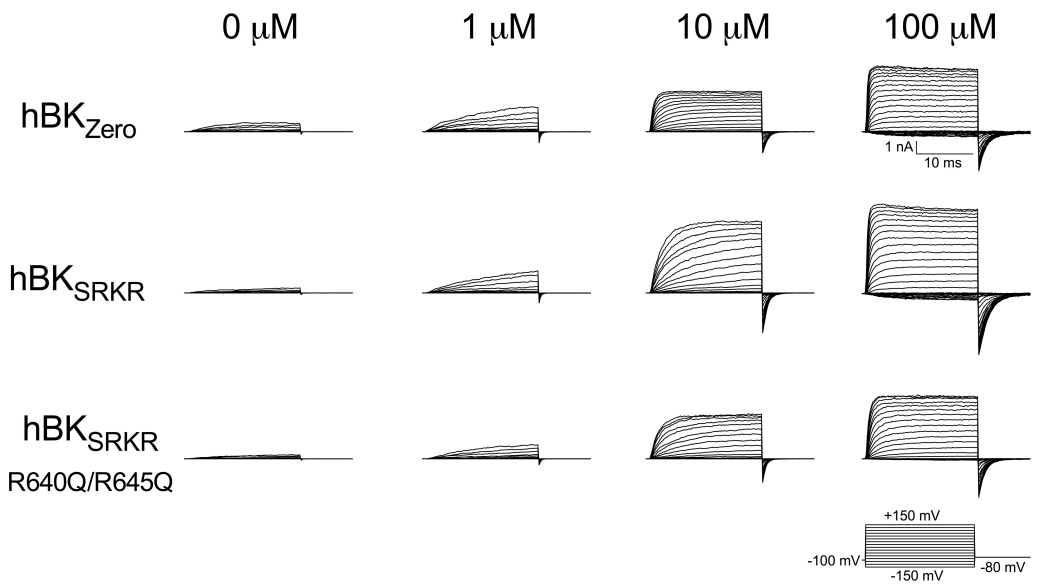

Figure 33: Currents recorded from hBK channel variants

Representative macroscopic BK current traces recorded at the indicated Ca^{2+} concentration from inside-out patches from hBK_{Zero}, hBK_{SRKR}, and $hBK_{SRKR\ R640Q/R645Q}$ channels. Currents were recorded from separate patches. Based upon previous experiments in our lab, we hypothesized that R640Q/R645Q would disrupt phosphorylation of S642, therefore eliminating the shift in G-V relationship between hBK_{Zero} and hBK_{SRKR}.

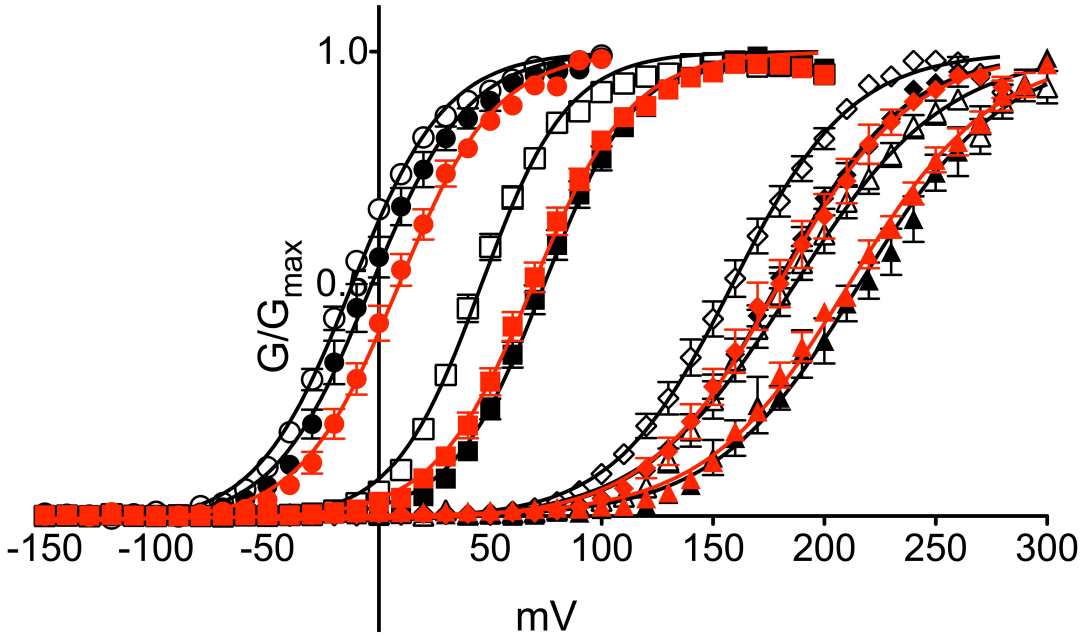

Figure 34: G-V relationships of hBK$_{Zero}$, hBK$_{SRKR}$, and hBK$_{SRKR\ R640Q/R645Q}$ currents

Based upon previous experiments in our lab, we hypothesized that R640Q/R645Q would disrupt phosphorylation of S642, therefore eliminating the shift in G-V relationship between hBK$_{Zero}$ and hBK$_{SRKR}$. Currents were recorded from hBK$_{Zero}$ (open symbols), hBK$_{SRKR}$ (black symbols), and hBK$_{SRKR\ R640Q/R645Q}$ channels at 0 (triangle), 1 (diamond), 10 (square) and 100 (circle) μM Ca^{2+}. $V_{1/2}$ values and number of patches used per variant for analysis are listed in Table 9.

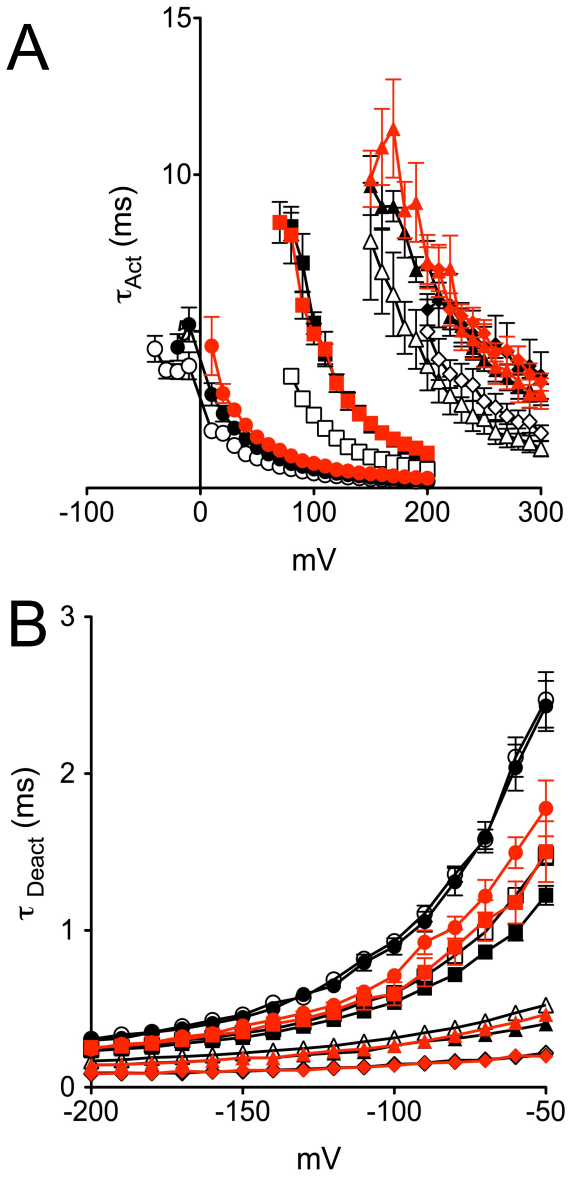

Figure 35: Activation and deactivation kinetics for $hBK_{R640Q/R645Q}$ currents

Activation kinetics were determined by fitting the rising phase of hBK_{Zero} (open symbol), hBK_{SRKR} (black symbols), and $hBK_{SRKR\ R640Q/R645Q}$ (red symbols) currents to single exponential functions at 0 (diamond), 1 (triangle), 10 (square), and 100 (circle) μM Ca^{2+}.

Construct	$V_{1/2}$ (mV)			
	100 μM	**10 μM**	**1 μM**	**0 μM**
mBK_{Zero}	-7 ± 2 (10)	46 ± 2 (10)	132 ± 3 (10)	186 ± 5 (9)
mBK_{SRKR}	-4 ± 1 (10)	79 ± 5 (9) * P < 0.0001	181 ± 4 (18) * P < 0.0001	211 ± 7 (8)
hBK_{Zero}	-14 ± 1 (14)	44 ± 2 (20)	154 ± 4 (8)	180 ± 6 (10)
hBK_{SRKR}	-5 ± 3 (10)	73 ± 3 (19) * P < 0.0001	174 ± 3 (10) * P < 0.05	225 ± 11 (8) * P < 0.001
hBK_{SRKR} R640Q/R645Q	7 ± 3 (10) * P < 0.0001	67 ± 2 (10) * P < 0.0001	177 ± 6 (7) * P < 0.05	212 ± 3 (11) * P < 0.01

Table 9: $V_{1/2}$ values for BK_{Zero} and BK_{SRKR} currents

Number of patches used to acquire data at each Ca^{2+} concentration is denoted in parenthesis. Significance (*, $P < 0.05$) was tested using an unpaired *t*-test within mouse constructs, and a one-way ANOVA with Bonferroni post-hoc tests within human constructs at each Ca^{2+} concentration. Comparisons were made against either mouse or human BK_{Zero} constructs.

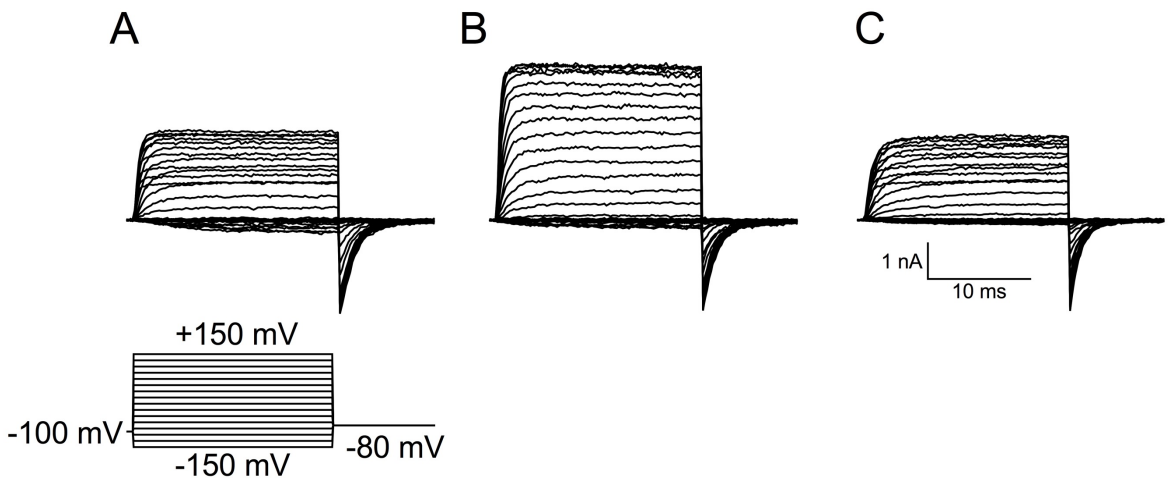

Figure 36: Na^+ inhibition of BK currents

(A) Baseline macroscopic BK currents were recorded in an inside-out patch configuration from hBK_{SRKR} channels in symmetrical K^+ solutions at 100 μM Ca^{2+}. Solution was pH'd to 7.2 using NaOH. Note the voltage-dependent inhibition of the current. (B) Upon perfusion of symmetrical K^+ solution pH'd with KOH, voltage-dependent inhibition was allieveated. (C) Upon re-perfusion of solutions pH'd with NaOH, voltage-dependent block returns. Currents were recorded from a single patch.

References

Atkinson, N.S., Robertson, G.A., and Ganetzky, B. (1991). A component of calcium-activated potassium channels encoded by the *Drosophila slo* locus. Science *253*, 551–555.

Baig, S.M., Koschak, A., Lieb, A., Gebhart, M., Dafinger, C., Nürnberg, G., Ali, A., Ahmad, I., Sinnegger-Brauns, M.J., Brandt, N., et al. (2010). Loss of $Ca_v1.3$ (CACNA1D) function in a human channelopathy with bradycardia and congenital deafness. Nat Neurosci *14*, 77–84.

Bao, L., Kaldany, C., Holmstrand, E.C., and Cox, D.H. (2004). Mapping the BK_{Ca} channel's 'Ca^{2+} bowl': side-chains essential for Ca^{2+} sensing. The Journal of General Physiology *123*, 475–489.

Baruscotti, M., Bucchi, A., Viscomi, C., Mandelli, G., Consalez, G., Gnecchi-Rusconi, T., Montano, N., Casali, K.R., Micheloni, S., Barbuti, A., et al. (2011). Deep bradycardia and heart block caused by inducible cardiac-specific knockout of the pacemaker channel gene *Hcn4*. Proc Natl Acad Sci USA *108*, 1705–1710.

Behrens, R., Nolting, A., Reimann, F., Schwarz, M., Waldschütz, R., and Pongs, O. (2000). hKCNMB3 and hKCNMB4, cloning and characterization of two members of the large-conductance calcium-activated potassium channel β subunit family. FEBS Letters *474*, 99–106.

Bentzen, B.H., Osadchii, O., Jespersen, T., Hansen, R.S., Olesen, S.-P., and Grunnet, M. (2009). Activation of big conductance Ca^{2+}-activated K^+ channels (BK) protects the heart against ischemia-reperfusion injury. Pflugers Arch *457*, 979–988.

Berkefeld, H., Sailer, C.A., Bildl, W., Rohde, V., Thumfart, J.-O., Eble, S., Klugbauer, N., Reisinger, E., Bischofberger, J., Oliver, D., et al. (2006). BK_{Ca}-Cav channel complexes mediate rapid and localized Ca^{2+}-activated K^+ signaling. Science *314*, 615–620.

Bilmen, J.G., Wootton, L.L., and Michelangeli, F. (2002). The mechanism of inhibition of the sarco/endoplasmic reticulum Ca^{2+} ATPase by paxilline. Arch Biochem Biophys *406*, 55–64.

Blom, N., Gammeltoft, S., and Brunak, S. (1999). Sequence and structure-based prediction of eukaryotic protein phosphorylation sites. J. Mol. Biol. *294*, 1351–1362.

Bogdanov, K.Y., Vinogradova, T.M., and Lakatta, E.G. (2001). Sinoatrial nodal cell ryanodine receptor and Na^+-Ca^{2+} exchanger: molecular partners in pacemaker regulation. Circulation Research *88*, 1254–1258.

Boyett, M.R., Honjo, H., Yamamoto, M., Nikmaram, M.R., Niwa, R., and Kodama, I. (1998). Regional differences in effects of 4-aminopyridine within the sinoatrial node. Am J Physiol *275*, H1158–H1168.

Brelidze, T.I., Niu, X., and Magleby, K.L. (2003). A ring of eight conserved negatively charged amino acids doubles the conductance of BK channels and prevents inward rectification. Proc Natl Acad Sci USA *100*, 9017–9022.

Brenner, R., Jegla, T.J., Wickenden, A., Liu, Y., and Aldrich, R.W. (2000a). Cloning and functional characterization of novel large conductance calcium-activated potassium channel β subunits, hKCNMB3 and hKCNMB4. Journal of Biological Chemistry *275*, 6453–6461.

Brenner, R., Peréz, G.J., Bonev, A.D., Eckman, D.M., Kosek, J.C., Wiler, S.W., Patterson, A.J., Nelson, M.T., and Aldrich, R.W. (2000b). Vasoregulation by the β1 subunit of the calcium-activated potassium channel. Nature *407*, 870–876.

Brenner, R., Chen, Q.H., Vilaythong, A., Toney, G.M., Noebels, J.L., and Aldrich, R.W. (2005). BK channel β4 subunit reduces dentate gyrus excitability and protects against temporal lobe seizures. Nat Neurosci *8*, 1752–1759.

Butler, A., Tsunoda, S., McCobb, D.P., Wei, A., and Salkoff, L. (1993). mSlo, a complex mouse gene encoding "maxi" calcium-activated potassium channels. Science *261*, 221–224.

Candia, S., Garcia, M.L., and Latorre, R. (1992). Mode of action of iberiotoxin, a potent blocker of the large conductance Ca^{2+}-activated K^+ channel. Biophys J *63*, 583–590.

Chen, L., Tian, L., MacDonald, S.H.-F., McClafferty, H., Hammond, M.S.L., Huibant, J.-M., Ruth, P., Knaus, H.-G., and Shipston, M.J. (2005). Functionally Diverse Complement of Large Conductance Calcium- and Voltage-activated Potassium Channel (BK) α-Subunits Generated from a Single Site of Splicing. Journal of Biological Chemistry *280*, 33599.

Chen, W.-T., Chen, Y.-C., Lu, Y.-Y., Kao, Y.-H., Huang, J.-H., Lin, Y.-K., Chen, S.-A., and Chen, Y.-J. (2013). Apamin modulates electrophysiological characteristics of the pulmonary vein and the Sinoatrial Node. Eur. J. Clin. Invest. *43*, 957–963.

Cho, H.-S., Takano, M., and Noma, A. (2003). The electrophysiological properties of spontaneously beating pacemaker cells isolated from mouse sinoatrial node. J Physiol (Lond) *550*, 169–180.

Clark, R.B., Mangoni, M.E., Lueger, A., Couette, B., Nargeot, J., and Giles, W.R. (2004). A rapidly activating delayed rectifier K^+ current regulates pacemaker activity in adult mouse sinoatrial node cells. Am J Physiol Heart Circ Physiol *286*, H1757–H1766.

Collins, F.S., Brooks, L.D., and Chakravarti, A. (1998). A DNA polymorphism discovery resource for research on human genetic variation. Genome Res. *8*, 1229–1231.

Cui, J., and Aldrich, R.W. (2000). Allosteric linkage between voltage and Ca^{2+}-dependent activation of BK-type mslo1 K^+ channels. Biochemistry *39*, 15612–15619.

Cui, J., Yang, H., and Lee, U.S. (2009). Molecular mechanisms of BK channel activation. Cell. Mol. Life Sci. *66*, 852–875.

Davies, A.G., Pierce-Shimomura, J.T., Kim, H., VanHoven, M.K., Thiele, T.R., Bonci, A., Bargmann, C.I., and McIntire, S.L. (2003). A central role of the BK potassium channel in behavioral responses to ethanol in C. elegans. Cell *115*, 655–666.

DiFrancesco, D. (2006). Serious workings of the funny current. Progress in Biophysics and Molecular Biology *90*, 13–25.

Díaz, L., Meera, P., Amigo, J., Stefani, E., Alvarez, O., Toro, L., and Latorre, R. (1998). Role of the S4 segment in a voltage-dependent calcium-sensitive potassium (hSlo) channel. J Biol Chem *273*, 32430–32436.

Du, W., Bautista, J.F., Yang, H., Diez-Sampedro, A., You, S.-A., Wang, L., Kotagal, P., Lüders, H.O., Shi, J., Cui, J., et al. (2005). Calcium-sensitive potassium channelopathy in human epilepsy and paroxysmal movement disorder. Nat Genet *37*, 733–738.

Dworetzky, S.I., Trojnacki, J.T., and Gribkoff, V.K. (1994). Cloning and expression of a human large-conductance calcium-activated potassium channel. Brain Res. Mol. Brain Res. *27*, 189–193.

Elkins, T., Ganetzky, B., and Wu, C.F. (1986). A Drosophila mutation that eliminates a calcium-dependent potassium current. Proc Natl Acad Sci USA *83*, 8415–8419.

England, S.K., Wooldridge, T.A., Stekiel, W.J., and Rusch, N.J. (1993). Enhanced single-channel K^+ current in arterial membranes from genetically hypertensive rats. Am J Physiol *264*, H1337–H1345.

Faber, E.S.L., and Sah, P. (2002). Physiological role of calcium-activated potassium currents in the rat lateral amygdala. Journal of Neuroscience *22*, 1618–1628.

Fadel, P.J., Ogoh, S., Keller, D.M., and Raven, P.B. (2003). Recent insights into carotid baroreflex function in humans using the variable pressure neck chamber. Exp Physiol *88*, 671–680.

Fakler, B., and Adelman, J.P. (2008). Control of K_{Ca} channels by calcium nano/microdomains. Neuron *59*, 873–881.

Filosa, J.A., Bonev, A.D., Straub, S.V., Meredith, A.L., Wilkerson, M.K., Aldrich, R.W., and Nelson, M.T. (2006). Local potassium signaling couples neuronal activity to

vasodilation in the brain. Nat Neurosci *9*, 1397–1403.

Giangiacomo, K.M., Garcia, M.L., and McManus, O.B. (1992). Mechanism of iberiotoxin block of the large-conductance calcium-activated potassium channel from bovine aortic smooth muscle. Biochemistry *31*, 6719–6727.

Giangiacomo, K.M., Becker, J., Garsky, C., Schmalhofer, W., Garcia, M.L., and Mullmann, T.J. (2008). Novel α-KTx sites in the BK channel and comparative sequence analysis reveal distinguishing features of the BK and KV channel outer pore. Cell Biochem Biophys *52*, 47–58.

Grimes, W.N., Li, W., Chávez, A.E., and Diamond, J.S. (2009). BK channels modulate pre- and postsynaptic signaling at reciprocal synapses in retina. Nat Neurosci *12*, 585–592.

Guglielmi, L., Servettini, I., Caramia, M., Catacuzzeno, L., Franciolini, F., D'Adamo, M.C., and Pessia, M. (2015). Update on the implication of potassium channels in autism: K+ channelautism spectrum disorder. Front. Cell. Neurosci. *9*.

Ha, T.S., Jeong, S.Y., Cho, S.W., Jeon, H.K., Roh, G.S., Choi, W.S., and Park, C.S. (2000). Functional characteristics of two BK_{Ca} channel variants differentially expressed in rat brain tissues. Eur. J. Biochem. *267*, 910–918.

Heginbotham, L., Lu, Z., Abramson, T., and MacKinnon, R. (1994). Mutations in the K^+ channel signature sequence. Biophysj *66*, 1061–1067.

Heppner, T.J., Bonev, A.D., and Nelson, M.T. (1997). Ca^{2+}-activated K^+ channels regulate action potential repolarization in urinary bladder smooth muscle. Am J Physiol *273*, C110–C117.

Herrera, G.M., Heppner, T.J., and Nelson, M.T. (2000). Regulation of urinary bladder smooth muscle contractions by ryanodine receptors and BK and SK channels. Am J Physiol Regul Integr Comp Physiol *279*, R60–R68.

Herrera, G.M., and Nelson, M.T. (2002). Differential regulation of SK and BK channels by Ca^{2+} signals from Ca^{2+} channels and ryanodine receptors in guinea-pig urinary bladder myocytes. J Physiol (Lond) *541*, 483–492.

Herrmann, S., Stieber, J., Stöckl, G., Hofmann, F., and Ludwig, A. (2007). HCN4 provides a "depolarization reserve" and is not required for heart rate acceleration in mice. Embo J *26*, 4423–4432.

Horrigan, F.T., and Aldrich, R.W. (2002). Coupling between voltage sensor activation, Ca^{2+} binding and channel opening in large conductance (BK) potassium channels. The Journal of General Physiology *120*, 267–305.

Hu, H., Shao, L.R., Chavoshy, S., Gu, N., Trieb, M., Behrens, R., Laake, P., Pongs, O., Knaus, H.G., Ottersen, O.P., et al. (2001). Presynaptic Ca^{2+}-activated K^+ channels

in glutamatergic hippocampal terminals and their role in spike repolarization and regulation of transmitter release. Journal of Neuroscience *21*, 9585–9597.

Imlach, W.L., Finch, S.C., Dunlop, J., Meredith, A.L., Aldrich, R.W., and Dalziel, J.E. (2008). The molecular mechanism of "ryegrass staggers," a neurological disorder of K^+ channels. J Pharmacol Exp Ther *327*, 657–664.

Imlach, W.L., Finch, S.C., Miller, J.H., Meredith, A.L., and Dalziel, J.E. (2010). A role for BK channels in heart rate regulation in rodents. PLoS ONE *5*, e8698.

Ireland, D.R., Davies, P.J., and McLachlan, E.M. (1998). The role of N-type Ca^{2+} channels in regulating excitability of guinea-pig sympathetic neurones. J. Auton. Nerv. Syst. *73*, 109–114.

Jaffe, D.B., Wang, B., and Brenner, R. (2011). Shaping of action potentials by type I and type II large-conductance Ca^{2+}-activated K^+ channels. Neuroscience.

Jiang, Y., Lee, A., Chen, J., Cadene, M., Chait, B.T., and MacKinnon, R. (2002). Crystal structure and mechanism of a calcium-gated potassium channel. Nature *417*, 515–522.

Jiao, H., Arner, P., Hoffstedt, J., Brodin, D., Dubern, B., Czernichow, S., Hooft, F.V., Axelsson, T., Pedersen, O., Hansen, T., et al. (2011). Genome wide association study identifies *KCNMA1* contributing to human obesity. BMC Medical Genomics *4*, 51.

Johnson, B.E., Glauser, D.A., Dan-Glauser, E.S., Halling, D.B., Aldrich, R.W., and Goodman, M.B. (2011). Alternatively spliced domains interact to regulate BK potassium channel gating. Proc Natl Acad Sci USA *108*, 20784–20789.

Johnson, E., Ringo, J., Bray, N., and Dowse, H. (1998). Genetic and pharmacological identification of ion channels central to the Drosophila cardiac pacemaker. J. Neurogenet. *12*, 1–24.

Kawada, T., Akiyama, T., Shimizu, S., Kamiya, A., Uemura, K., Sata, Y., Shirai, M., and Sugimachi, M. (2010). Large conductance Ca^{2+}-activated K^+ channels inhibit vagal acetylcholine release at the rabbit sinoatrial node. Autonomic Neuroscience : Basic & Clinical *156*, 149–151.

Kim, H.-J., Lim, H.-H., Rho, S.-H., Bao, L., Lee, J.-H., Cox, D.H., Kim, D.H., and Park, C.-S. (2008). Modulation of the Conductance-Voltage Relationship of the BK_{Ca} Channel by Mutations at the Putative Flexible Interface between Two RCK Domains. Biophys J *94*, 446–456.

Klassen, T., Davis, C., Goldman, A., Burgess, D., Chen, T., Wheeler, D., McPherson, J., Bourquin, T., Lewis, L., Villasana, D., et al. (2011). Exome Sequencing of Ion Channel Genes Reveals Complex Profiles Confounding Personal Risk Assessment in Epilepsy. Cell *145*, 1036–1048.

Knaus, H.-G., Mcmanus, O.B., Lee, S.H., Schmalhofer, W.A., Garcia-Calvo, M., Helms, L.M.H., Sanchez, M., Giangiacomo, K., and Reuben, J.P. (1994). Tremorgenic Indole Alkaloids Potently Inhibit Smooth Muscle High-Conductance Calcium-Activated Potassium Channels. Biochemistry *33*, 5819–5828.

Kodama, I., Boyett, M.R., Nikmaram, M.R., Yamamoto, M., Honjo, H., and Niwa, R. (1999). Regional differences in effects of E-4031 within the sinoatrial node. Am J Physiol *276*, H793–H802.

Kodama, I., Nikmaram, M.R., Boyett, M.R., Suzuki, R., Honjo, H., and Owen, J.M. (1997). Regional differences in the role of the Ca^{2+} and Na^{+} currents in pacemaker activity in the sinoatrial node. Am J Physiol *272*, H2793–H2806.

Koval, O.M., Fan, Y., and Rothberg, B.S. (2007). A role for the S0 transmembrane segment in voltage-dependent gating of BK channels. The Journal of General Physiology *129*, 209–220.

Lai, M.H., Wu, Y., Gao, Z., Anderson, M.E., Dalziel, J.E., and Meredith, A.L. (2014). BK channels regulate sinoatrial node firing rate and cardiac pacing in vivo. Am J Physiol Heart Circ Physiol *307*, H1327–H1338.

Lakatta, E.G., Maltsev, V.A., and Vinogradova, T.M. (2010). A coupled SYSTEM of intracellular Ca^{2+} clocks and surface membrane voltage clocks controls the timekeeping mechanism of the heart's pacemaker. Circulation Research *106*, 659–673.

Larson, E.D., St Clair, J.R., Sumner, W.A., Bannister, R.A., and Proenza, C. (2013). Depressed pacemaker activity of sinoatrial node myocytes contributes to the age-dependent decline in maximum heart rate. Proc Natl Acad Sci USA *110*, 18011–18016.

Latorre, R., and Miller, C. (1983). Conduction and selectivity in potassium channels. Journal of Membrane Biology.

Laumonnier, F., Roger, S., Guérin, P., Molinari, F., M'rad, R., Cahard, D., Belhadj, A., Halayem, M., Persico, A.M., Elia, M., et al. (2006). Association of a functional deficit of the BK_{Ca} channel, a synaptic regulator of neuronal excitability, with autism and mental retardation. Am J Psychiatry *163*, 1622–1629.

Lee, S.H., Ripke, S., Neale, B.M., Faraone, S.V., Purcell, S.M., Perlis, R.H., Mowry, B.J., Thapar, A., Goddard, M.E., Witte, J.S., et al. (2013). Genetic relationship between five psychiatric disorders estimated from genome-wide SNPs. Nat Genet *45*, 984–994.

Lei, M., Huang, C.L.-H., and Zhang, Y. (2008). Genetic Na^{+} channelopathies and sinus node dysfunction. Progress in Biophysics and Molecular Biology *98*, 171–178.

Lei, M., Jones, S.A., Liu, J., Lancaster, M.K., Fung, S.S.-M., Dobrzynski, H., Camelliti,

P., Maier, S.K.G., Noble, D., and Boyett, M.R. (2004). Requirement of neuronal- and cardiac-type sodium channels for murine sinoatrial node pacemaking. J Physiol (Lond) *559*, 835–848.

Li, B., Krishnan, V.G., Mort, M.E., Xin, F., Kamati, K.K., Cooper, D.N., Mooney, S.D., and Radivojac, P. (2009). Automated inference of molecular mechanisms of disease from amino acid substitutions. Bioinformatics *25*, 2744–2750.

Liao, Z., Lockhead, D., Larson, E.D., and Proenza, C. (2010). Phosphorylation and modulation of hyperpolarization-activated HCN4 channels by protein kinase A in the mouse sinoatrial node. The Journal of General Physiology *136*, 247–258.

Locknar, S.A., Barstow, K.L., Tompkins, J.D., Merriam, L.A., and Parsons, R.L. (2004). Calcium-induced calcium release regulates action potential generation in guinea-pig sympathetic neurones. J Physiol (Lond) *555*, 627–635.

Lu, Y., Ma, X., Sabharwal, R., Snitsarev, V., Morgan, D., Rahmouni, K., Drummond, H.A., Whiteis, C.A., Costa, V., Price, M., et al. (2009). The ion channel ASIC2 is required for baroreceptor and autonomic control of the circulation. Neuron *64*, 885–897.

Ma, Z., Lou, X.J., and Horrigan, F.T. (2006). Role of charged residues in the S1-S4 voltage sensor of BK channels. The Journal of General Physiology *127*, 309–328.

Mangoni, M.E., and Nargeot, J. (2001). Properties of the hyperpolarization-activated current (I_f) in isolated mouse sino-atrial cells. Cardiovasc Res *52*, 51–64.

Mangoni, M.E., and Nargeot, J. (2008). Genesis and regulation of the heart automaticity. Physiol Rev *88*, 919–982.

Mangoni, M.E., Couette, B., Bourinet, E., Platzer, J., Reimer, D., Striessnig, J., and Nargeot, J. (2003). Functional role of L-type $Ca_v1.3$ Ca^{2+} channels in cardiac pacemaker activity. Proc Natl Acad Sci USA *100*, 5543–5548.

Mangoni, M.E., Traboulsie, A., Leoni, A.-L., Couette, B., Marger, L., Le Quang, K., Kupfer, E., Cohen-Solal, A., Vilar, J., Shin, H.-S., et al. (2006). Bradycardia and slowing of the atrioventricular conduction in mice lacking $Ca_V3.1/\alpha1G$ T-type calcium channels. Circulation Research *98*, 1422–1430.

Marger, L., Mesirca, P., Alig, J., Torrente, A., Dubel, S., Engeland, B., Kanani, S., Fontanaud, P., Striessnig, J., Shin, H.-S., et al. (2011). Pacemaker activity and ionic currents in mouse atrioventricular node cells. Channels (Austin) *5*, 241–250.

Marty, A. (1983). Ca^{2+}-dependent K^+ channels with large unitary conductance. Trends Neurosci 6, 262-265.

McCobb, D.P., Fowler, N.L., Featherstone, T., Lingle, C.J., Saito, M., Krause, J.E., and Salkoff, L. (1995). A human calcium-activated potassium channel gene expressed

in vascular smooth muscle. Am J Physiol *269*, H767–H777.

McGahon, M.K., Dash, D.P., Arora, A., Wall, N., Dawicki, J., Simpson, D.A., Scholfield, C.N., McGeown, J.G., and Curtis, T.M. (2007). Diabetes Downregulates Large-Conductance Ca^{2+}-Activated Potassium β1 Channel Subunit in Retinal Arteriolar Smooth Muscle. Circulation Research *100*, 703–711.

Meera, P., Wallner, M., and Toro, L. (2000). A neuronal beta subunit (KCNMB4) makes the large conductance, voltage- and Ca^{2+}-activated K+ channel resistant to charybdotoxin and iberiotoxin. Proc Natl Acad Sci USA *97*, 5562–5567.

Meera, P., Wallner, M., Jiang, Z., and Toro, L. (1996). A calcium switch for the functional coupling between α (hslo) and beta subunits ($K_{V,Ca}$β) of maxi K channels. FEBS Letters *385*, 127–128.

Meera, P., Wallner, M., Song, M., and Toro, L. (1997). Large conductance voltage- and calcium-dependent K^+ channel, a distinct member of voltage-dependent ion channels with seven N-terminal transmembrane segments (S0-S6), an extracellular N terminus, and an intracellular (S9-S10) C terminus. Proc Natl Acad Sci USA *94*, 14066–14071.

Meredith, A.L., Thorneloe, K.S., Werner, M.E., Nelson, M.T., and Aldrich, R.W. (2004). Overactive bladder and incontinence in the absence of the BK large conductance Ca^{2+}-activated K^+ channel. J Biol Chem *279*, 36746–36752.

Meredith, A.L., Wiler, S.W., Miller, B.H., Takahashi, J.S., Fodor, A.A., Ruby, N.F., and Aldrich, R.W. (2006). BK calcium-activated potassium channels regulate circadian behavioral rhythms and pacemaker output. Nat Neurosci *9*, 1041–1049.

Monfredi, O., Maltsev, V.A., and Lakatta, E.G. (2013). Modern concepts concerning the origin of the heartbeat. Physiology *28*, 74–92.

Montgomery, J.R., and Meredith, A.L. (2012). Genetic activation of BK currents in vivo generates bidirectional effects on neuronal excitability. Proc Natl Acad Sci USA *109*, 18997–19002.

Montgomery, J.R., Whitt, J.P., Wright, B.N., Lai, M.H., and Meredith, A.L. (2013). Mis-expression of the BK K^+ channel disrupts suprachiasmatic nucleus circuit rhythmicity and alters clock-controlled behavior. AJP: Cell Physiology *304*, C299–C311.

Nelson, M.T., Cheng, H., Rubart, M., Santana, L.F., Bonev, A.D., Knot, H.J., and Lederer, W.J. (1995). Relaxation of arterial smooth muscle by calcium sparks. Science *270*, 633–637.

Ng, P.C., and Henikoff, S. (2003). SIFT: Predicting amino acid changes that affect protein function. Nucleic Acids Research *31*, 3812–3814.

Ono, K., Shibata, S., and Iijima, T. (2000). Properties of the delayed rectifier potassium current in porcine sino-atrial node cells. J Physiol (Lond) *524 Pt 1*, 51–62.

Park, W.S., Kang, S.H., Son, Y.K., Kim, N., Ko, J.-H., Kim, H.K., Ko, E.A., Kim, C.D., and Han, J. (2007). The mitochondrial Ca^{2+}-activated K^+ channel activator, NS 1619 inhibits L-type Ca^{2+} channels in rat ventricular myocytes. Biochemical and Biophysical Research Communications *362*, 31–36.

Pedarzani, P., Kulik, A., Müller, M., Ballanyi, K., and Stocker, M. (2000). Molecular determinants of Ca^{2+}-dependent K^+ channel function in rat dorsal vagal neurones. J Physiol (Lond) *527 Pt 2*, 283–290.

Perez, G.J., Bonev, A.D., and Nelson, M.T. (2001). Micromolar Ca^{2+} from sparks activates Ca^{2+}-sensitive K^+ channels in rat cerebral artery smooth muscle. Am J Physiol, Cell Physiol *281*, C1769–C1775.

Platzer, J., Engel, J., Schrott-Fischer, A., Stephan, K., Bova, S., Chen, H., Zheng, H., and Striessnig, J. (2000). Congenital deafness and sinoatrial node dysfunction in mice lacking class D L-type Ca^{2+} channels. Cell *102*, 89–97.

Rae, J., Cooper, K., Gates, P., and Watsky, M. (1991). Low access resistance perforated patch recordings using amphotericin B. J Neurosci Methods *37*, 15–26.

Raffaelli, G., Saviane, C., Mohajerani, M.H., Pedarzani, P., and Cherubini, E. (2004). BK potassium channels control transmitter release at CA3-CA3 synapses in the rat hippocampus. J Physiol (Lond) *557*, 147–157.

Ramanathan, K., Michael, T.H., Jiang, G.J., Hiel, H., and Fuchs, P.A. (1999). A molecular mechanism for electrical tuning of cochlear hair cells. Science *283*, 215–217.

Ramensky, V., Bork, P., and Sunyaev, S. (2002). Human non-synonymous SNPs: server and survey. Nucleic Acids Research *30*, 3894–3900.

Reinhart, P.H., Chung, S., Martin, B.L., Brautigan, D.L., and Levitan, I.B. (1991). Modulation of calcium-activated potassium channels from rat brain by protein kinase A and phosphatase 2A. J Neurosci *11*, 1627–1635.

Rockman, H.A., Wachhorst, S.P., Mao, L., and Ross, J. (1994). ANG II receptor blockade prevents ventricular hypertrophy and ANF gene expression with pressure overload in mice. Am J Physiol *266*, H2468–H2475.

Rosenblatt, K.P., Sun, Z.P., Heller, S., and Hudspeth, A.J. (1997). Distribution of Ca^{2+}-activated K^+ channel isoforms along the tonotopic gradient of the chicken's cochlea. Neuron *19*, 1061–1075.

Rothberg, B.S., and Magleby, K.L. (2000). Voltage and Ca^{2+} activation of single large-conductance Ca^{2+}-activated K^+ channels described by a two-tiered allosteric

gating mechanism. The Journal of General Physiology *116*, 75–99.

Sanchez, M., and McManus, O. (1996). Paxilline inhibition of the alpha-subunit of the high-conductance calcium-activated potassium channel. Neuropharmacology *35*, 963–968.

Sanguinetti, M.C., and Bennett, P.B. (2003). Antiarrhythmic drug target choices and screening. Circulation Research *93*, 491–499.

Sausbier, M., Hu, H., Arntz, C., Feil, S., Kamm, S., Adelsberger, H., Sausbier, U., Sailer, C.A., Feil, R., Hofmann, F., et al. (2004). Cerebellar ataxia and Purkinje cell dysfunction caused by Ca^{2+}-activated K+ channel deficiency. Proc Natl Acad Sci USA *101*, 9474–9478.

Sausbier, M., Arntz, C., Bucurenciu, I., Zhao, H., Zhou, X.-B., Sausbier, U., Feil, S., Kamm, S., Essin, K., Sailer, C.A., et al. (2005). Elevated blood pressure linked to primary hyperaldosteronism and impaired vasodilation in BK channel-deficient mice. Circulation *112*, 60–68.

Schreiber, M., and Salkoff, L. (1997). A novel calcium-sensing domain in the BK channel. Biophys J *73*, 1355–1363.

Shao, L.R., Halvorsrud, R., Borg-Graham, L., and Storm, J.F. (1999). The role of BK-type Ca^{2+}-dependent K^+ channels in spike broadening during repetitive firing in rat hippocampal pyramidal cells. J Physiol (Lond) *521 Pt 1*, 135–146.

Shelley, C., Whitt, J.P., Montgomery, J.R., and Meredith, A.L. (2013). Phosphorylation of a constitutive serine inhibits BK channel variants containing the alternate exon "SRKR". The Journal of General Physiology *142*, 585–598.

Shen, K.Z., Lagrutta, A., Davies, N.W., Standen, N.B., Adelman, J.P., and North, R.A. (1994). Tetraethylammonium block of Slowpoke calcium-activated potassium channels expressed in Xenopus oocytes: evidence for tetrameric channel formation. Pflugers Arch *426*, 440–445.

Shipston, M. (2001). Alternative splicing of potassium channels: a dynamic switch of cellular excitability. Trends in Cell Biology.

Shruti, S., Clem, R.L., and Barth, A.L. (2008). A seizure-induced gain-of-function in BK channels is associated with elevated firing activity in neocortical pyramidal neurons. Neurobiol Dis *30*, 323–330.

Singh, H., Lu, R., Bopassa, J.C., Meredith, A.L., Stefani, E., and Toro, L. (2013). mitoBK$_{Ca}$ is encoded by the *Kcnma1* gene, and a splicing sequence defines its mitochondrial location. Proc Natl Acad Sci USA *110*, 10836–10841.

Solaro, C.R., Prakriya, M., Ding, J.P., and Lingle, C.J. (1995). Inactivating and noninactivating Ca^{2+}- and voltage-dependent K^+ current in rat adrenal chromaffin

cells. J Neurosci *15*, 6110–6123.

Storm, J.F. (1987). Action potential repolarization and a fast after-hyperpolarization in rat hippocampal pyramidal cells. J Physiol (Lond) *385*, 733–759.

Sweet, T.-B., and Cox, D.H. (2009). Measuring the influence of the BK_{Ca} β1 subunit on Ca^{2+} binding to the BK_{Ca} channel. The Journal of General Physiology *133*, 139–150.

Takamatsu, H., Nagao, T., Ichijo, H., and Adachi-Akahane, S. (2003). L-type Ca^{2+} channels serve as a sensor of the SR Ca^{2+} for tuning the efficacy of Ca^{2+}-induced Ca^{2+} release in rat ventricular myocytes. J Physiol (Lond) *552*, 415–424.

Talukder, G., and Aldrich, R.W. (2000). Complex voltage-dependent behavior of single unliganded calcium-sensitive potassium channels. Biophysj *78*, 761–772.

Tseng-Crank, J., Foster, C.D., Krause, J.D., Mertz, R., Godinot, N., DiChiara, T.J., and Reinhart, P.H. (1994). Cloning, expression, and distribution of functionally distinct Ca^{2+}-activated K^+ channel isoforms from human brain. Neuron *13*, 1315–1330.

Tseng-Crank, J., Godinot, N., Johansen, T.E., Ahring, P.K., Strøbaek, D., Mertz, R., Foster, C.D., Olesen, S.P., and Reinhart, P.H. (1996). Cloning, expression, and distribution of a Ca^{2+}-activated K+ channel β-subunit from human brain. Proc Natl Acad Sci USA *93*, 9200–9205.

Uebele, V.N., Lagrutta, A., Wade, T., Figueroa, D.J., Liu, Y., McKenna, E., Austin, C.P., Bennett, P.B., and Swanson, R. (2000). Cloning and functional expression of two families of β-subunits of the large conductance calcium-activated K^+ channel. J Biol Chem *275*, 23211–23218.

Vinogradova, T.M., Bogdanov, K.Y., and Lakatta, E.G. (2002). β-Adrenergic stimulation modulates ryanodine receptor Ca^{2+} release during diastolic depolarization to accelerate pacemaker activity in rabbit sinoatrial nodal cells. Circulation Research *90*, 73–79.

Vinogradova, T.M., Zhou, Y.-Y., Maltsev, V., Lyashkov, A., Stern, M., and Lakatta, E.G. (2004). Rhythmic ryanodine receptor Ca^{2+} releases during diastolic depolarization of sinoatrial pacemaker cells do not require membrane depolarization. Circulation Research *94*, 802–809.

Wallner, M., Meera, P., and Toro, L. (1996). Determinant for β-subunit regulation in high-conductance voltage-activated and Ca^{2+}-sensitive K^+ channels: an additional transmembrane region at the N terminus. Proc Natl Acad Sci USA *93*, 14922–14927.

Wallner, M., Meera, P., and Toro, L. (1999). Molecular basis of fast inactivation in voltage and Ca^{2+}-activated K^+ channels: a transmembrane β-subunit homolog.

Proc Natl Acad Sci USA *96*, 4137–4142.

Wan, E., Kushner, J.S., Zakharov, S., Nui, X.-W., Chudasama, N., Kelly, C., Waase, M., Doshi, D., Liu, G., Iwata, S., et al. (2013). Reduced vascular smooth muscle BK channel current underlies heart failure-induced vasoconstriction in mice. Faseb J *27*, 1859–1867.

Wang, B., Jaffe, D.B., and Brenner, R. (2014). Current understanding of iberiotoxin-resistant BK channels in the nervous system. Front Physiol *5*, 382.

Wang, B., Rothberg, B.S., and Brenner, R. (2009). Mechanism of increased BK channel activation from a channel mutation that causes epilepsy. The Journal of General Physiology *133*, 283–294.

Wang, Z.W., Saifee, O., Nonet, M.L., and Salkoff, L. (2001). SLO-1 potassium channels control quantal content of neurotransmitter release at the C. elegans neuromuscular junction. Neuron *32*, 867–881.

Weisbrod, D., Peretz, A., Ziskind, A., Menaker, N., Oz, S., Barad, L., Eliyahu, S., Itskovitz-Eldor, J., Dascal, N., Khananshvili, D., et al. (2013). SK4 Ca^{2+} activated K^+ channel is a critical player in cardiac pacemaker derived from human embryonic stem cells. Proc Natl Acad Sci USA *110*, E1685–E1694.

Werner, M.E., Zvara, P., Meredith, A.L., Aldrich, R.W., and Nelson, M.T. (2005). Erectile dysfunction in mice lacking the large-conductance calcium-activated potassium (BK) channel. J Physiol (Lond) *567*, 545–556.

Wu, X., Yang, Y., Gui, P., Sohma, Y., Meininger, G.A., Davis, G.E., Braun, A.P., and Davis, M.J. (2008). Potentiation of large conductance, Ca^{2+}-activated K^+ (BK) channels by $\alpha5\beta1$ integrin activation in arteriolar smooth muscle. J Physiol (Lond) *586*, 1699–1713.

Wu, Y., Gao, Z., Chen, B., Koval, O.M., Singh, M.V., Guan, X., Hund, T.J., Kutschke, W., Sarma, S., Grumbach, I.M., et al. (2009). Calmodulin kinase II is required for fight or flight sinoatrial node physiology. Proc Natl Acad Sci USA *106*, 5972–5977.

Wu, Y., Yang, Y., Ye, S., and Jiang, Y. (2010). Structure of the gating ring from the human large-conductance Ca^{2+}-gated K^+ channel. Nature.

Xia, X.M., Ding, J.P., and Lingle, C.J. (1999). Molecular basis for the inactivation of Ca^{2+}- and voltage-dependent BK channels in adrenal chromaffin cells and rat insulinoma tumor cells. J Neurosci *19*, 5255–5264.

Xia, X.-M., Zeng, X., and Lingle, C.J. (2002). Multiple regulatory sites in large-conductance calcium-activated potassium channels. Nature *418*, 880–884.

Xie, J., and McCobb, D.P. (1998). Control of alternative splicing of potassium channels

by stress hormones. Science *280*, 443–446.

Xu, H., Garver, H., Galligan, J.J., and Fink, G.D. (2011). Large-conductance Ca^{2+}-activated K^+ channel β1-subunit knockout mice are not hypertensive. Am J Physiol Heart Circ Physiol *300*, H476–H485.

Xu, W., Liu, Y., Wang, S., McDonald, T., Van Eyk, J.E., Sidor, A., and O'Rourke, B. (2002). Cytoprotective role of Ca^{2+}- activated K^+ channels in the cardiac inner mitochondrial membrane. Science *298*, 1029–1033.

Xu, Z.J., and Adams, D.J. (1992). Resting membrane potential and potassium currents in cultured parasympathetic neurones from rat intracardiac ganglia. J Physiol (Lond) *456*, 405–424.

Yan, J., and Aldrich, R.W. (2010). LRRC26 auxiliary protein allows BK channel activation at resting voltage without calcium. Nature *466*, 513–516.

Yan, J., and Aldrich, R.W. (2012). BK potassium channel modulation by leucine-rich repeat-containing proteins. Proc Natl Acad Sci USA *109*, 7917–7922.

Yan, J., Olsen, J.V., Park, K.-S., Li, W., Bildl, W., Schulte, U., Aldrich, R.W., Fakler, B., and Trimmer, J.S. (2008). Profiling the phospho-status of the BK_{Ca} channel α subunit in rat brain reveals unexpected patterns and complexity. Mol Cell Proteomics *7*, 2188–2198.

Yang, J., Krishnamoorthy, G., Saxena, A., Zhang, G., Shi, J., Yang, H., Delaloye, K., Sept, D., and Cui, J. (2010). An epilepsy/dyskinesia-associated mutation enhances BK channel activation by potentiating Ca^{2+} sensing. Neuron *66*, 871–883.

Yuan, P., Leonetti, M.D., Hsiung, Y., and MacKinnon, R. (2012). Open structure of the Ca^{2+} gating ring in the high-conductance Ca^{2+}-activated K^+ channel. Nature *481*, 94–97.

Yuan, P., Leonetti, M.D., Pico, A.R., Hsiung, Y., and MacKinnon, R. (2010). Structure of the human BK channel Ca^{2+}-activation apparatus at 3.0 A resolution. Science *329*, 182–186.

Yusifov, T., Savalli, N., Gandhi, C.S., Ottolia, M., and Olcese, R. (2008). The RCK2 domain of the human BK_{Ca} channel is a calcium sensor. Proc Natl Acad Sci USA *105*, 376–381.

Zhang, G., and Horrigan, F.T. (2005). Cysteine modification alters voltage- and Ca^{2+}-dependent gating of large conductance (BK) potassium channels. The Journal of General Physiology *125*, 213–236.

Zhang, G., Xu, R., Heinemann, S.H., and Hoshi, T. (2006). Cysteine oxidation and rundown of large-conductance Ca^{2+}-dependent K^+ channels. Biochemical and Biophysical Research Communications *342*, 1389–1395.

Zhang, G., Huang, S.-Y., Yang, J., Shi, J., Yang, X., Moller, A., Zou, X., and Cui, J. (2010). Ion sensing in the RCK1 domain of BK channels. Proc Natl Acad Sci USA *107*, 18700–18705.

Zhou, Y., Tang, Q.-Y., Xia, X.-M., and Lingle, C.J. (2010). Glycine311, a determinant of paxilline block in BK channels: a novel bend in the BK S6 helix. The Journal of General Physiology *135*, 481–494.

Zhou, Y., and Lingle, C.J. (2014). Paxilline inhibits BK channels by an almost exclusively closed-channel block mechanism. The Journal of General Physiology *144*, 415–440.